Monitoring of greenhouse gases and aerosols at Svalbard and Birkenes in 2022

Annual report

Stephen M. Platt, Tove Svendby, Ove Hermansen, Chris Lunder,
Markus Fiebig, Ann Mari Fjæraa, Georg Hansen, Norbert Schmidbauer,
Cathrine Lund Myhre and Kerstin Stebel

NILU report 24/2023

NILU report 24/2023 Norwegian Environment Agency **M-2615|2023**	ISBN: 978-82-425-3137-7 ISSN: 2464-3327	CLASSIFICATION: A – Unclassified (open report)
DATE 22.11.2023	SIGNATURE OF RESPONSIBLE PERSON Aasmund Fahre Vik, Deputy CEO and CTO	NUMBER OF PAGES 99
TITLE Monitoring of greenhouse gases and aerosols at Svalbard and Birkenes in 2022		PROJECT LEADER Wenche Aas
Annual report		NILU PROJECT NO. O-113007/O-121002
AUTHOR(S) Stephen M. Platt, Tove Svendby, Ove Hermansen, Chris Lunder, Markus Fiebig, Ann Mari Fjæraa, Georg Hansen, Norbert Schmidbauer, Cathrine Lund Myhre and Kerstin Stebel		QUALITY CONTROLLER Kjetil Tørseth
REPORT PREPARED FOR Norwegian Environment Agency Postboks 5672 Sluppen, 7485 Trondheim		CONTRACT REF. Contract number 17078061/21087006

ABSTRACT

This annual report for 2022 summarizes the activities and results of the greenhouse gas monitoring at the Zeppelin Observatory, situated on Svalbard, during the period 2001-2022, and the greenhouse gas monitoring and aerosol observations from Birkenes for 2009-2022.

NORWEGIAN TITLE

Overvåkning av klimagasser og partikler på Svalbard og Birkenes i 2022: Årsrapport.

KEYWORDS

Greenhouse gases/ Drivhusgasser	Aerosols/ Partikler	Climate gases/ Klimagasser	Halocarbons/ Halokarboner

ABSTRACT (in Norwegian)

Denne årsrapporten for 2022 presenterer aktiviteter og måleresultater fra klimagassovervåkingen ved Zeppelinobservatoriet på Svalbard for årene 2001-2022 og klimagassmålinger og klimarelevante partikkelmålinger fra Birkenes for 2009-2022.

PUBLICATION TYPE: Digital document (pdf)	COVER PICTURE: Source: Kjetil Tørseth, NILU

Citation: Platt, S.M., Svendby, T., Hermansen, O., Lunder, C., Fiebig, M., Fjæraa, A.M., Hansen, G., Schmidbauer, N., Myhre, C.L. and Stebel, K. (2023). Monitoring of greenhouse gases and aerosols at Svalbard and Birkenes in 2022. Annual report. (NILU report 24/2023). Kjeller: NILU.

NILU's ISO Certifications: NS-EN ISO 9001 and NS-EN ISO 14001. NILU's Accreditation: NS-EN ISO/IEC 17025.

Contents

Contents **3**

Summary **4**

Sammendrag **5**

1 Atmospheric methane on the wrong path **6**

2 Monitoring of greenhouse gases and aerosols at Svalbard and Birkenes in 2022 ..... **9**

2.1 Greenhouse gases 12

2.1.1 Carbon dioxide (CO_2) 14

2.1.2 Methane (CH_4) 15

2.1.3 Methane isotopic signature 17

2.1.4 Nitrous Oxide (N_2O) 18

2.1.5 Volatile organic compounds (VOC) 19

2.1.6 Carbon monoxide (CO) 22

2.1.7 Chloromethane at the Zeppelin Observatory 23

2.1.8 Bromomethane at the Zeppelin Observatory 25

2.1.9 Chlorofluorocarbons (CFCs) at the Zeppelin Observatory 26

2.1.10 Hydrochlorofluorocarbons (HCFCs) at the Zeppelin Observatory 28

2.1.11 Hydrofluorocarbons (HFCs) at Zeppelin Observatory 30

2.1.12 Halons measured at the Zeppelin Observatory 34

2.1.13 Other chlorinated hydrocarbons at the Zeppelin Observatory 35

2.1.14 Perfluorinated compounds at Zeppelin Observatory 37

2.2 Aerosol properties 40

2.2.1 Aerosol properties at Birkenes 40

2.2.2 Aerosol properties at Zeppelin 43

2.2.3 Aerosol properties at Trollhaugen 46

References **50**

Appendix A Data Tables **57**

Appendix B Description of instruments and methodologies **75**

Appendix C Abbreviations **95**

Summary

Key facts and figures from the monitoring programme for greenhouse gases. We present the monitoring of greenhouse gases and aerosols at Svalbard and Birkenes in 2022, providing insights into the main greenhouse gases—carbon dioxide (CO_2), methane (CH_4), and nitrous oxide (N_2O)—as well as other trace gases and aerosol physical-chemical properties relevant to Earth's climate. Our main findings in brief:

- Our observations show a consistent global increase in CO_2, which so far is not slowing down. CO_2 Levels increased by 2.4 and 2.6 ppm to 419.6 and 423.9 ppm from 2021 to 2022 at Zeppelin and Birkenes, respectively. CO_2 mixing ratios are not expected to fall until at least 2040, even under the most stringent "Shared socioeconomic pathways" (SSP) defined by the intergovernmental panel on climate change (IPCC), required to limit global mean surface temperature rise to 1.5°C (SSP1 1.9). This is due to the long lifetime of CO_2.
- Data from Birkenes and Zeppelin show accelerating increases in methane (CH_4), threatening the Paris agreement goal of limiting warming to 2°C or preferably 1.5°C. CH_4 Levels increased by 17.6 and 13.8 ppb to 1999.6 and 2005.5 ppb from 2021 to 2022 at Zeppelin and Birkenes, respectively. This was a record increase in CH_4 at Zeppelin.
- On 26th September 2022 the natural gas pipelines Nord Stream 1 and 2, between Russia and Germany in the Baltic Sea, were sabotaged resulting in an estimated leak of 150,000 tons of CH_4. Despite likely being the largest ever leak of CH_4 from a single point-source it is insignificant to the global climate, since the emissions were far lower than from sources such as wetlands (400,000 tons, daily)
- Nitrous Oxide (N_2O) is a powerful greenhouse gas and levels continue to increaseN_2O levels increased by 1.31 ppb to 335.5 ppb at Zeppelin.
- Several of the ozone depleting substances such as chlorofluorocarbons (CFCs) and their replacements also have very high global warming potentials. Those controlled by the Montreal protocols are declining. An important exception is CFC-115, which has begun to increase since ~2017, though it is still at a low concentration. The increase may be due to its use in HFC production. The Montreal Protocol does not forbid this use case.
- Perfluorinated compounds are some of the most extreme greenhouse gases. While all are currently at very low levels, the high warming potentials of these compounds means they must be followed closely. All are increasing in concentration.

Sammendrag

Viktige fakta og tall fra overvåkingsprogrammet for klimagasser. Vi presenterer resultater og analyser fra overvåkingen av klimagasser og aerosoler på Svalbard og Birkenes i 2022 for å gi innsikt i de viktigste klimagassene - karbondioksid (CO_2), metan (CH_4) og lystgass (N_2O) - samt andre sporstoffer og fysisk-kjemiske egenskaper til aerosoler som er relevante for klima. Her er oppsummering av de viktigste funnene:

- Observasjonene viser at CO_2 nivået øker globalt, og så langt er det ingen tegn på at økningen avtar. CO_2-nivåene økte med 2.4 ppm på Zeppelin og 2.6 ppm på Birkenes fra 2021 til 2022, og årlige middelverdier ble målt til 419.6 og 423.9 ppm på hhv Zeppelin og Birkenes i 2022. FNs klimapanel har definert en rekke "sosioøkonomiske utviklingsbaner" (Shared Socioeconomic Pathways, SSPs), men CO_2-nivået forventes ikke å avta før tidligst i 2040, selv under de strengeste SSP-kravene for å begrense den globale gjennomsnittstemperaturen til 1.5°C (SSP1 1.9). Dette skyldes den lange levetiden til CO_2.
- Data fra Birkenes og Zeppelin viser akselererende økning i metan (CH_4), noe som truer Paris-avtalens mål om å begrense oppvarmingen til 2°C eller aller helst 1.5°C. CH_4-nivåene økte med 17.6 ppb og 13.8 ppb på hhv Zeppelin og Birkenes fra 2021 til 2022, og årlige middelverdier i 2022 ble målt til hhv 1999.6 ppb og 2005.5 ppb på de to stasjonene. Dette var en rekordstor økning av CH_4 på Zeppelin.
- Den 26. september 2022 ble naturgassrørledningene Nord Stream 1 og 2, mellom Russland og Tyskland i Østersjøen, sabotert. Dette resulterte i en estimert lekkasje på 150 000 tonn CH_4. Til tross for at det sannsynligvis er den største punktkildelekkasjen av CH_4 noensinne, er den relativt ubetydelig for det globale klimaet, ettersom metanutslippet fra og våtmarker er langt høyere (~400 000 tonn daglig)
- Lystgass (N_2O) er en kraftig klimagass og nivået fortsetter å øke. N_2O-nivået økte med 1.31 ppb på Zeppelin, til en årlig middelverdi på 335.5 ppb i 2022.
- Flere av de ozonnedbrytende stoffene, som klorfluorkarboner (KFKer) og deres erstatningsstoffer, har også svært høyt globalt oppvarmingspotensial (GWP). De stoffene som er kontrollert av Montreal-protokollene har gått ned. Et unntak er CFC-115, som har vist en økning etter ~2017, men konsentrasjonen er fortsatt relativt lav. Økningen skyldes trolig at gassen brukes i HFK-produksjon.
- Perfluorerte forbindelser er noen av de mest ekstreme klimagassene. Konsentrasjonene er fremdeles svært lave, men på grunn av det høye oppvarmingspotensialet til disse forbindelsene, må utviklingen følges nøye. Konsentrasjonen øker for alle disse gassene.

1 Atmospheric methane on the wrong path

Meeting the Paris Agreement goal of keeping warming to 1.5, or even to 2°C, will require an international effort to put societies and economies on a pathway to lower emissions. The latest assessment report of the intergovernmental panel on climate change (IPCC AR6; IPCC 2021) describes a range of such 'Shared socioeconomic pathways' (SSPs). The expected pathways under four such scenarios for CH_4 are shown in Figure 1 (top left), expressed as the relative change in CH_4 on the pathways over time, with 2020 as the reference year. SSP1 1.9 (blue) and SSP2 2.6 (red) represent successful efforts to limit warming to 1.5, and 2°C respectively. Both scenarios imply an immediate reduction in CH_4, starting already in 2020. The two other scenarios in the figure, SSP2 4.5 and SSP3 7.0 represent an intermediate and very high emission scenario which will lead to an estimated 2.7°C and 3.6°C of warming, respectively. While SSP3 7.0 is considered 'unlikely' by the IPCC and while it is not too late for CH_4 to follow a different path, the data from Zeppelin and Birkenes (Figure 1, top left, orange and green lines, respectively) show that CH_4 is so far following the high emission scenario.

Although carbon dioxide (CO_2) is the most important gas, the ongoing increases in CH_4 jeopardize the Paris Agreement goals. This is because it is already responsible for significant warming (~25% compared to CO_2) and is a powerful greenhouse gas with a global warming potential 28 times that of CO_2 (see Box 1). Hence, the further CH_4 diverges from the SSP1 1.9 and 2.6 pathways, the deeper the reductions in the other main gases, CO_2 and N_2O, will need to be. The main cause of ongoing increase in CH_4, which came as a surprise when it began around 2005, is thought to be increased emissions from microbes in tropical wetland soils. This is consistent with the isotopic signature of atmospheric methane (see also Sect. 2.1.3).

Box 1: Key facts on Methane

- CH_4 is formed when organic compounds are broken down in anoxic conditions
- Around half of atmospheric emissions are from anthropogenic activity, half from natural sources
- The two largest sources are agriculture and waste (206-217 Tg/year) and wetlands (149-181 Tg/ year). Both of these are microbial sources
- The main sink is via reaction with OH radicals. CH_4 concentrations are high enough to impact OH levels overall, such that CH_4 influences its own lifetime and that of other atmospheric hydrocarbons
- The atmospheric life time is ~12 years and the global warming potential (GWP) is ~28 over a 100 year period

Tracking the impact of the global methane pledge. One of the dangers of wetland emissions is the potential for uncontrollable climate feedbacks. On the other hand, the short lifetime of CH_4 allows for a rapid impact of any cuts in human emissions. Due to the high risks of increasing methane and the high rewards offered by emission reductions, the Global Methane Pledge, ratified in 2021 by over 100 countries including Norway, which aims to voluntarily reduce global methane emissions by at least 30% from 2020 levels by 2030, is a hugely important initiative. Following the impact of the pledge in the years to come is an important task. NILU, supported by the monitoring activities at Zeppelin and Birkenes, and as part of the integrated carbon observing system (ICOS) is at the forefront of this effort. Using inversion models (box 2) we investigate when and where CH_4 emissions are higher or lower than expected. As an example, Figure 1 (top right) shows that the inversion model suggests that in June 2022, CH_4 emissions were lower than expected for much of Norway, but higher on the southwest coast.

Box 2: Inversion modelling.
Inversion models to relate changes in observed atmospheric concentrations to changes in fluxes using statistics. The initial estimate the 'prior' is updated to a 'posterior' flux such that the fluxes result in a better fit to the observations. Priors can come from emission inventories (anthropogenic flux) or land models (e.g., for wetlands). The difference between such a prior estimate and a revised posterior estimate is shown in Figure 1.

Nord stream leaks a wake-up call. On 26th September 2022 the natural gas pipelines Nord Stream 1 and 2, between Russia and Germany in the Baltic Sea, were sabotaged. CH_4 immediately began leaking out of the pipelines and bubbled up at the ocean surface near the coast of Sweden and Bornholm (Denmark). The Birkenes Observatory picked up the signal on the 27th, with the highest CH_4 concentration ever seen at the site. We modelled the air currents over the site and used this information, combined with the observations from Birkenes and other nearby stations to provide an estimate of the flux from the leaks and to predict the path of the methane plume as it moved over Northern Europe (Figure 1, bottom). Our initial estimate was a leak of 40 000 tonnes of CH_4, which we later revised upwards to 150 000 tonnes, since the first data released on the 27th did not include the full CH_4 spike as it had automatically been flagged as erroneous and removed. These numbers would mean that the Nord Stream pipeline sabotage actions resulted in likely the largest single ever point source leak of methane. However, it is important to note that these numbers represent a short-term emission. Over a full year the Nord Stream leaks are dwarfed by the global human emissions due to agriculture of ~560 000 tonnes and the emissions from wetlands of ~400 000 tonnes daily. Furthermore, these emissions occur all day, every day, every month, every year, and are as shown in Figure S-1, increasing. Consequently, while the climate impact of the leaks is thus minimal (0.01 to 0.03% of the methane emitted globally every year) they highlight the true scale of the emissions happening all the time from other sources globally. Lastly, while natural gas may be considered a relatively low carbon fuel source compared to, e.g., coal, such leaks do occur from natural gas and storage, and although it occurs more slowly, it also builds up over time.

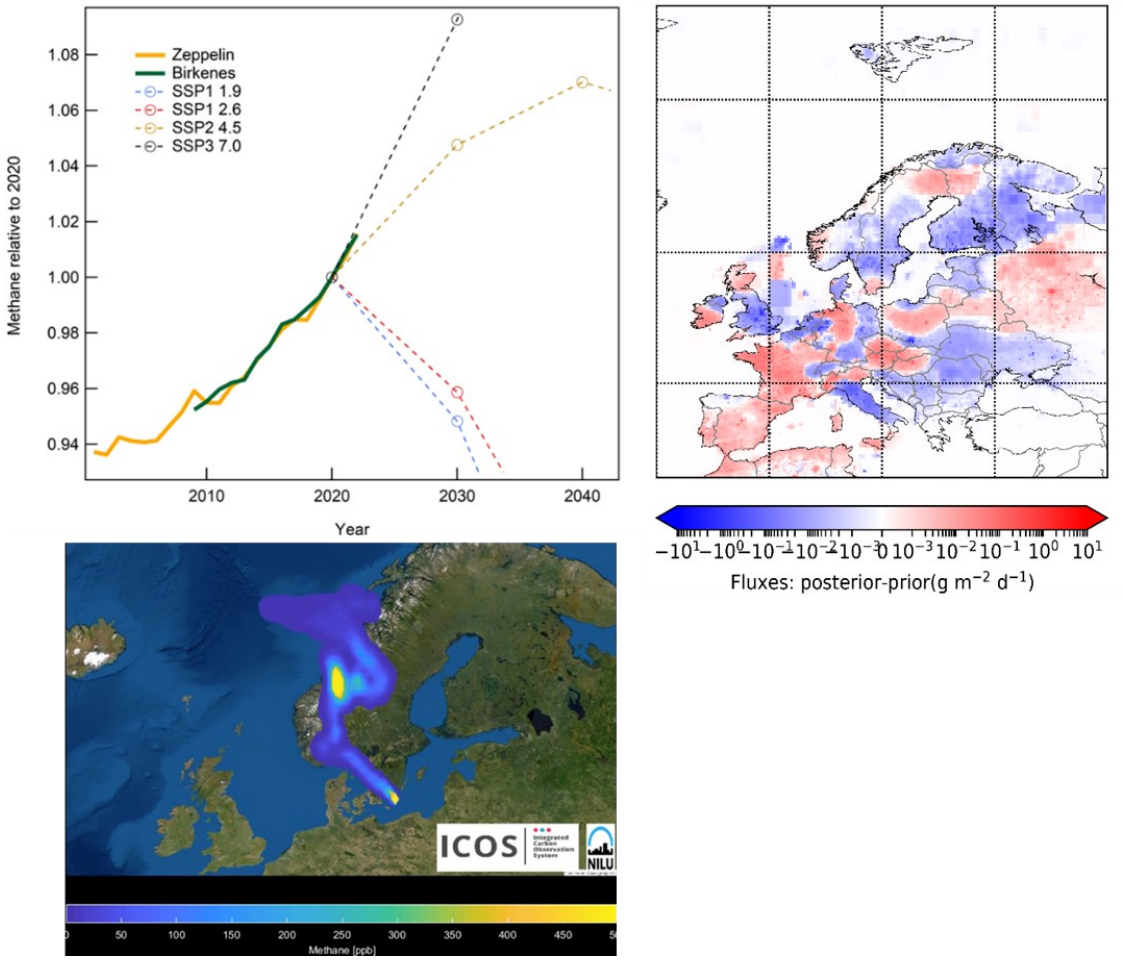

Figure S-1: Top left: Relative increase in methane compared to 2020 for Zeppelin (orange) and Birkenes (green) and the Intergovernmental Panel on Climate Change (IPCC) methane levels under selected shared socioeconomic pathways (SSP), dashed lines. SSPs from IPCC AR6 Annex III (IPCC, 2021). SSP1 1.9 (blue) and SSP1 2.6 are the methane concentration pathways the world needs to follow to meet the 1.5°C and 2°C Paris agreement targets, respectively. Top Right: The difference between the predicted (prior) methane fluxes from the inventories and the refined (posterior, updated with observations). Higher than predicted is red, lower than predicted is blue- Fluxes in grams per m^2 per day, as indicated by the colour bar. From https://shiny.nilu.no/ICOS/. Bottom: modelled plume of the Nord stream gas leak on 27th September.

2 Monitoring of greenhouse gases and aerosols at Svalbard and Birkenes in 2022

Monitoring of greenhouse gases and aerosols at Svalbard and Birkenes in 2022 is the third of three reports on the state of the atmosphere in Norway, Svalbard, and Antarctica. The previous reports are Monitoring of long-range transported air pollutants in Norway (Aas et al., 2023), and Monitoring of the atmospheric ozone layer and natural ultraviolet radiation (Svendby et al., 2023). In this Section, we include the full programme, i.e., all compounds (Greenhouse gases in Section 1.1, aerosol in Section 1.2), methodology (Appendix II), and updates on the status of the various instruments. We discuss long-term climate relevant features of the various components while significant changes seen in 2022 or other recent years are included in the previous summary section.

The monitoring programme for greenhouse gases and aerosols began in 1999 under a contract between the Norwegian Environment agency and NILU. Under this programme, we measure the long-term developments of the main greenhouse gases (CO_2, CH_4, N_2O), climate-relevant trace gases and aerosol properties (Table 1), at two Norwegian sites: Zeppelin, Birkenes (Figure 1). Additional measurements are performed by NILU at Trollhaugen, Antarctica, which we also include in the report for completeness. Our measurements support national and international stakeholders and policy makers and the scientific community by contributing to an improved understanding of the drivers of climate change, the effect on atmospheric composition of natural and anthropogenic emissions, and the impacts of mitigation activities. The programme is set up to meet national and international obligations (Table 1), covering the major atmospheric components influencing global warming. These include measurements of most of the main greenhouse gases shown in Figure 2 and parameters influencing the aerosol effects also shown in the figure (Sect. 2).

Figure 1: NILU's atmospheric monitoring site at Zeppelin, Svalbard (78.90°N, 11.88°E, 472 m a.s.l., above sea level, see also Platt et al. 2022) and Birkenes in Southern Norway (58.38°N, 8.25°E, 219 m a.s.l., see also Ytrri et al. 2021). Trollhaugen, in Antarctica (72.012°S, 2.53°E) is not shown. All three sites experience minimal local pollution making them ideal for long-term monitoring of the background atmosphere.

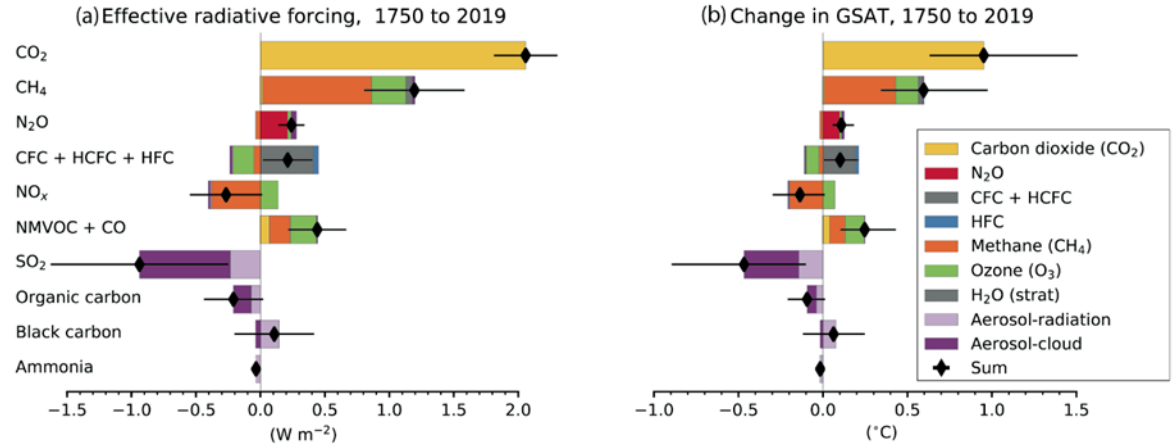

Figure 2: The change in effective radiative forcing (a) and global surface average temperature (GSAT, b) between 1750 and 2019 due to changes in the listed atmospheric components (carbon dioxide, CO_2; methane, CH_4; nitrous oxide, N_2O; chlorofluorocarbons, CFC+ hydro chlorofluorocarbons, HCFC+ hydrofluorocarbons HFC; oxides of nitrogen, NO_X; non-methane volatile organic compounds, NMVOC, sulfate aerosol SO_2, organic carbon, black carbon, ammonia), according to the IPCC AR6, 2021.

Table 1: Summary of the measurement programme at Birkenes, Zeppelin, and Troll Observatories.

Component	Birkenes Start	Zeppelin Start	Troll Start	International network	Comment
Trace gases					
CO2	2009	2012	(-)	ICOS	Zeppelin: since 1988 by Univ. Stockholm, ICOS class 1 site since 2017. Birkenes: COS class 2 site since 2020- Trollhaugen is not in ICOS.
CH4	2009	2001	(-)	ICOS	ICOS labelling as above
N2O	(-)	2009	(-)	ICOS	ICOS labelling and implementation in 2017
CO	(-)	2001	(-)	ICOS	ICOS labelling and implementation in 2017
	CFCs				
CFC-11*, CFC-12*, CFC-113* CFC-115*	(-)	2001		AGAGE	* These components are not within the required precision of AGAGE, but a part of the AGAGE quality assurance programme. This is related to the measurements in the period 2001 to 2010, before the installation of the Medusa instrument. After 2010, the measurements are with the same precision as the rest of the measurements in the AGAGE network.
	HCFCs				
HCFC-22, HCFC-141b, HCFC-142b	(-)	2001		AGAGE	
	HFCs				
HFC-125, HFC-134a, HFC-152a, **HFC-23**, **HFC-227ea**, **HFC-236fa**, **HFC-245fa**, **HFC-365mfc**, **HFC-32**, **HFC-4310mee**, **HFC-143a**	(-)	2001		AGAGE	Blue text indicates the extension and components added to the program in 2015.
	PFCs				
PFC-14, PFC-116 , PFC-218, PFC-318	(-)	2001		AGAGE	Blue text indicates the extension and components added to the program in 2015.
	Halons				
H-1211, H-1301 , **H-2402**	(-)	2001		AGAGE	Blue text indicates the extension and components added to the program in 2015.

Component	Birkenes Start	Zeppelin Start	Troll Start	International network	Comment
	Other chlorinated hydrocarbons				
CH3Cl, CH3Br, CH2Cl2, CHCl3, CCl4, CH3CCl3, CHClCCl2*, CCl_2CCl_2*	(-)	2001		AGAGE	Blue text indicates the extension and components added to the program in 2015.
	Other fluorinated				
SF6 , NF3	(-)	2001		AGAGE	Blue text indicates the extension and components added to the program in 2015.
SO2F2	(-)	2016		AGAGE	
	VOCs				
C2H6 – ethane, C3H8 – propane, C4H10 – butane, C5H12 – pentane, C6H6 – benzene, C6H5CH3 – toluene	(-)	2010		ACTRIS, EMEP	VOCs were included in the national monitoring programme from 2015, but the measurements are harmonised back to 2010.
	Aerosol properties				
Aerosol Optical depth	2009	2002	2014	ACTRIS	Zeppelin: spectral {368,412,500,862 nm} in collaboration with WORCC (in Ny-Ålesund); Birkenes spectral {spectral at 340, 380, 440, 500, 675, 870, 1020, 1640 nm} in collaboration with Univ. Valladolid
Particle Number Size Distribution (PNSD)	2009	2020	2022	ACTRIS,EMEP	Zeppelin: fine and coarse mode (0.01 µm < Dp < 10 µm), coarse mode. Birkenes fine and coarse mode (0.01 µm < Dp < 10 µm), Trollhaugen: fine mode (0.01 µm < Dp < 0.8 µm)
Number Size Distribution of Refractory Particles	2009	(-)	(-)		Zeppelin: fine mode (0.01 µm < Dp < 0.8 µm), NILU.
Aerosol Scattering Coefficient	2019	2015	2014	ACTRIS	Birkenes: spectral {450,550,700 nm}; Zeppelin spectral {450, 550, 700 nm}
Aerosol Absorption Coefficient	2017	2015	2020	ACTRIS	7-wavelength {370,470,520,590,660,880,950}. Trollhaugen and Birkenes have has additional 3-wavelength {470,522,660 nm}

Table 2: National and international agreements supported by the Norwegian national monitoring of greenhouse gases and aerosols.

Agreement	Date Ratified	Parties	Summary of Obligation
Paris Agreement[1]	4th Nov 2016	194/198 Parties including Norway	Limit global warming to 2°C or preferably 1.5°C or below. Commit to emission reduction targets, e.g., EU aiming for 55% reduction by 2030.
Global Methane Pledge[2]	4th Nov 2021	100+ Parties including Norway	Voluntarily reduce global methane emissions by at least 30% from 2020 levels by 2030. Improve reporting transparency.
Montreal Protocol & Kigali Amendment[3]	16th September 1987 & 15th October 2016	197 Parties including Norway	Monreal: Reduce ozone-depleting substances. Kigali: Cut hydrofluorocarbons (HFCs) use by over 80% in the 21st century to combat global warming.
Klimaloven[4]	-	Norway	Cut greenhouse gas emissions by at least 50 to 55% by 2030 compared to 1990 levels.

[1]https://unfccc.int/process/the-paris-agreement/status-of-ratification; [2]https://www.globalmethanepledge.org/;
[3]http://ec.europa.eu/clima/policies/strategies/2030/ and
http://www.consilium.europa.eu/uedocs/cms_data/docs/pressdata/en/ec/145397.pdf
[4]https://lovdata.no/dokument/NL/lov/2017-06-16-60

2.1 Greenhouse gases

Table 3 summarises the main results for 2022 and the trends over the period 2001 to 2022, including 2022 global annual mean values from the Bulletin of the American Meteorological Society (BAMS) (Blunden et al., 2023). All peak concentrations of the measured gases are significantly lower at Zeppelin than at other sites at the Northern hemisphere, due to the station's remote location. Birkenes is closer to the main source areas and the regional vegetation is important for regulating the carbon cycle, resulting in much larger variability in the concentration level compared to the Arctic region. Most greenhouse gases and other climate gases have numerous sources, both anthropogenic and natural. Trends and future changes in concentrations are thus determined by the future balance of their sources and sinks.

Table 3: Greenhouse gases measured at Zeppelin and Birkenes; lifetimes in years, global warming potential (GWP) for 100 year horizon and annual mean for 2022, change last year, and trends per year over the measurement period. Red is increasing and blue is decreasing trends. Global means for 2022, taken from Bulletin of the American Meteorological Society (Vimont et al., 2023) and WMO (2023), are included for comparison. All concentrations are mixing ratios in ppt, except for methane, nitrous oxide and carbon monoxide (ppb) and carbon dioxide (ppm). Trend calculations described in Appendix II.

Component	Chemical formula	Life-time	GWP	Global mean 2022	Annual mean 2022	Absolute change from last year	Trend/yr
Carbon dioxide - Zeppelin	CO_2	**	1	417.9	419.7	2.4	2.5
Carbon dioxide - Birkenes					423.9	2.6	2.5
Methane - Zeppelin	CH_4	11.8	28	1923	1999.6	17.6	7.1
Methane - Birkenes					2005.5	13.8	9.4
Carbon monoxide	CO	few months	-	335.8	115.0	-13.0	-0.8
Nitrous oxide	N_2O	109	273	-	335.8	1.31	1.03
Chlorofluorocarbons							
CFC-11	CCl_3F	52	5 560	219.6	220.7	-1.86	-1.77
CFC-12	CF_2Cl_2	102	11 200	489.7	494.3	-3.67	-2.71
CFC-113	CF2ClCFCl2	93	6 520	67.8	68.7	-0.46	-0.62

Component	Chemical formula	Life-time	GWP	Global mean 2022	Annual mean 2022	Absolute change from last year	Trend/yr
CFC-115	CF_3CF_2Cl	540	9 600	-	8.9	0.09	0.03
Hydrochlorofluorocarbons							
HCFC-22	$CHClF_2$	11.9	1 960	248.8	258.0	-0.61	5.20
HCFC-141b	$C_2H_3FCl_2$	9.4	860	24.6	26.0	-0.21	0.47
HCFC-142b	CH_3CF_2Cl	18	2 300	21.2	22.1	-0.54	0.41
Hydrofluorocarbons							
HFC-125	CHF_2CF_3	30	3 740	37.0	43.5	4.11	1.93
HFC-134a	CH_2FCF_3	14	1 530	124.5	132.1	6.12	5.28
HFC-152a	CH_3CHF_2	1.6	164	7.4	10.8	0.13	0.36
HFC-23	CHF_3	228	14 600	35.9	36.6	1.02	1.08
HFC-365mfc	$CH_3CF_2CH_2CF_3$	8.9	914	1.07	1.36	0.01	0.06
HFC-227ea	CF_3CHFCF_3	36	3 600	2.04	2.26	0.19	0.13
HFC-236fa	$CF_3CH_2CF_3$	213	8 690	-	0.24	0.02	0.01
HFC-245fa	$CHF_2CH_2CF_3$	7.7	858	-	3.97	0.14	0.20
HFC-32	CH_2F_2	5.4	771	26.3	37.7	4.97	2.65
HFC-4310mee	$C_5H_2F_{10}$	17	1 600	-	0.32	0.01	0.01
HFC-143a	CH_3CF_3	51	5 810	27.5	30.5	1.70	1.56
Perfluorinated compounds							
PFC-14	CF_4	50 000	7 380	88.5	88.99	1.01	0.97
PFC-116	C_2F_6	10 000	12 400	5.15	5.20	0.10	0.09
PFC-218	C_3F_8	2600	9 290	0.74	0.75	0.02	0.02
PFC-318	$c\text{-}C_4F_8$	3200	10 200	1.99	2.04	0.08	0.06
Sulphurhexafluoride	SF_6	3 200	25 200	11.02	11.24	0.40	0.30
Nitrogen trifluoride	NF_3	569	17 400	-	3.10	0.33	0.18
Sulphuryl fluoride	SO_2F_2	36	4 630	-	3.01	0.14	0.11
Halons							
H-1211	$CBrClF_2$	16	1 930	2.93	3.09	-0.09	-0.07
H-1301	$CBrF_3$	72	7 200	3.31	3.39	0.003	0.02
H-2402	$CBrF_2CBrF_2$	28	2 170	0.397	0.39	-0.004	-0.01
Halogenated compounds							
Chloromethane	CH_3Cl	0.9	5.5	547.5	515.00	3.95	-0.45
Bromomethane	CH_3Br	0.8	2.4	6.61	6.61	-0.14	-0.14
Dichloromethane	CH_2Cl_2	0.49	11.2	-	71.38	2.56	2.02
Trichloromethane	$CHCl_3$	0.5	20.6	-	12.28	-0.44	0.18
Carbon tetrachloride	CCl_4	32	2200	75.5	74.96	-1.20	-0.94
Trichloroethane	CH_3CCl_3	5	161	1.1	0.97	-0.40	-1.51
Trichloroethene	$CHClCCl_2$	0.02	0.04	-	0.21	-0.10	-0.01
Tetrachloroethene	CCl_2CCl_2	0.30	6.3	-	2.00	-0.14	-0.10
Volatile Organic Compounds (VOC)							

Component	Chemical formula	Life-time	GWP	Global mean 2022	Annual mean 2022	Absolute change from last year	Trend/yr
Ethane	C_2H_6	Ca 78 days*		-	1487.54	-54.23	-0.29
Propane	C_3H_8	Ca 18 days*		-	462.75	107.72	-15.18
Butane	C_4H_{10}	Ca 8 days*		-	169.71	52.71	-6.28
Pentane	C_5H_{12}	Ca 5 days*		-	55.67	13.43	-2.05
Benzene	C_6H_6	Ca 17 days*		-	60.25	-7.97	-1.40
Toluene	$C_6H_5CH_3$	Ca 2 days*		-	18.36	-1.86	-1.28

**The lifetimes of VOCs are strongly dependent on season, sunlight, other components etc. The estimates are global averages given in C. Nicholas Hewitt (ed.): Reactive Hydrocarbons in the Atmosphere, Academic Press, 1999, p. 313. The times series for these are short and the trend is very uncertain.*

2.1.1 Carbon dioxide (CO_2)

Key findings for CO_2: Our observations show a consistent global increase in CO_2, which so far is not slowing down. Annual variability results from higher emissions and less uptake from vegetation during the Northern hemisphere winter. Short term variability often occurs due to long range transport of air from polluted regions.

CO_2 emissions are primarily from fossil fuel burning and cement production. Global fossil CO_2 emissions have consistently increased over the past decades (Figure 3) except for a few years marked by international crises. NILU initiated CO_2 measurements at the Zeppelin Observatory in 2012, though ITM, University of Stockholm, began measurements in 1989. Continuous CO_2 measurements have been conducted at Birkenes since May 2009. Birkenes exhibits larger CO_2 variations than Zeppelin due to its proximity to sources. Zeppelin experiences the greatest variability during winter and spring, while Birkenes shows substantial variations year-round. Both sites experience episodes of elevated CO_2, often due to long-range transport of pollution. Generally, high levels occur when meteorological conditions lead to transport from Central Europe or the UK at Birkenes, and from Central Europe or Russia at Zeppelin. Annual increases compared to the global mean are shown in Figure 4.

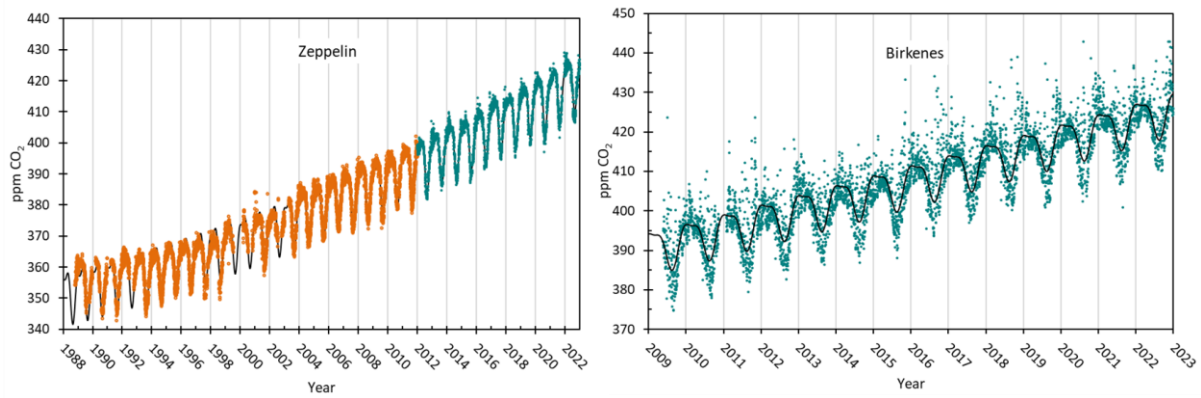

Figure 3: Left: daily mean CO_2 concentrations at the Zeppelin Observatory from mid-1988 to 2022. Prior to 2012, ITM University of Stockholm provided all data (orange) subsequent data from NILU are shown in green. Right: daily mean CO_2 at Birkenes (green). The black solid lines for both are the empirical, fitted, mixing ratio, with fit coefficients yielding the trend. This trend calculation is described in Appendix II.

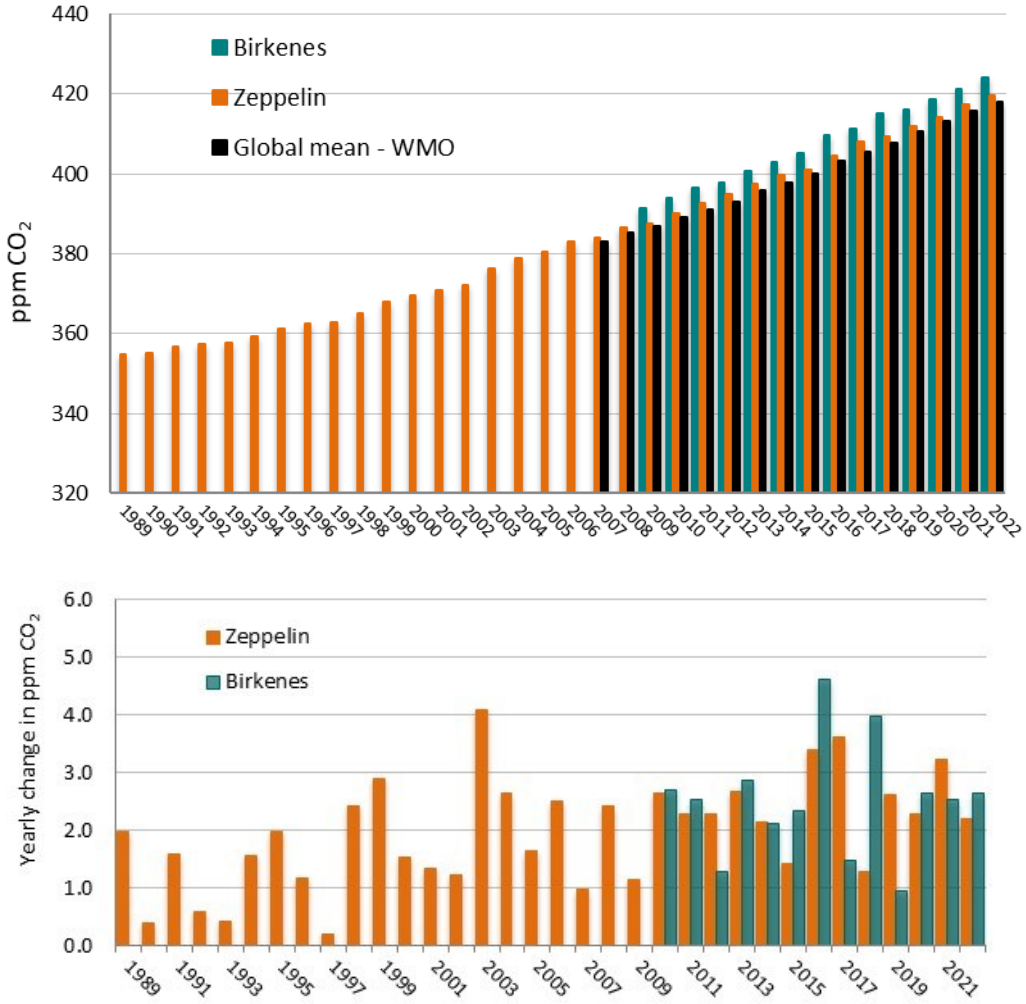

Figure 4: Upper panel: the annual mean concentrations of CO_2 measured at Zeppelin Observatory for the period 1989 to 2022 shown in orange. Prior to 2012, ITM University of Stockholm provides all data. The annual mean values from Birkenes are shown as green bars. The global mean values as given by WMO (2008 to 2023) are included in black. The yearly annual increases are shown in the lower panel, orange for Zeppelin, green for Birkenes.

2.1.2 Methane (CH_4)

Key findings for CH_4: Data from Birkenes and Zeppelin show accelerating increases in CH_4, threatening the Paris agreement goal of limiting warming to 2°C or preferably 1.5°C. The seasonal pattern in the time series is a result of higher CH_4 removal rates in Summer via the main sink, the OH radical, which is produced via reactions involving sunlight. As is the case for CO_2, long range transport from polluted regions causes episodes of high concentration.

CH_4 is the 2nd most important greenhouse gas, due to a high GWP of ~28, and plays central role in atmospheric chemistry. The atmospheric lifetime[1] of methane is 11.8 years (IPCC 2021), when indirect effects (e.g., on OH radical levels) are included. Excluding indirect effects, the lifetime is ~9 to 10 years. CH_4 in the environment is formed when organic compounds are broken down in anoxic conditions. This is either by thermogenesis (mainly combustion) or biogenesis (mainly microbial), and is due to biogenic or anthropogenic activity, each accounting for around half of the global atmospheric methane

[1] Time taken to decay to 1/e, 1/2.7, of original levels.

burden (Saunois et al., 2020). The main cause of the ongoing methane increases since ~2006 (Figure 6 and Figure 7) is thought to be increased Tropical wetland activity and extent, i.e., increased methanogenic bacterial activity. The main sink is removal by free hydroxyl radicals (OH) to eventually produce water and CO_2. A small fraction is also removed by surface deposition and reaction with Cl. Since the reaction with OH also represents a significant loss path for the OH itself, additional CH_4 emission will consume additional OH and thereby increasing its own lifetime, implying further increases in atmospheric CH_4 concentrations (and in those of all other compounds significantly removed by OH, i.e., most VOCs) (Isaksen and Hov, 1987; Prather et al., 2001), i.e. a positive feedback. Of concern are other possible climate feedbacks involving CH_4 including thawing permafrost (which may release trapped CH_4 and widen wetland extent) and decomposing gas hydrates.

There has been an increase in the concentrations of CH_4 at both Zeppelin and Birkenes over the last years (Figure 5), and in general the concentrations are higher at Birkenes than at Zeppelin (Figure 6). A seasonal variation is clearly visible for both, although stronger at Birkenes than Zeppelin. This is due to longer distance to the sources at Zeppelin, and thus the sink through reaction with OH dominates the variation. The larger variations at Birkenes are explained by both the regional sources in Norway, as well as a stronger impact of pollution transported from central Europe or UK. Meanwhile the big difference between global mean (Figure 6), and the observations at Zeppelin and Birkenes is due higher emissions in the Northern hemisphere.

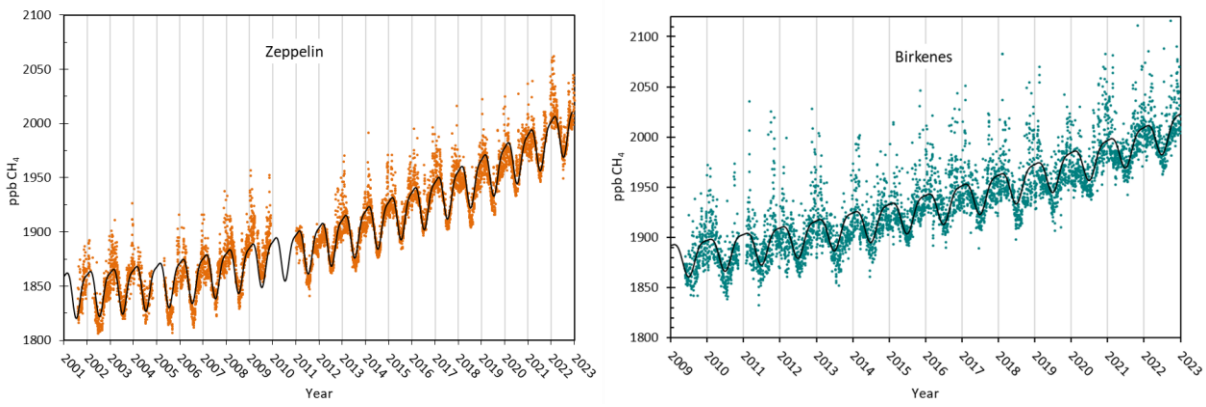

Figure 5: Left: daily averaged CH_4 mixing ratios for the period 2001 to 2022 at the Zeppelin Observatory and the empirical fitted methane mixing ratio (black). Right: daily averaged CH_4 mixing ratios for 2009 to 2022 at the Birkenes Observatory and the empirical fitted methane mixing ratio (black). The black solid lines for both are the empirical, fitted, mixing ratio, with fit coefficients yielding the trend. This trend calculation is described in Appendix II.

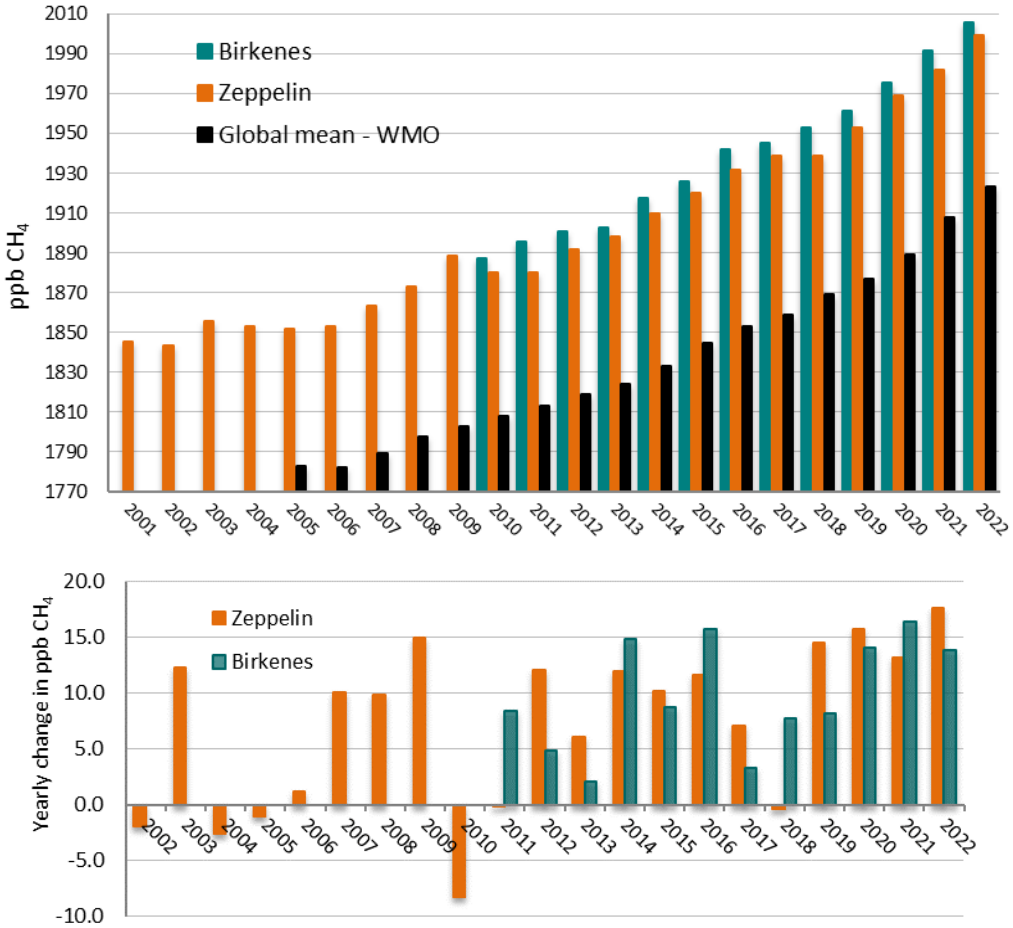

Figure 6: Upper: Development of the annual mean CH_4 mixing ratio at the Zeppelin Observatory (orange bars) for the period 2001 to 2022, Birkenes for the period 2010 to 2022 in green bars, compared to global mean provided by WMO as black bars (WMO, 20223). Lower: yearly increases for Zeppelin (orange) and Birkenes (green). The annual means are based on the measured CH_4 values, however, model fitted values are used to fill in gaps if measurements are missing.

2.1.3 Methane isotopic signature

Key findings for CH_4 isotopic signature: The isotopic signature of CH_4 ($\delta^{13}C_{CH4}$) has decreased at the same time as the atmospheric CH_4 concentration has increased. This likely reflects increased emissions in Tropical Wetland regions. This is particularly concerning because it is more difficult to control natural emission sources compared to manmade emission sources.

The isotopic signature of CH_4 (expressed as $\delta^{13}C_{CH4}$) varies by emission source (France et al., 2016) and hence measurements of the isotopic signature provide additional information on the changing balance of CH_4 sources and sinks (Table 4). Careful interpretation of the signature is necessary, in combination with CH_4 observations in the previous section, and knowledge of relevant Earth Systems (e.g., land use change via models). Changes in $\delta^{13}C_{CH4}$ signature at Zeppelin support the hypothesis of an increase in microbial activity from wetlands (more negative signature, Figure 7).

Table 4: The main CH_4 sources and sinks in tera-grams (Tg) per year (yr) according to Saunois et al., (2020). The effect of a change in the sink is given in the right column. For example, increasing fossil fuel emission will tend to increase the background $\delta^{13}C_{CH4}$ signal to more positive values. Also included are small Arctic sources which must be followed closely, since although fluxes are low, the reservoirs are large and vulnerable to climate change.

Source or Sink	Flux [Tg yr-1]	Effect on $\delta^{13}C_{CH4}$ of increased emission or increased sink
Main Sources and Sinks		
Fossil fuels	128	**More positive**
Agriculture	206	**More negative**
Biomass burning	30	**More positive**
Wetlands	149	**More negative**
OH radical	-595	**More negative**
Low flux, potential for high future disruption		
Oceanic	14	**More negative**

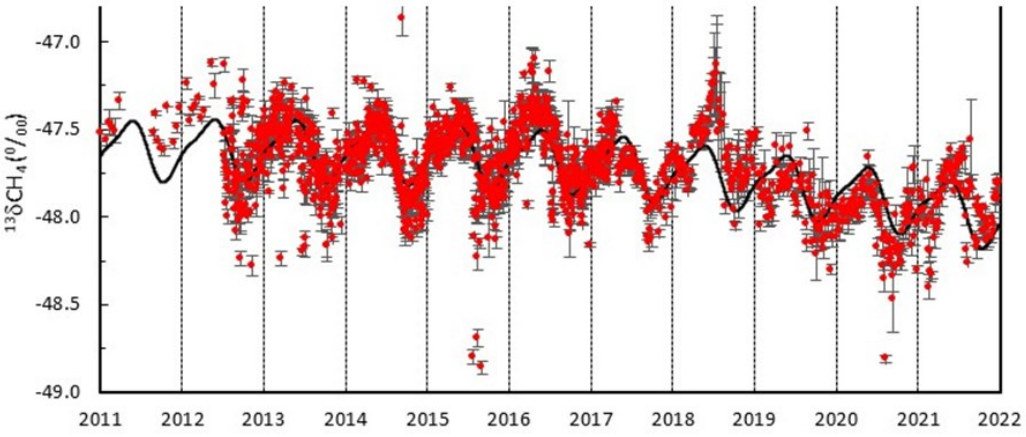

Figure 7: Long term measurements the ^{13}C isotopic signature of CH_4 ($\delta^{13}C$-CH_4, red) at the Zeppelin Observatory, Svalbard 78°N. The black solid line is the empirical, fitted, mixing ratio, with fit coefficients yielding the trend. This trend calculation is described in Appendix II.

2.1.4 Nitrous Oxide (N_2O)

Key findings for N_2O: Nitrous Oxide (N_2O) is a powerful greenhouse gas and levels continue to increase. Around half of emissions are manmade.

Nitrous Oxide (N_2O) is a greenhouse gas with both natural and anthropogenic sources including the oceans, tropical forests, soil, biomass burning, cultivated soil, animal manure, use of synthetic fertilizers, and various industrial processes. There are high uncertainties in the major soil, agricultural, combustion and oceanic sources of N_2O. Anthropogenic sources contribute approximately to 45% of total global N_2O emission according to the Global Carbon Project. Frozen peat soils in Arctic tundra are a potential source (Repo et al., 2009), but studies identify tropical and sub-tropical regions as the largest source regions (Thompson et al., 2013). N_2O is an important greenhouse gas with a radiative forcing of 0.21 W m^{-2} since 1750 (IPCC, 2021). N_2O is also the major source of the ozone-depleting nitric oxide (NO) and nitrogen dioxide (NO_2) in the stratosphere, thus the component is also influencing the stratospheric ozone layer (WMO, 2018).

In 2009, NILU installed a new instrument at Zeppelin measuring N_2O with high time resolution of 15 minutes. The instrument was in full operation in April 2010 and has later been upgraded to comply with ICOS. There has been a gradual increase in N_2O at Zeppelin since the measurements started in

Figure 8. Annual means at the Zeppelin Observatory compared to the WMO global data are shown in Figure 9.

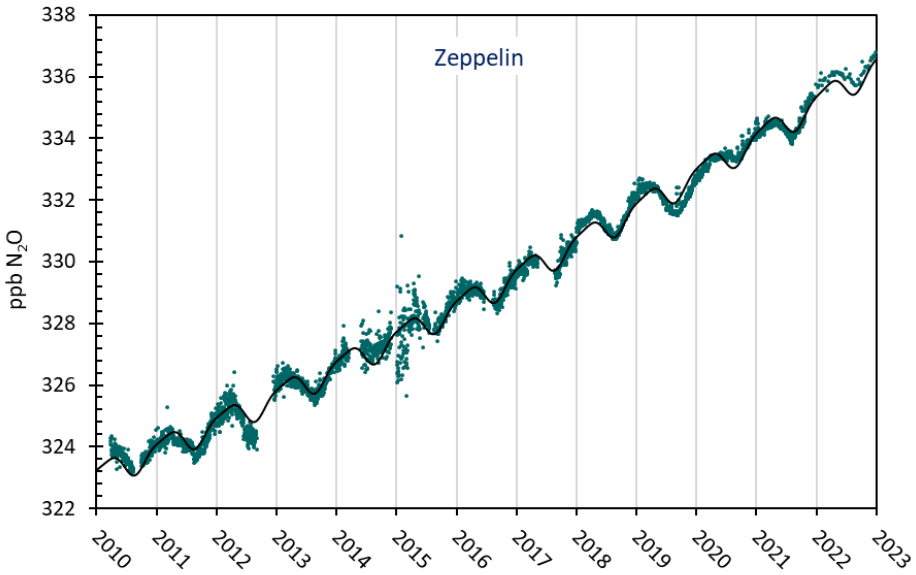

Figure 8: Measurements of N_2O at the Zeppelin Observatory for 2010 to 2022.The black line is empirical modelled N_2O mixing ratio. The black solid line is the empirical, fitted, mixing ratio, with fit coefficients yielding the trend. This trend calculation is described in Appendix II.

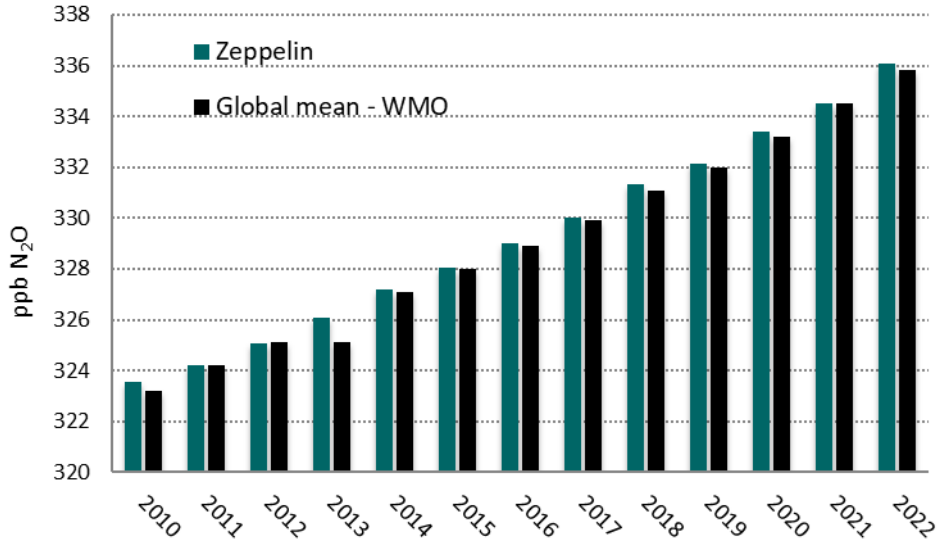

Figure 9: Annual mean concentration of N_2O at the Zeppelin Observatory for 2010 to 2022.

2.1.5 Volatile organic compounds (VOC)

Key findings for Volatile Organic Compounds (VOCs): There is currently no significant trend for any VOCs. Seasonal variability is a result of higher removal rates in summer via the main sink, the OH radical, which is produced via reactions involving sunlight. Short term variability results from long range transport from more polluted regions.

Volatile Organic Compounds (VOCs) represent a large group of carbon-based compounds that have a high vapour pressure and easily evaporate at room temperature. Six different volatile VOCs (ethane,

propane, butane, pentane, benzene, and toluene) have been measured at Zeppelin since September 2010. The annual mean concentrations vary from one year to another and for most compounds it is not possible to draw any conclusions about developments and trends. VOC oxidation contributes to tropospheric ozone production and influences photochemical processes, both impacting climate and air quality. Sources of VOCs are both natural (mostly geological but also from wildfires) and anthropogenic (fossil fuels). CH_4 and VOCs are co-emitted from oil and natural gas sources.

In 2010 a Medusa-GCMS instrument was installed at Zeppelin, which made it possible to perform online VOC measurements. Figure 10 shows the daily mean observations of the four non-methane hydrocarbons included in the programme in 2010: ethane, propane, butane, and pentane.

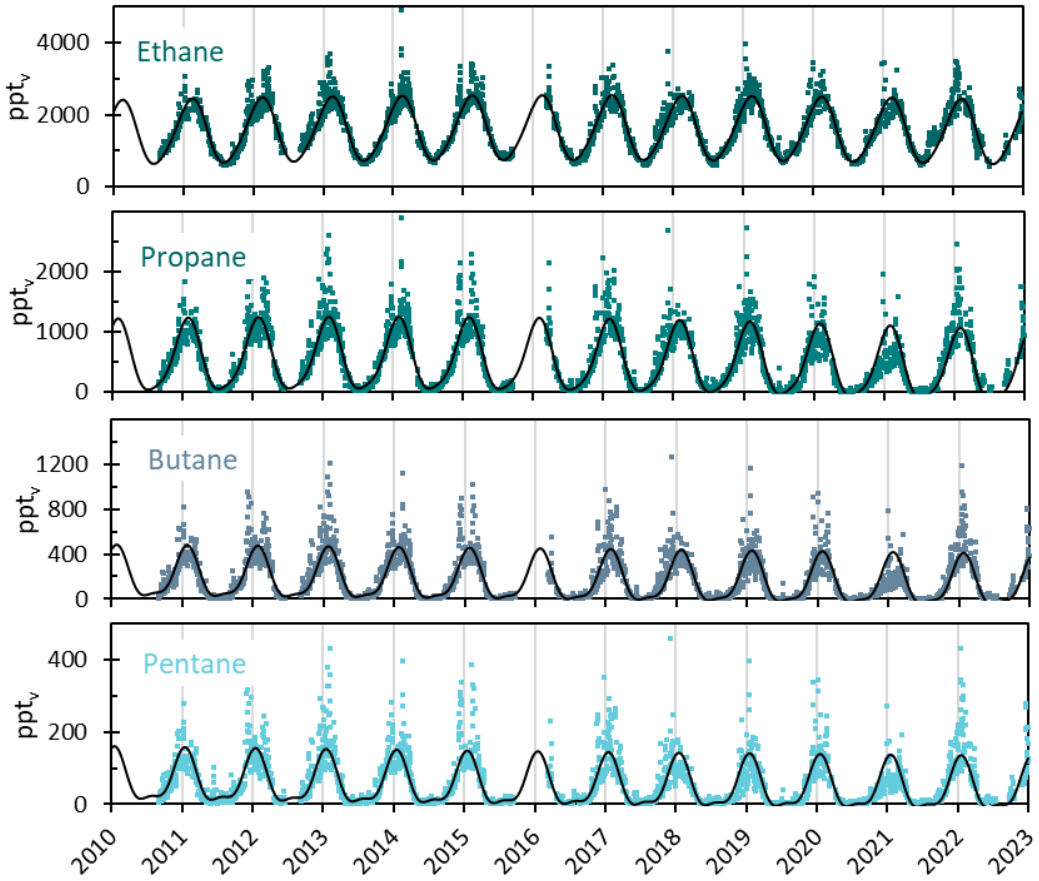

Figure 10: Observations of daily averaged mixing ratios of ethane, propane, butane, and pentane for the period September 2010 to 2022 at the Zeppelin Observatory. The black solid lines for both are the empirical, fitted, mixing ratio, with fit coefficients yielding the trend. This trend calculation is described in Appendix II.

Due to the short lifetimes, ranging from a few days for pentane to 2 to 3 months for ethane, the annual cycles are very strong and are regulated by OH reactions. The annual mean from 2011 to 2022 are shown in Figure 11. As seen from the figure the annual mean concentrations vary from one year to another and for most compounds it is not possible to draw any definite conclusions about development and trend. Figure 12 shows the daily mean observations of benzene and toluene at Zeppelin for the period 2010 to 2022. After an upgrade of the Medusa-GCMS in fall 2017, the benzene and toluene values became unrealistically low. This was purely a technical issue with no implication for the background levels of these gases. The upgrade was required to measure the low concentrations of the halogenated gases. Thus, the measurements performed in 2018 to 2020 are mainly missing.

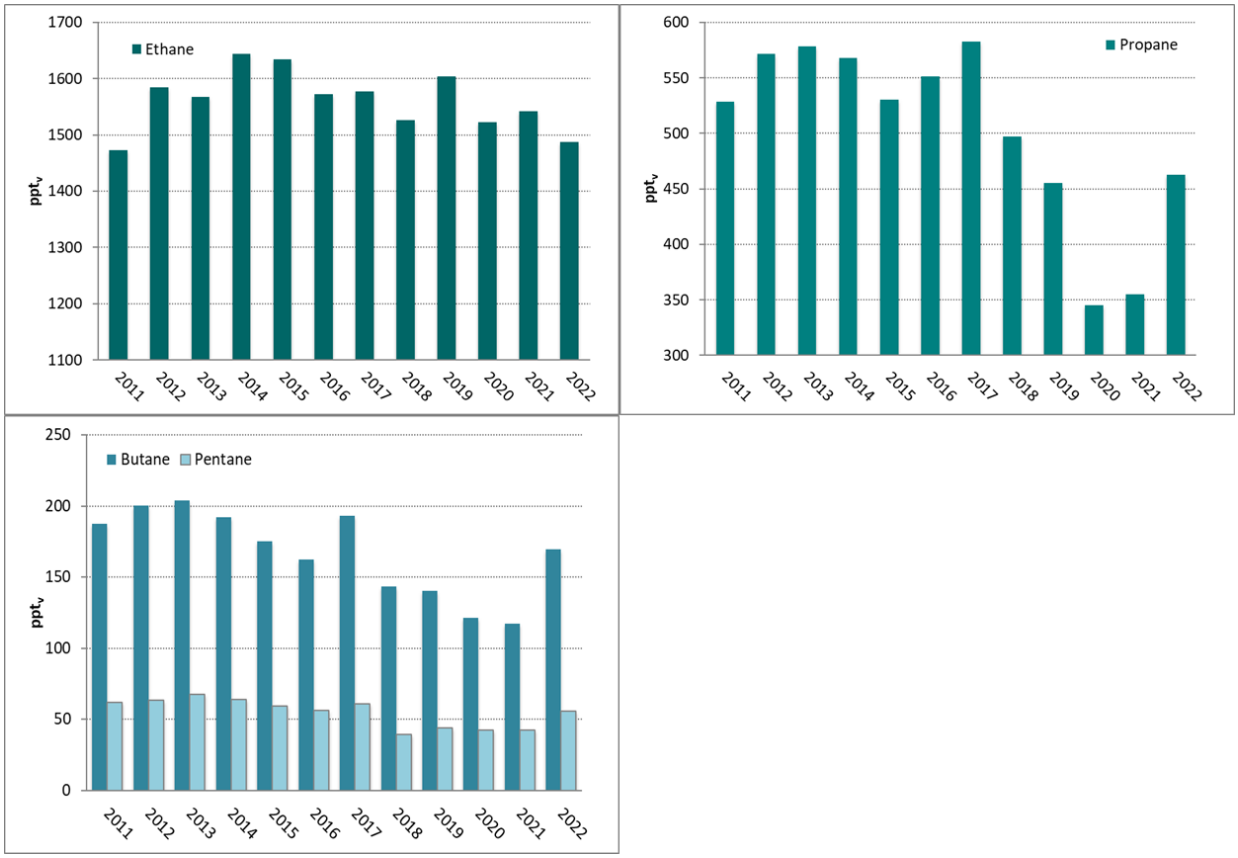

Figure 11: Development of the annual means of the measured non-methane hydrocarbons at the Zeppelin Observatory for the period 2011 to 2022. Upper left panel in dark green: ethane, upper right panel: propane, and lower panel: butane and pentane. All values in ppt.

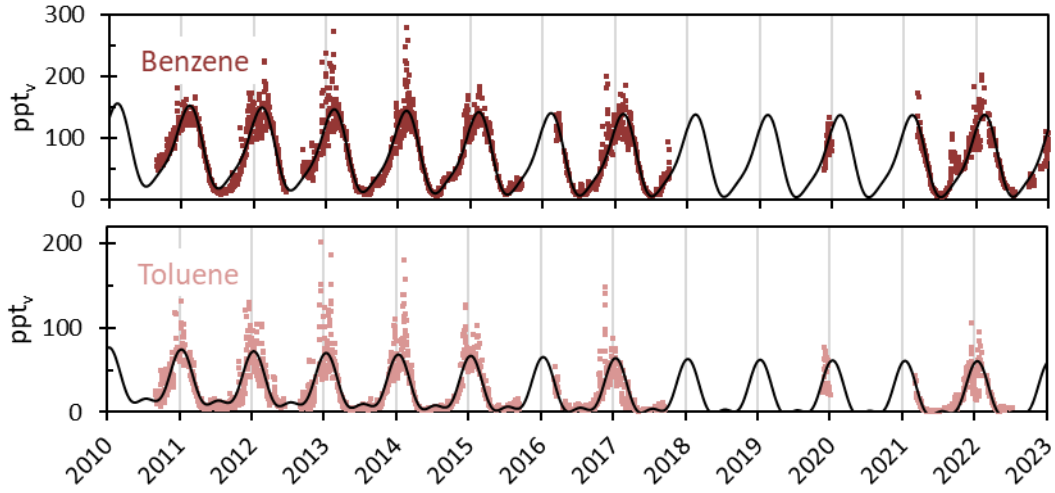

Figure 12: Daily averaged mixing ratio of benzene (upper panel) and toluene (lower panel) for the period September 2010 to 2022 at the Zeppelin Observatory (pink dots). The black solid lines for both are the empirical, fitted, mixing ratio, with fit coefficients yielding the trend. This trend calculation is described in Appendix II.

As can be seen from the figure there are strong annual variations, mainly explained by the reactions induced by sunlight. The annual means of benzene and toluene for the period 2011 to 2022 are presented in Figure 13. As explained above annual mean values were not calculated from the

measurements in 2018 to 2022, which makes the trend estimates very uncertain. The shaded and patterned bars in Figure 13 imply that the annual means 2018-2020 primarily are based on model values (i.e. the black curve in Figure 12).

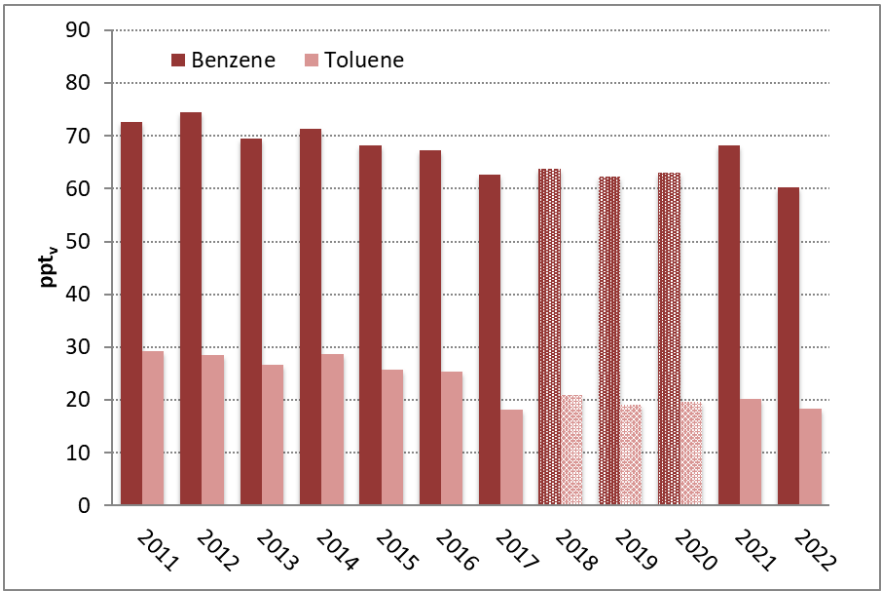

Figure 13: Development of the annual means of benzene (brown) and toluene (light red) for the period 2011 to 2022 at the Zeppelin Observatory. All concentrations are in ppt. Note that benzene and toluene in 2018 to 2020 mainly are based on model data.

2.1.6 Carbon monoxide (CO)

Key findings for Carbon monoxide (CO): CO levels are stable after a small decline between 2002 to 2010. Large spikes are often associated with long range transport.

Atmospheric carbon monoxide (CO) has both natural and anthropogenic sources. CO is produced when various organic gases are oxidized, such as methane, VOCs emitted from fossil fuel, and gases from biomass burning. Additionally, emissions from plants and ocean are important sources. CO is not considered as a direct greenhouse gas, as it does not absorb terrestrial thermal IR energy strongly enough. However, CO modulates the level of methane and production of tropospheric ozone, which are both very important greenhouse gases. Hence, CO is considered as a climate gas although not a greenhouse gas. CO also plays a key role in the control of OH radicals. CO at Zeppelin is included in the current monitoring programme and for ICOS and the observed CO mixing ratios for the period September 2001 to 2022 are shown in Figure 14. CO concentrations show characteristic seasonal variations with a clear annual cycle with a late winter (February to March) maximum and a late summer (August) minimum. This seasonal cycle is driven by variations in OH concentration as a sink, emission by industries and biomass burning, and transport of air on a large scale. As seen from the figure there are also peak values which are due to long-range transport of polluted air to Zeppelin and the Arctic. The development of the annual CO means at Zeppelin for the period 2001 to 2022 is presented in Figure 15. Overall, the CO concentration at Zeppelin shows a decrease during the period 2003 to 2009, and stable levels the last years with a small peak in 2010.

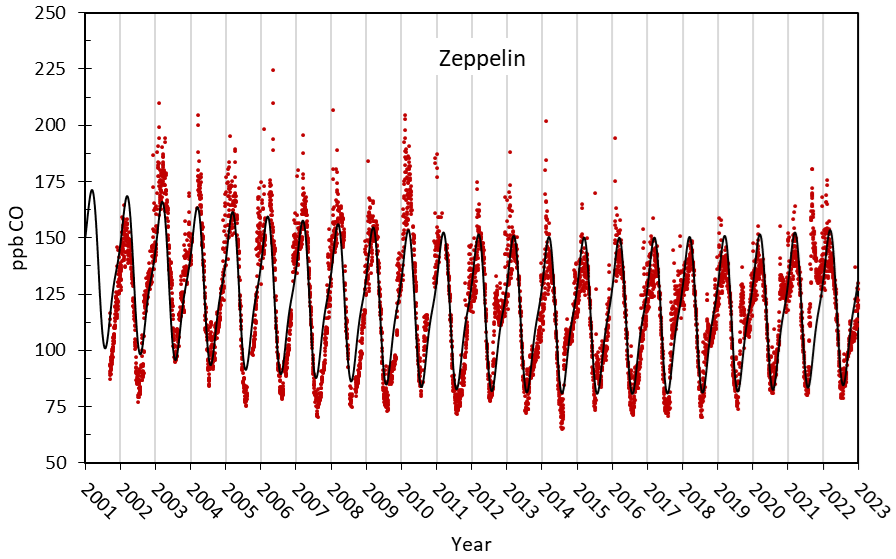

Figure 14: Daily averaged carbon monoxide (CO) from September 2001 to 2022 at the Zeppelin observatory (red dots). The black solid line is the empirical, fitted, mixing ratio, with fit coefficients yielding the trend. This trend calculation is described in Appendix II.

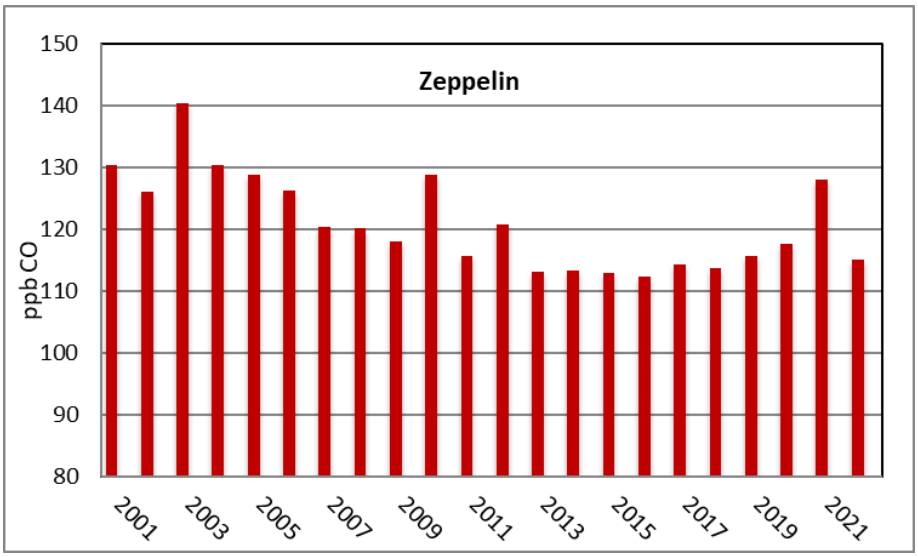

Figure 15: Development of the annual means of carbon monoxide at Zeppelin.

2.1.7 Chloromethane at the Zeppelin Observatory

Key findings for Chloromethane (CH_3Cl): CH_3Cl is ozone depleting but not regulated under the Kyoto and Montreal protocols because it is emitted naturally. Levels are stable and are lower at Zeppelin than the global average due to higher emissions in the Tropics.

Chloromethane (or methyl chloride, CH_3Cl) is the most abundant chlorine containing organic gas in the atmosphere, contributing ~16% of total chlorine from the well-mixed gases in the troposphere (WMO, 2014b). It is a strong contributor to ozone depletion. Its main sources are natural, including the oceans, biomass burning, fungi, wetlands, rice paddies, and tropical forests and hence this compound is not regulated through the Montreal or the Kyoto protocols. CH_3Cl has a relatively high mixing ratio and contributes to the stratospheric chlorine burden. The results of the measurements of this gas for the

period 2001 to 2022 are shown in Figure 16. The lifetime of chloromethane is only one year, resulting in large seasonal fluctuations due to rapid changes in emission, as shown in Figure 16.

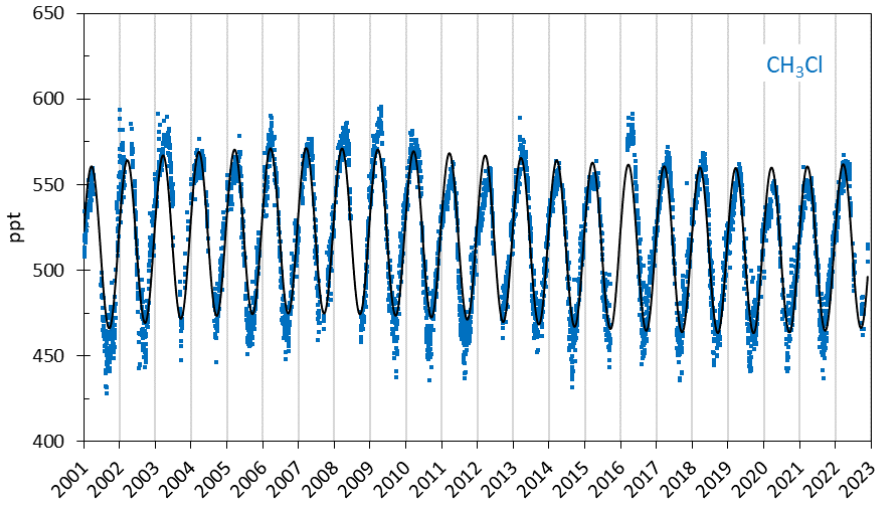

Figure 16: Daily averaged chloromethane, CH_3Cl, for the period 2001 to 2022 at the Zeppelin Observatory (blue dots). The black solid line is the empirical, fitted, mixing ratio, with fit coefficients yielding the trend. This trend calculation is described in Appendix II.

The annual means of chloromethane for the period 2001 to 2022 are shown in Figure 17. Days with missing observations are filled with empirical fitted data. Only small changes have been observed since the measurements started in 2001. The black bars in Figure 17 show that the global annual means, published by BAMS in "State of Climate" 2016 to 2022 (Last report: Blunden et al. 2023), are 30 to 40 ppt (6 to 7%) higher than the annual mean values at the Zeppelin Observatory. This is likely explained by strong emission sources in the tropics, resulting in increased CH_3Cl mixing ratios towards lower latitudes (Umezawa et al., 2014). Zeppelin is less affected by this, due to the short lifetime.

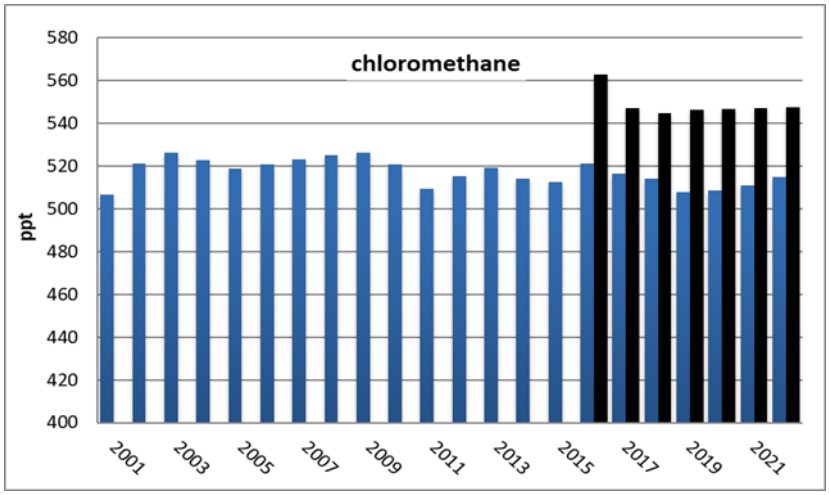

Figure 17: Development of Chloromethane annual means measured at the Zeppelin Observatory for the period 2001 to 2022. Global annual means for 2016 to 2022 are included as black bars. All units are in ppt.

2.1.8 Bromomethane at the Zeppelin Observatory

Key findings for Methyl bromide (CH_3Br): CH_3Br is a potent greenhouse gas and ozone depleting substance with both natural and anthropogenic sources. Levels have declined following successful implantation of the Kyoto and Montreal protocols and are currently stable.

Bromomethane, also known as Methyl bromide (CH_3Br), is significant atmospheric bromine reservoir, and is a key player in ozone layer depletion. This compound has dual origins—natural and anthropogenic— with natural sources such as the ocean, plants, and soil acting as both emitters and absorbers. The main anthropogenic source is fumigants for pest control. Additional anthropogenic contributors include leaded gasoline combustion, biomass burning, and emissions from specific crop species. Despite its natural occurrence, the human-induced release of bromomethane contributes to ozone layer depletion. The combined organic bromine levels from halons and bromomethane reached a peak in the mid-1990s and have declined and stabilised since 2001. Stratospheric bromide abundance has also started to decline (WMO, 2018). Figure 18 shows daily averaged CH_3Br mixing ratios from 2001 to 2022. CH_3Br is a potent greenhouse gas, twice as effective as CO_2, with a relatively short lifetime of 0.8 years (Myhre et al., 2013b). This short lifespan accounts for the compound's annual and seasonal variations.

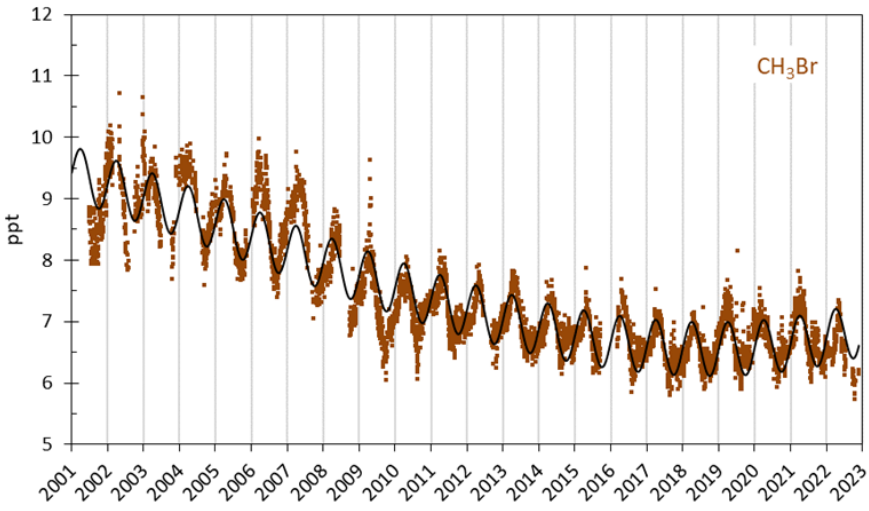

Figure 18: Observations of Bromomethane, CH_3Br, for the period 2001 to 2022 at the Zeppelin Observatory. Brown dots: daily averages mixing ratios from the observations. The black solid line is the empirical, fitted, mixing ratio, with fit coefficients yielding the trend. This trend calculation is described in Appendix II.

The development of the annual means for the period 2001 to 2022 is presented in Figure 19. The decline in bromomethane from 2001 to around 2015 is explained by a considerable reduction in emissions; the use of CH_3Br has decreased steadily following the implementation of the Montreal Protocol. The global mean mixing ratios published by BAMS in "State of the Climate" is close to the annual mean values observed at the Zeppelin Observatory.

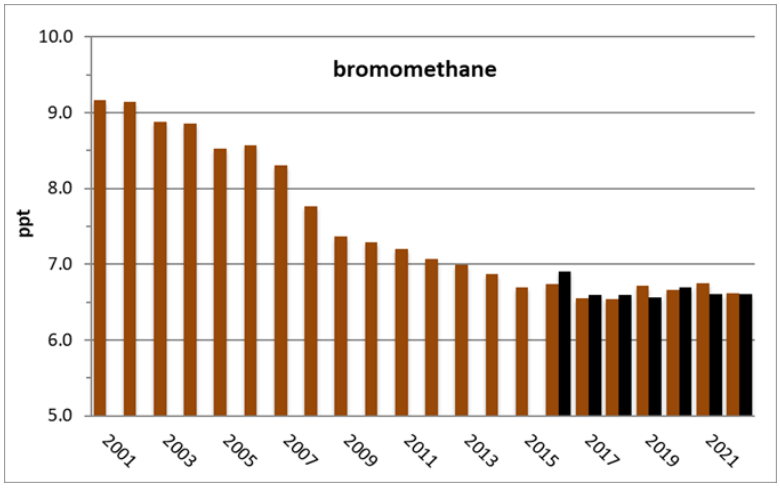

Figure 19: Development of the annual means of bromomethane measured at the Zeppelin Observatory for the period 2001 to 2022. The global annual mean for 2016 to 2022 are included as black bars.

2.1.9 Chlorofluorocarbons (CFCs) at the Zeppelin Observatory

Key findings for chlorofluorocarbons (CFCs): CFCs are regulated under the Montreal Protocol as ozone depleting substances. They are also potent greenhouse gases. Following the protocol, all four CFCs measured Zeppelin (-11, -12, -113, -115) declined. However, CFC-115 has begun to increase since ~2017, though it is still at a low concentration. The increase may be due to its use in HFC production. The Montreal Protocol does not forbid this use case, and future developments in CFC-115 should be followed closely.

We measure four chlorofluorocarbons (CFCs) at the Zeppelin: CFCs -11, -12, -113, and -115 (Figure 20). These are the main four ODSs. The main sources of these compounds were foam blowing, aerosol propellant, refrigerants, solvents, and the electronics industry. Peak CFC production was ~1985, with peak emission two years later in 1987. Note however, that CFC-115 is used in the production of HFCs, and this use-case is not regulated under the Montreal Protocol (MP). The lifetimes of these compounds are long, from 45 to over one thousand years (Table 3) and combined with strong infrared absorption properties, their GWPs are high. However, the development of the CFC -11, -12, and - 113 levels, as seen at the global background site Zeppelin is promising and in accordance with the MP. While still not posing a threat due to low levels, and still in accordance with the MP, CFC-115 has increased since around 2017. This development must be followed closely.

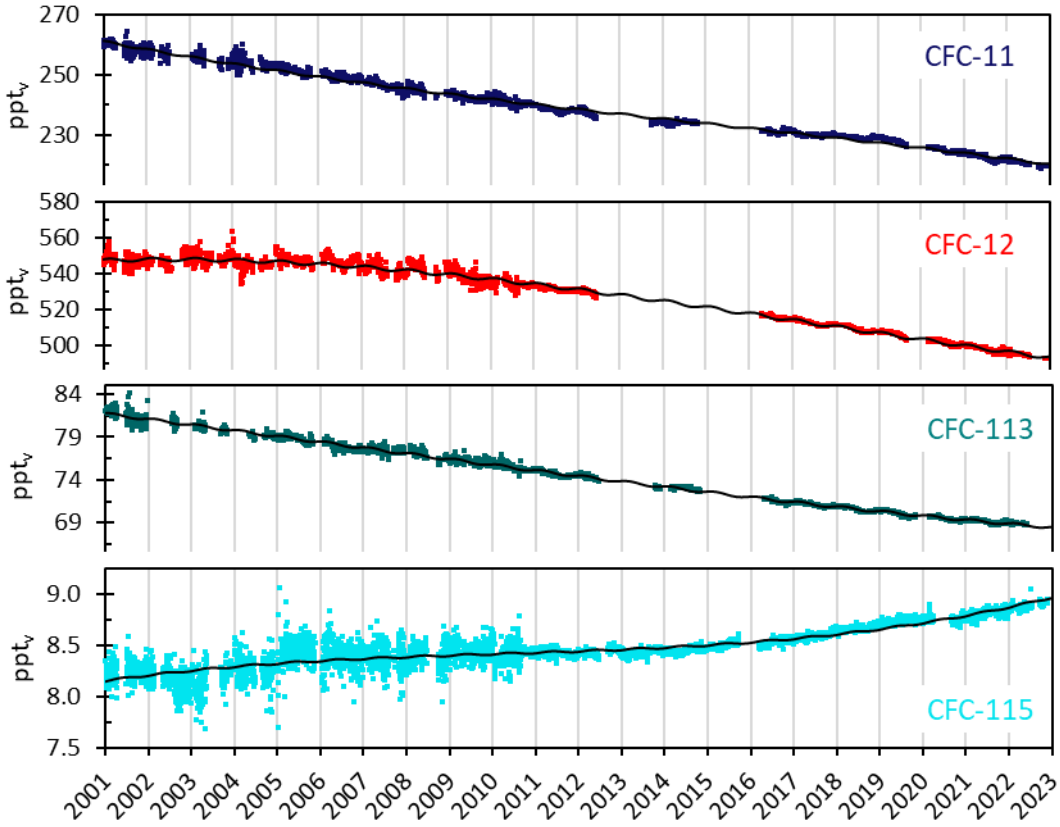

Figure 20: Daily averaged mixing ratios of the monitored CFCs at the Zeppelin observatory for the period 2001 to 2022: CFC-11 (dark blue), CFC-12 (red), CFC-113 (green) and CFC-115 (light blue). The black solid lines are the empirical, fitted, mixing ratios, with fit coefficients yielding the trend. This trend calculation is described in Appendix II.

The 2001 to 2022 annual means for all the observed CFCs at Zeppelin are shown in Figure 21. The global annual means in 2016 to 2022 as reported in "State of the Climate", BAMS (Dlugokencky et al., 2018 and 2019; Hall et al., 2017 and 2020; Lan et al., 2021 and 2022, Blunden et al, 2023) are included as black bars for comparison. As can be seen, the observed concentrations at Zeppelin are close to the global mean for these compounds, as the lifetimes are long and there are hardly any present-day emissions.

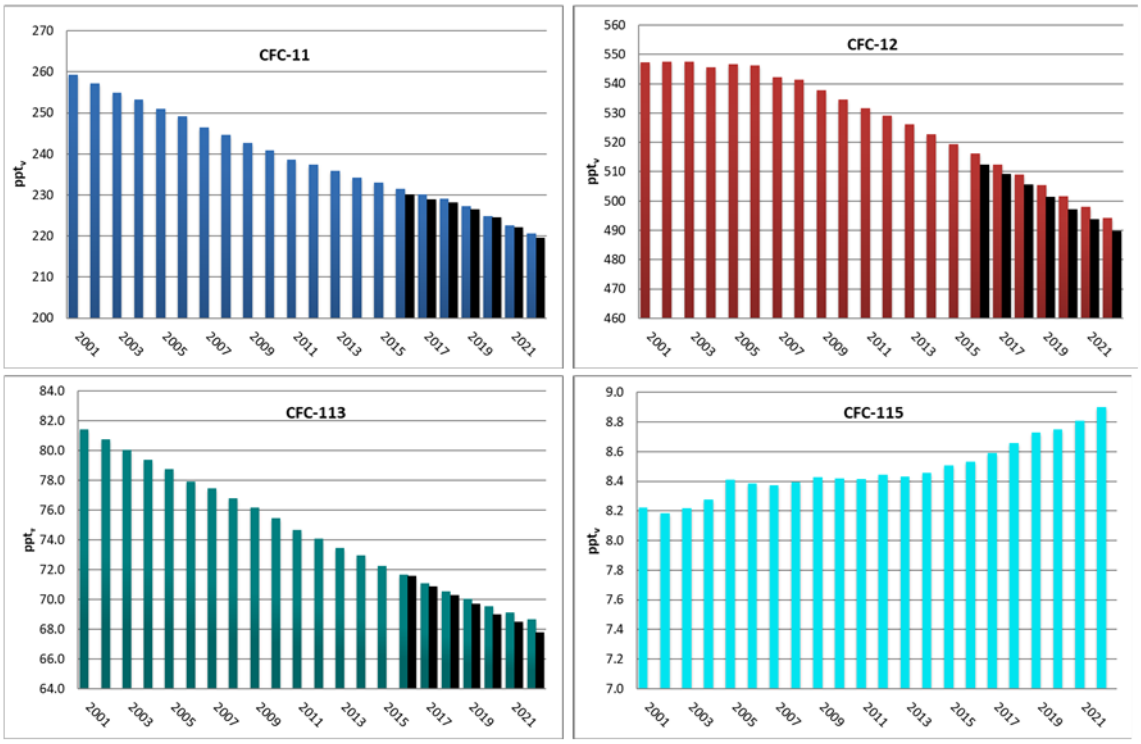

Figure 21: Development of CFC annual means at the Zeppelin Observatory for the period 2001 to 2022. Upper left panel: CFC-11, upper right panel: CFC-12, lower left panel: CFC-113, lower right panel: CFC-115. See Appendix I for data quality and uncertainty. The global annual means for 2016 to 2022 are included as black bars. All units are in ppt.

2.1.10 Hydrochlorofluorocarbons (HCFCs) at the Zeppelin Observatory

Key findings for hydrochlorofluorocarbons (HCFCs): HCFCs are stable or in decline, in accordance with the Montreal Protocol.

Hydrochlorofluorocarbons (HCFCs) are the 1st generation replacement gases for CFCs. Their lifetimes are rather long (Table 3), and although not as stable and persistent in the atmosphere as CFCs, they can still reach the stratosphere where they can destroy the ozone layer. Consequently, these gases are regulated through the MP. The Norwegian monitoring programme includes three HCFC species: HCFC-22 (removed from AGAGE since 2019), HCFC-141b and HCFC-142b. These compounds are mainly used as refrigerants, foam blowing agents and solvents. All these gases potentially have a strong warming effect due to their high GWPs, e.g., HCFC-142b has the highest GWP, with a warming potential 2300 times stronger than CO_2, per kg gas emitted (Table 3). The daily averaged observations of the three HCFCs are shown in Figure 22 for 2001 to 2022.

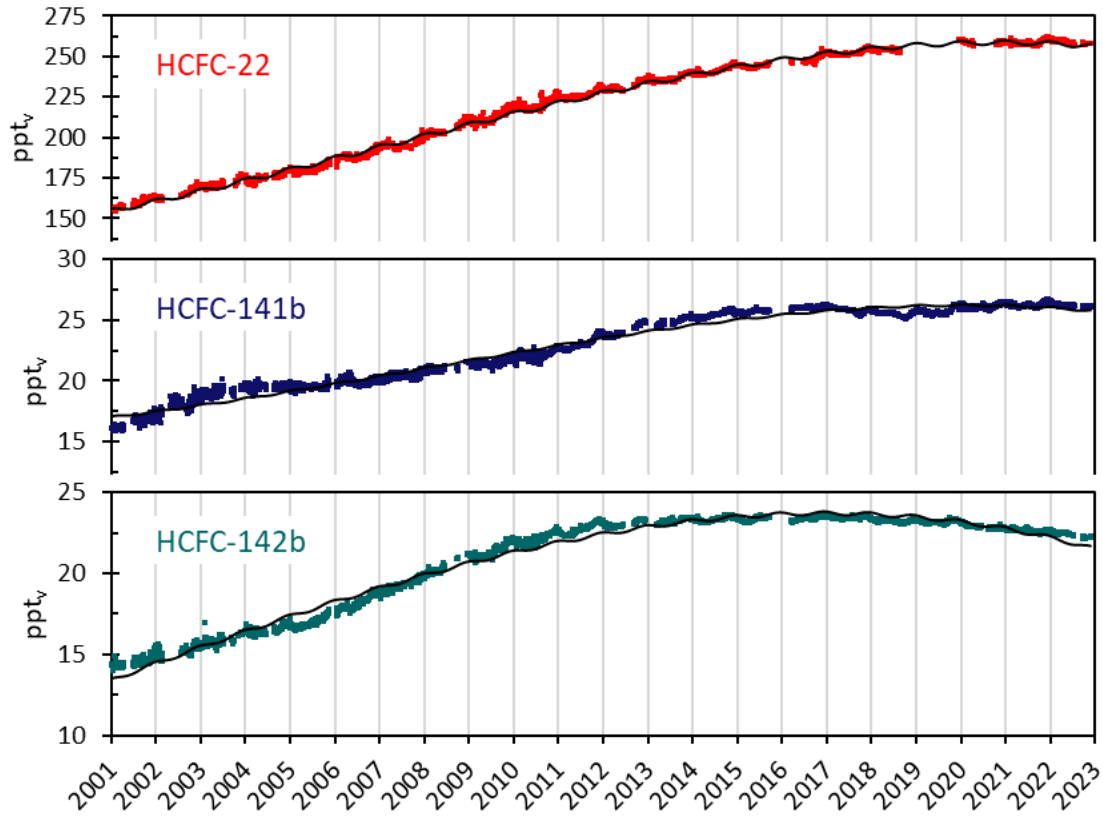

Figure 22: Daily averaged mixing ratios of the monitored HCFCs for the period 2001 to 2022 at the Zeppelin observatory: HCFC-22 (red), HCFC-141b (dark blue), and HCFC-142b (green). The black solid lines are the empirical, fitted, mixing ratios, with fit coefficients yielding the trend. This trend calculation is described in Appendix II.

Prior to ~2010 HCFC-22, HCFC-141b and HCFC-142b were increasing, see Figure 23, which also includes the global annual means for 2016 to 2022 (Hall et al. 2017 and 2020; Dlugokencky et al. 2018 and 2019; Lan et al., 2021 and 2022). The subsequent stabilisation or reduction in levels (for HCFC-142b) is promising. The observed concentrations at Zeppelin are 4 to 6% higher than the global means, due to location in the northern Hemisphere, closer to emission sources. Finally, however, despite the promising trend, with lifetimes in the order of 10 to 20 years, it is important to continue monitoring the development of the HCFCs for many years to come, as they have a significant influence on the ozone layer and are also strong greenhouse gases.

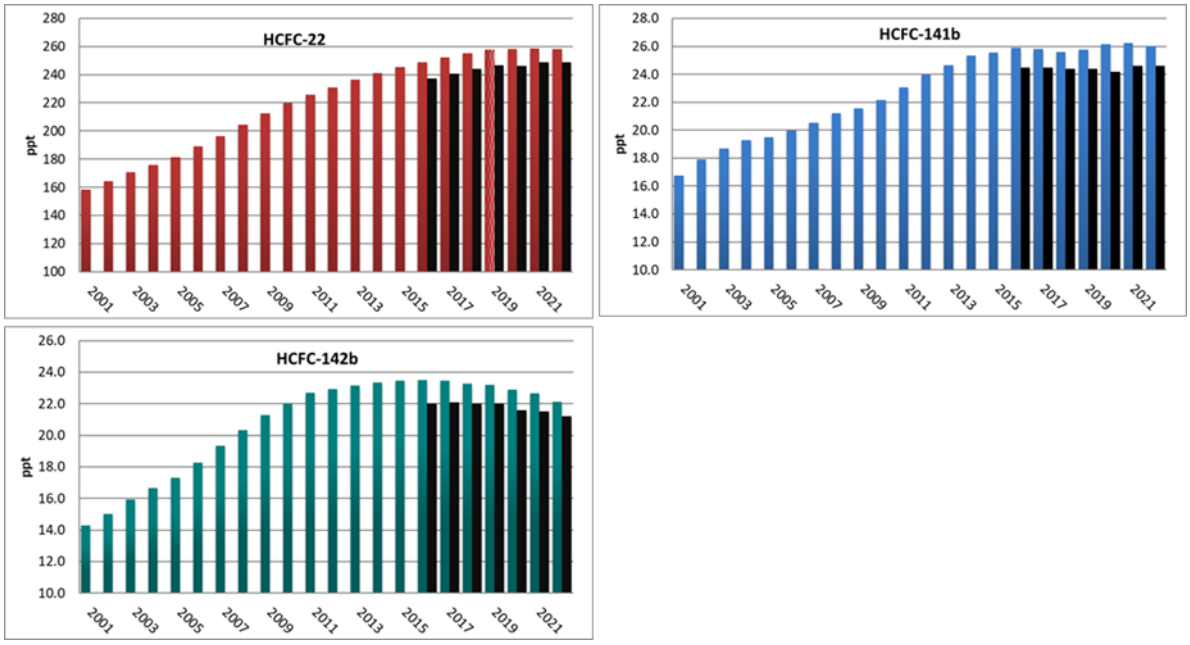

Figure 23: Development of the annual means of observed HCFCs at the Zeppelin Observatory for 2001 to 2022. HCFC-22 (red), HCFC-141b (blue), and HCFC-142b (green). The global annual means in 2016 to 2022 are included as black bars. All units are in ppt.

2.1.11 Hydrofluorocarbons (HFCs) at Zeppelin Observatory

Key findings for hydrofluorocarbons (HFCs): HFCs are 2nd generation CFC replacements, with much lower than ozone depleting potential than both CFCs and HCFCs. They are, however, strong greenhouse gases. Almost all are increasing in concentration, albeit from a low level at present, and these compounds should be monitored closely.

HFCs are 2nd generation replacements of CFCs, meaning that they are considered as better alternatives to the CFCs with respect to the ozone layer than HCFCs, as they do not contain chlorine or bromine. However, many of these compounds are strong greenhouse gases. For example, HFC-23 has a GWP of 12400 (Table 3). The phase-out of HFCs under the Montreal Protocol was under negotiation for many years and the successful agreement in Kigali, October 2016, was an important step. Presently, the contribution to global warming posed by HFCs is very limited. However, most of the compounds are increasing rapidly. The compounds are strong infrared absorbers with high GWP hence it is crucial to reduce future emissions.

For the period 2001 to 2022, three compounds have been measured at the Zeppelin Observatory: HFC-125, HFC-134a, and HFC-152a. HFC-125 is mainly used as a refrigerant and fire suppression agent. HFC-134a is used as a temperature control for domestic refrigeration and automobile air conditioners, whereas HFC-152a is used as a refrigerant and propellant for aerosol sprays and in gas duster products. Since 1990, when HFC-134a was almost undetectable in the atmosphere, the concentration of this gas has risen massively, and HFC-134a is currently the HFC with highest atmospheric concentration.

In 2015 five new HFCs were included in the Norwegian monitoring programme: HFC-23, HFC-365mfc, HFC-227ea, HFC-236fa, and HFC-245fa. In 2016, three additional HFCs were introduced to the programme: HFC-32, HFC-143a, and HFC-4310mee. All these species have been measured at Zeppelin since 2010, but they have not been analysed or reported to an international data base until 2016. The development of HFC-23 should be followed carefully since this gas has a relatively high concentration and an extremely high GWP. HFC-23 is a by-product of the production of HCFC-22 and is also used in the semiconductor industry. In addition, it is a useful refrigerant and fire suppressant.

Generally, the new HFCs are used for refrigeration and air conditioning, foam blowing, and fire extinguishing. Both HFC-245fa and HFC-365mfc are substitutes for HCFC-141b in foam blowing applications. HFC-236fa is also a foaming agent, in addition to a fire suppression agent and a refrigerant. HFC-227ea is mainly used to suppress fire in data equipment and telecommunication facilities, and in protection of flammable liquids and gases. HFC-227ea is also used as an aerosol propellant in pharmaceutical dose inhalers for e.g., asthma medication.

The three new HFCs introduced to the monitoring programme in 2016, are mainly used for refrigeration (HFC-32 and HFC-143a). In addition, HFC-143a is applied as propellant in canned air products for cleaning electronic equipment. HFC-4310mee is mainly used as a cleaning solvent in the electronics industry.

The seasonal cycles in HFC mixing ratios are closely linked to the lifetimes and variations in the incoming solar radiation. HFC-152a has the shortest lifetime (1.6 year), and as seen in Figure 24, HFC-152a has the most distinct seasonal cycle. The gas is mainly destroyed in the lowest part of the atmosphere by photolysis and reactions with OH.

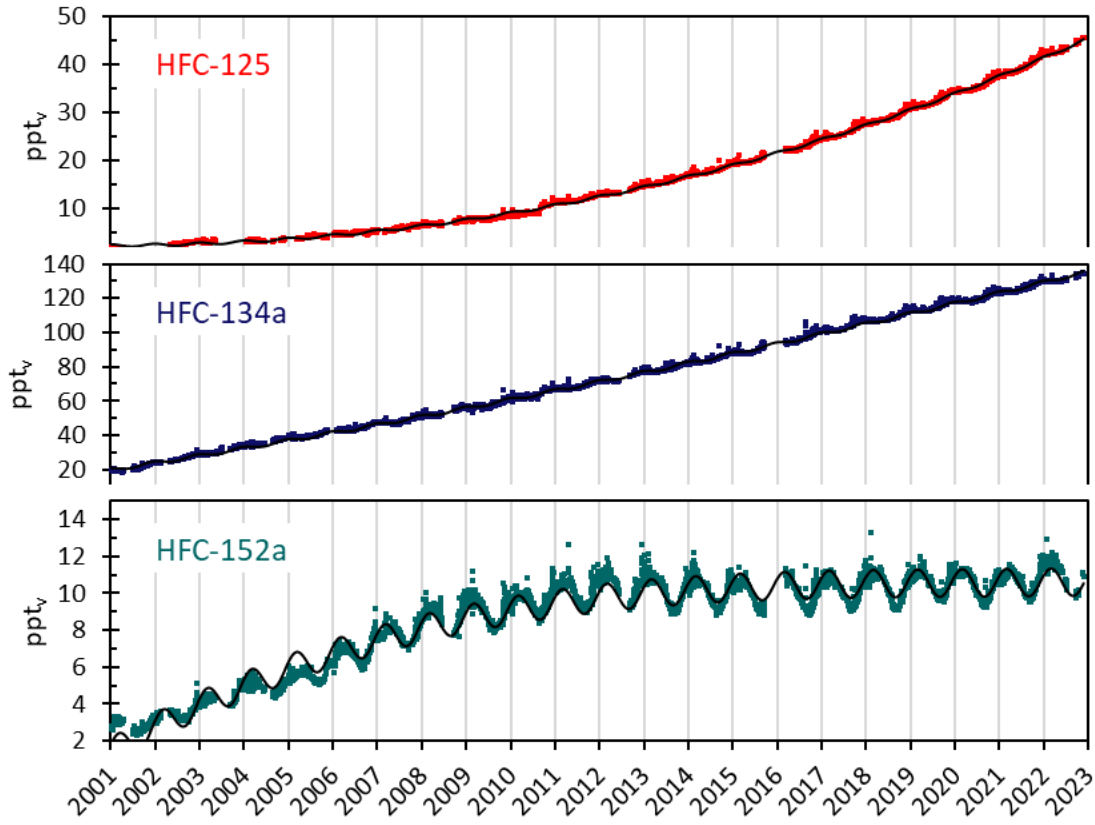

Figure 24: Daily averaged concentrations of the monitored HFCs for the period 2001 to 2022 at the Zeppelin observatory: HFC-125 (red), HFC-134a (dark blue), and HFC-152a (green). The black solid lines are the empirical, fitted, mixing ratios, with fit coefficients yielding the trend. This trend calculation is described in Appendix II.

HFCs shown in Figure 24 have increased significantly since 2001. HFC-152a has a shorter lifetime than the other HCFCs and hence the response to emissions changes is faster. This is clearly illustrated in Figure 25 and Figure 26 where there are apparent changes in the growth rate.

The eight new HFCs included in the programme in 2015 and 2016 are shown in Figure 25, which clearly demonstrates that the concentrations of all HFCs have increased steadily since 2010. The compounds generally increase by 4-10%/yr, except from HFC-32 which has an average increase of 17%/yr.

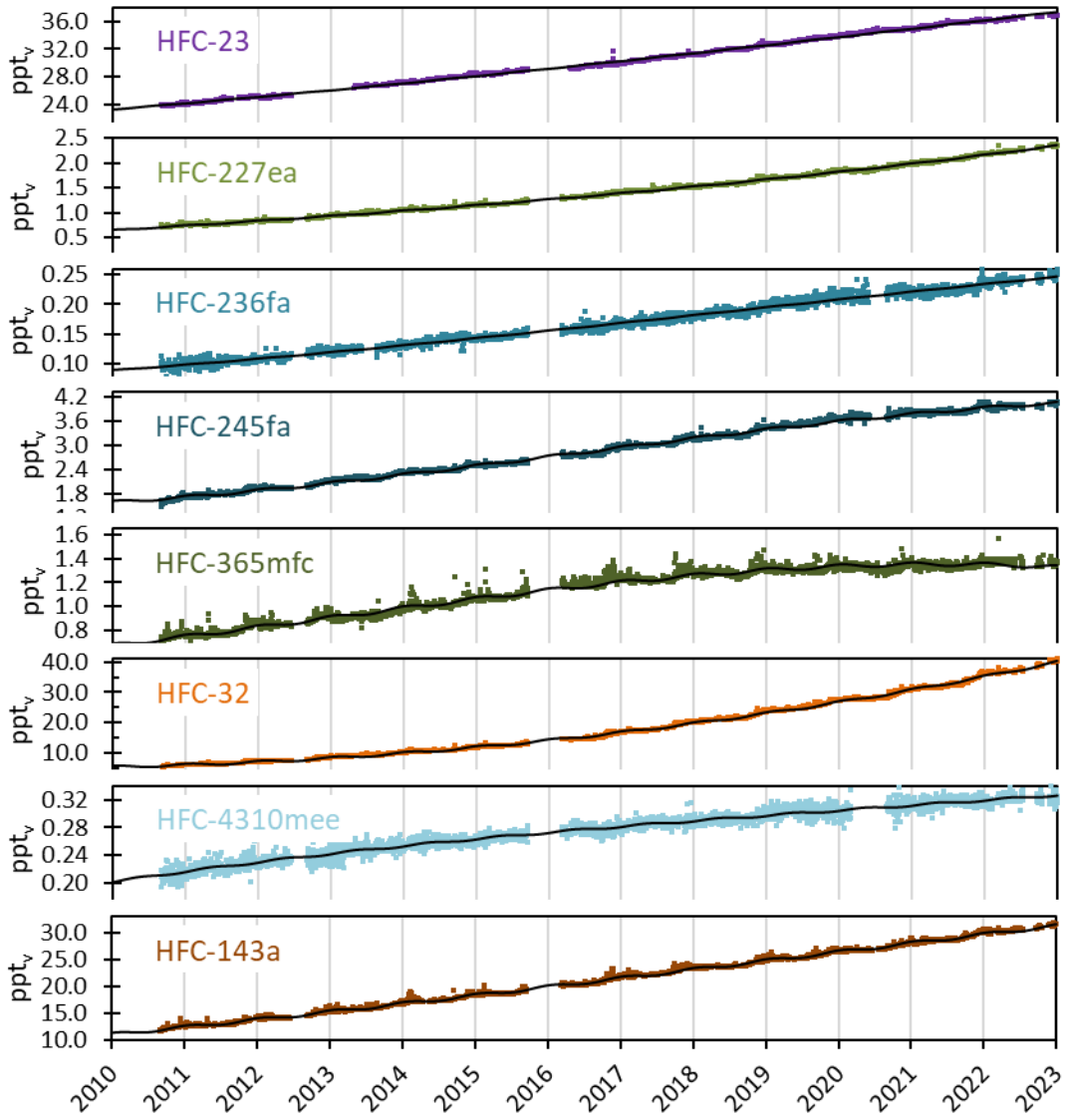

Figure 25: Daily averaged concentrations of monitored HFCs at the Zeppelin observatory for the period 2010 to 2022: HFC-23 (violet), HFC-227ea (light green), HFC-236fa (blue), HFC-245fa (dark blue), HFC-365mfc (dark green), HFC-32 (orange), HFC-4310mee (light blue), and HFC-143a (brown). The black solid lines are the empirical, fitted, mixing ratios, with fit coefficients yielding the trend. This trend calculation is described in Appendix II.

The development of annual means of all reported HFCs are shown in Figure 26. The global annual means of 2016 to 2022 as given in Hall et al. (2017; 2020), Dlugokencky et al. (2018; 2019), and Lan et al. (2021; 2022) are included as black bars for comparison. As for HCFCs the concentrations at Zeppelin are higher than the global means. Also, the increasing tendency for most HFCs is clear, even if the concentrations are still very low, particularly for the new HFC-365mfc, HFC-245fa, HFC-236fa, HFC-227ea, and HFC-4310mee.

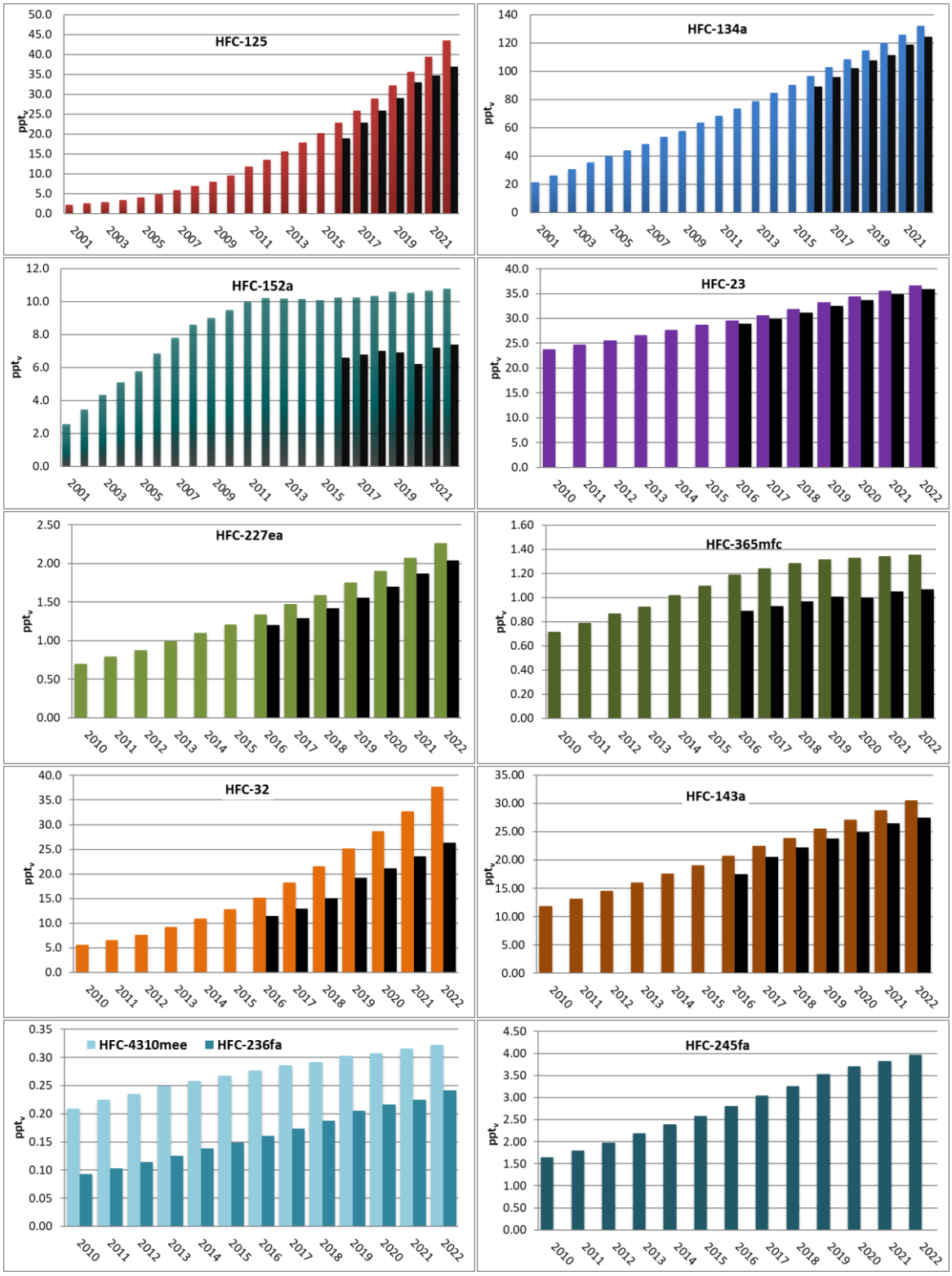

Figure 26: Development of the annual means of observed HFCs at the Zeppelin Observatory. For the period 2001 to 2022: HFC-125 (red), HFC-134a (blue), and HFC-152a (dark green). For the period 2010 to 2022: HFC-23 (violet), HFC-227ea (light green), HFC-365mfc (dark green), HFC-32 (orange), HFC-143 (brown), and light to dark blue: HFC-4310mee, HFC-236fa, and HFC-245fa. The global annual means in 2016 to 2022 included as black bars, when available.

2.1.12 Halons measured at the Zeppelin Observatory

Key findings for halons: Halons are bromine-containing greenhouse gases which are more ozone depleting than CFCs, though they are less likely to reach the stratosphere (location of the ozone layer). We measure three of these compounds at Zeppelin: H-1301 (levels of which are stable due to its long, 72-year lifetime), and H-1211 and H-2404 (levels of which are declining).

Halons are greenhouse gases containing bromine. Regulations for halons are also important to protect the ozone layer: If bromine reaches the stratosphere (high atmosphere), it is even more effective in destroying ozone than chlorine from CFCs. The halons are regulated through the Montreal Protocol and the concentration of most of these substances are decreasing. The main source of halons has been fire extinguishers. From 2001 to 2015 two halons were measured and analysed at the Zeppelin observatory: H-1301 and H-1211. In 2016 H-2402 was also included in the monitoring programme, where data were analysed back to 2010. H-2402 was used primarily in the former USSR and was the main halon fire suppressant in that region.

The ambient concentrations of the three halons are fairly low,- below 4 ppt. Figure 27 shows the daily average concentrations of the monitored halons at Zeppelin. The halon trend analyses, listed in Table 3 are visualized in Figure 27. The annual mean of H-1301 is stable, while H-1211 and H-2404 are delclining. This is explained by the shorter lifetime of the latter two compounds (16 years for H-1211, 28 years for H-2402) compared to H-1301 (72 years). A comparison to the global average of H-1211 and H-2402 is shown in Figure 28.

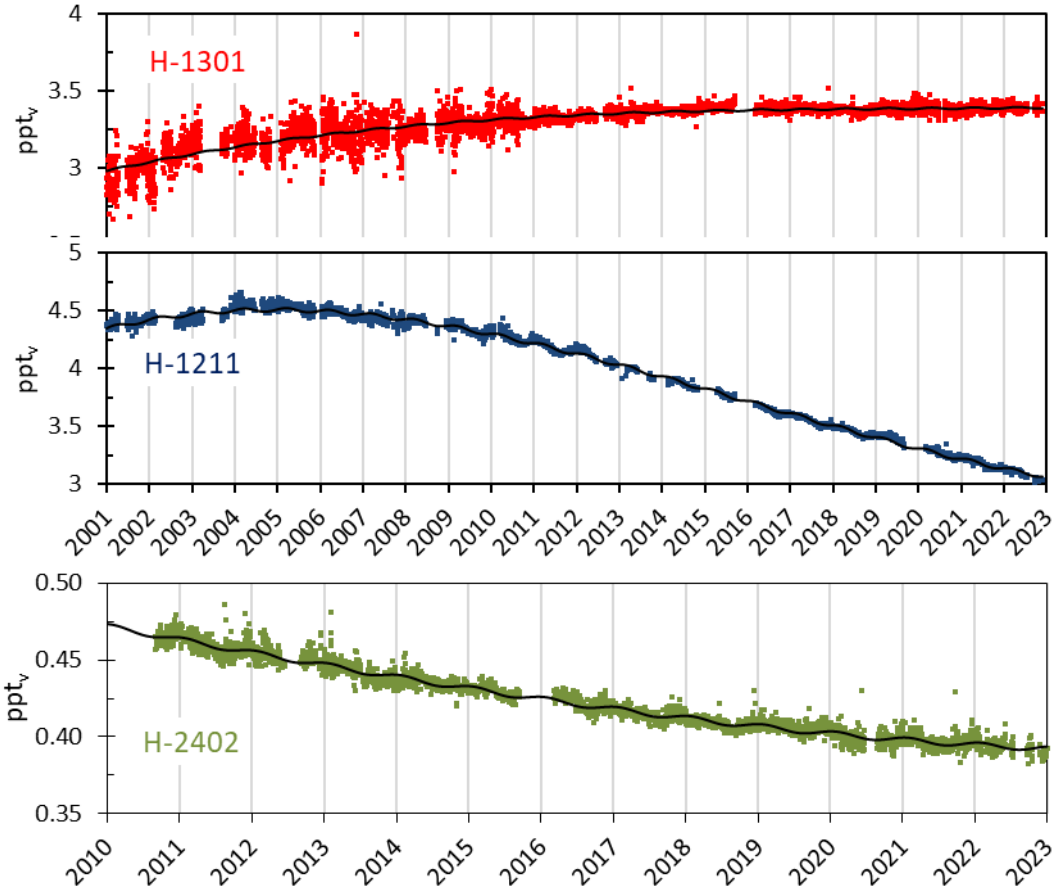

Figure 27: Daily averaged concentrations of the monitored halons at the Zeppelin Observatory. For the period 2001 to 2022: H-1301 (red) and H-1211 (blue). For the period 2010 to 2022: H-2402 (green). The black solid lines are the empirical, fitted, mixing ratios, with fit coefficients yielding the trend. This trend calculation is described in Appendix II.

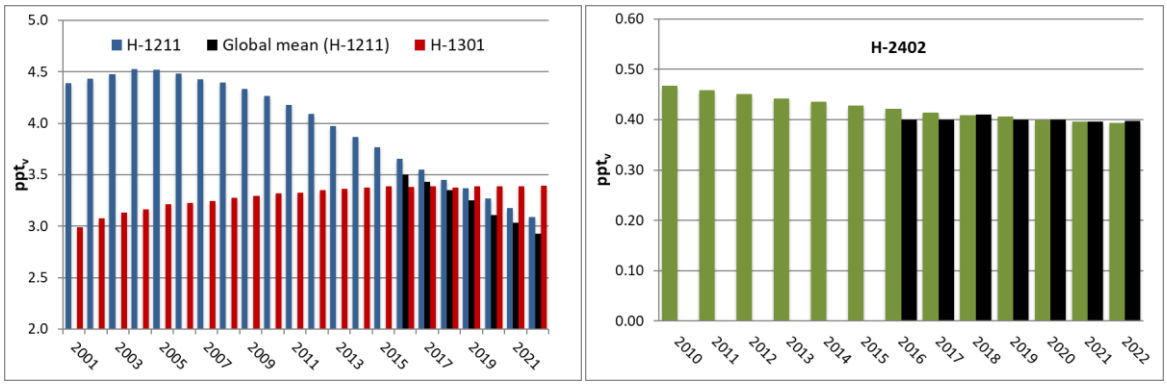

Figure 28: Development of the annual means of the observed halons at the Zeppelin Observatory. Red: H-1301, blue: H-1211, and green: H-2402. The global annual means in 2016 to 2022 are included as black bars. All units are in ppt.

2.1.13 Other chlorinated hydrocarbons at the Zeppelin Observatory

Key findings for other chlorinated hydrocarbons: Other chlorinated hydrocarbons at the Zeppelin Observatory: Trichloroethane (or methyl chloroform, CH_3CCl_3), dichloromethane (CH_2Cl_2), trichloromethane (or chloroform, $CHCl_3$), trichloroethene (TCE, $CHClCCl_2$), carbon tetrachloride (CCL_4) and tetrachloroethene (PCE, CCl_2CCl_2). Levels of trichloroethane, PCE, TCE and carbon tetrachloride are all stable or in decline. Dichloromethane and trichloroethane levels have increased or fluctuated in recent years. The reason is unclear since both are from a mix of natural and anthropogenic sources. It is important to follow developments in all of these compounds since they are ozone depleting if they are able to reach the stratosphere despite their short lifetimes.

We measure the following additional chlorinated hydrocarbons at the Zeppelin Observatory: Trichloroethane (or methyl chloroform, CH_3CCl_3), dichloromethane (CH_2Cl_2), trichloromethane (or chloroform, $CHCl_3$), trichloroethene (TCE, $CHClCCl_2$), carbon tetrachloride (CCL_4), and tetrachloroethene (PCE, CCl_2CCl_2). The daily average concentrations and annual means are shown in Figure 29 and Figure 30. The main anthropogenic sources of all these substances are solvents, while some, such as trichloromethane have significant natural sources including vegetation and the oceans.

Trichloroethane (CH_3CCl_3), which is controlled under the Montreal Protocol, has been declining steadily since the peak the early 1990s. Dichloromethane has a lifetime of less than 6 months and responds rapidly to emissions changes. Levels are increasing. Natural dichloromethane sources, which account for ~10% of the total, are mainly from biomass burning and the oceans. Trichloromethane (light blue) has a lifetime of ~6 months, thus the response to emission changes is also relatively rapid. The reason for many of the rapid changes observed is not yet clear, but they are likely explained by variations in natural emissions, since these dominate the atmospheric trichloromethane burden (Laturnus et al., 2002).

Even if trichloromethane and dichloromethane have relatively short lifetimes, modelling studies imply that chlorine from these compounds can reach the lower stratosphere and potentially destroy stratospheric ozone (Hossaini et al., 2017). Thus, sustained growth in these compounds might offset some of the gains achieved by the Montreal Protocol, further delaying recovery of Earth's ozone layer.

The atmospheric concentrations of trichloroethene (TCE; green) and tetrachloroethene (PCE; grey) are low, and the measured annual variabilities are quite high, especially before 2011 due to instrumental limitations (see Appendix II). This makes it difficult to draw conclusions about trends and development of these species.

The concentration of carbon tetrachloride (CCl_4) has been measured at Zeppelin since 2010. This compound was once a popular solvent in organic chemistry, but because of its adverse health effects it is rarely used any more. Today CCl_4 is sometimes applied as a solvent for infrared spectroscopy.

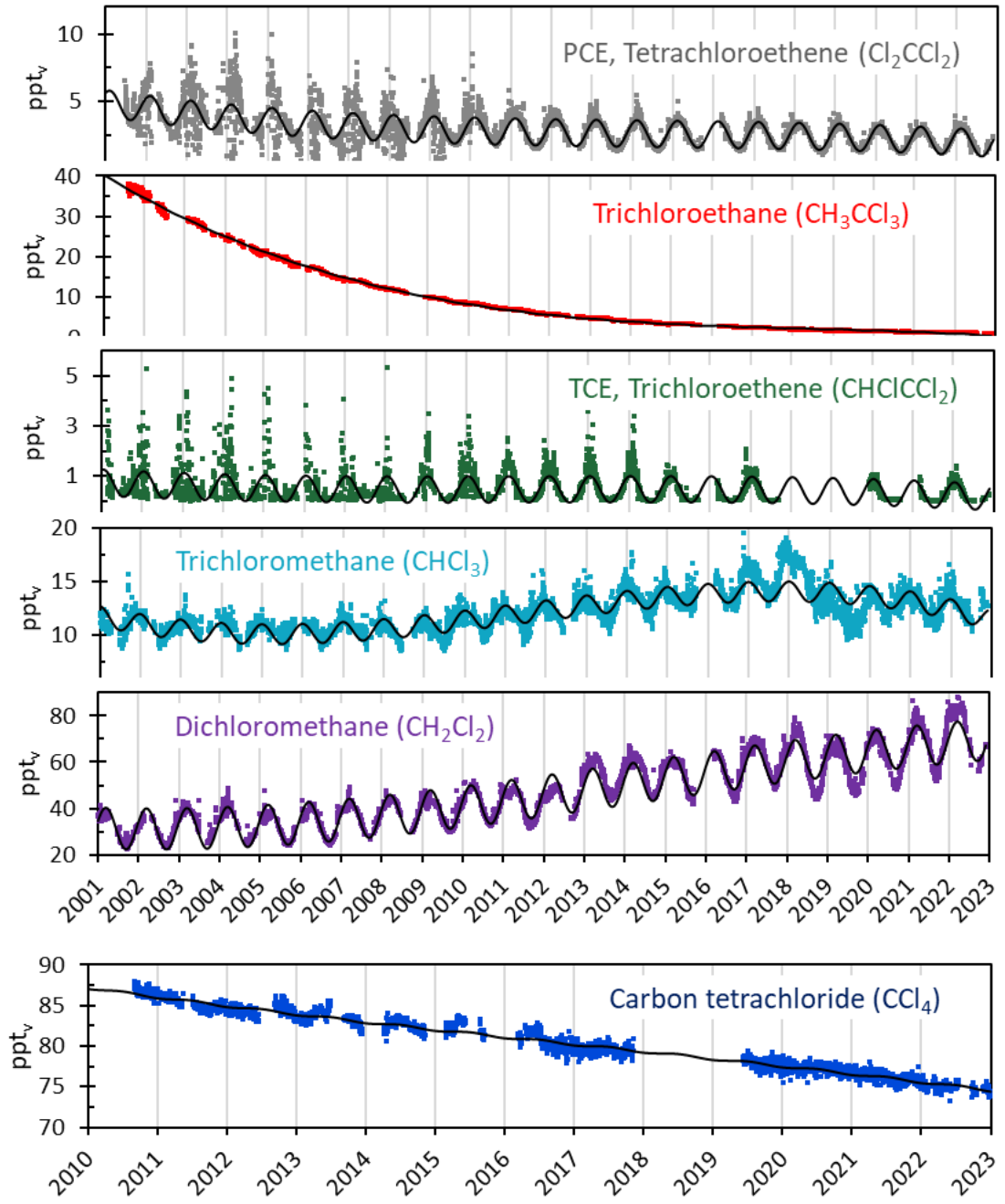

Figure 29: Daily averaged concentrations of chlorinated hydrocarbons at the Zeppelin observatory: For the period 2001 to 2022: Tetrachloroethene (grey), trichloroethane (red), trichloroethene (green), trichloromethane (light blue), and dichloromethane (violet). For the period 2010 to 2022: carbon tetrachloride (dark blue). The black solid lines are the empirical, fitted, mixing ratios, with fit coefficients yielding the trend. This trend calculation is described in Appendix II.

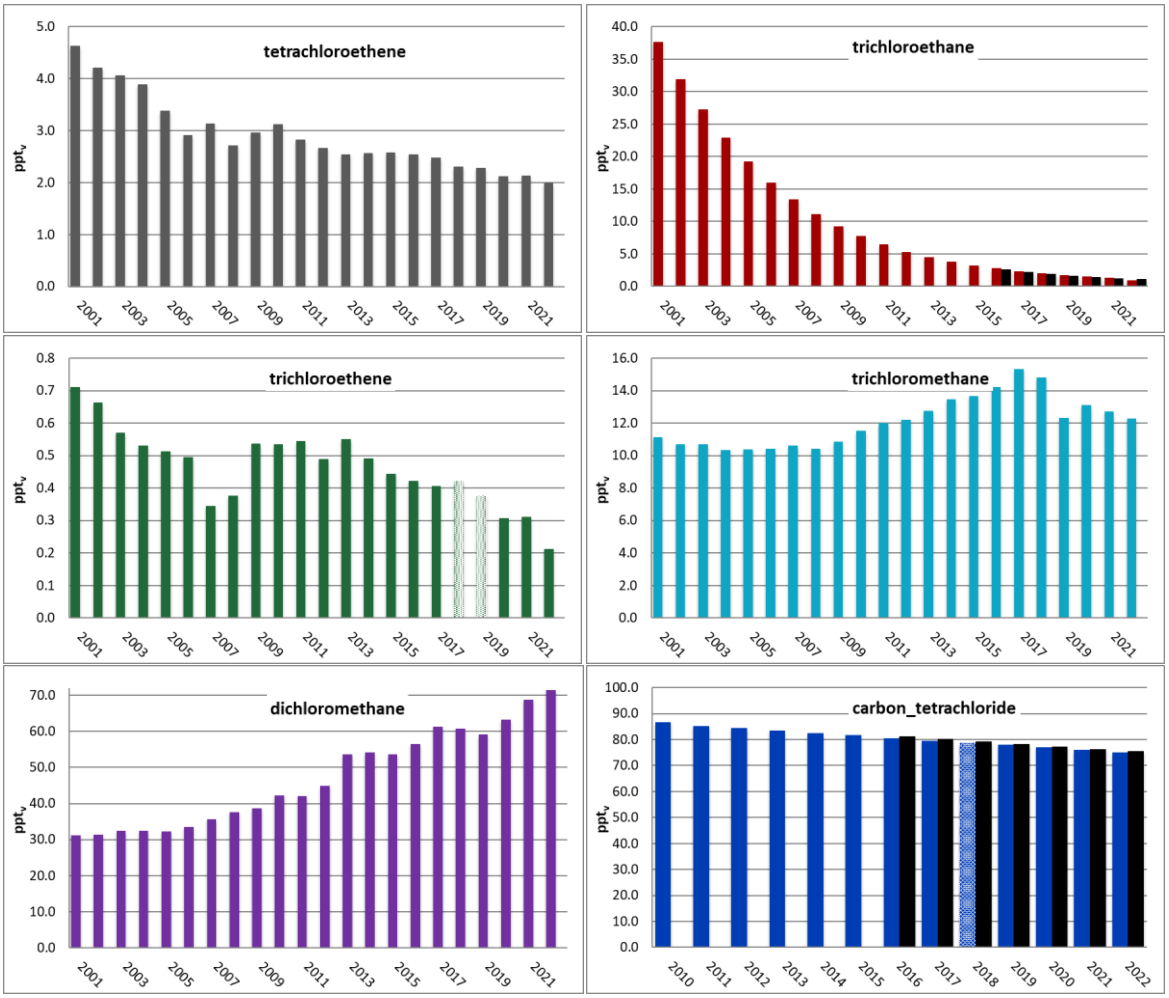

Figure 30: Annual means of the chlorinated hydrocarbons. Upper panel: tetrachloroethane (grey) and trichloroethane (red). Mid panel: trichloroethene (TCE, green) and trichloromethane (light blue). Lower panel: dichloromethane (violet) and carbon tetrachloride (CCl_4, dark blue). The global annual means for CH_3CCl_3 and CCl_4 in 2016 to 2022 are included as black bars, when available. All units are in ppt.

2.1.14 Perfluorinated compounds at Zeppelin Observatory

Key findings for perfluorinated compounds: As a group, the perfluorinated compounds are some of the most extreme greenhouse gases. E.g., sulfurhexafluoride, SF_6, has a global warming potential of 25200. While all are currently at very low levels, the high warming potentials of these compounds means they must be followed closely. All are increasing in concentration.

Perfluorinated compounds, including SF_6, NF_3, and SO_2F_2 (Figure 31, Figure 32), are extremely potent and long-lived (up to 50000 years) greenhouse gases. For example, SF_6, emitted mainly from magnesium production and the electrical industry, has been monitored since 2001, and has a warming potential 25200 times greater than CO_2. SO_2F_2, used as a pesticide fumigant, has a lifetime of 36 years and a GWP of 4630, while NF_3, employed in electronics manufacturing, has a 569-year lifetime and a GWP of 17400. These compounds raise concerns due to their extended atmospheric persistence and strong infrared absorption, impacting climate change. Monitoring improvements in 2015 and 2016 enabled the inclusion of NF_3 data from 2016 onwards. The concentrations at Zeppelin are slightly higher than the global means.

We also monitor PFCs - 14, -116, -218, and -318, at Zeppelin. PFC-14, used in refrigeration and electronics, has a 50000-year atmospheric lifetime and a GWP of 7380. PFC-116, found in semiconductor manufacturing, has a 10000-year lifetime and a GWP of 12400. PFC-218, used in

electronics and medicine, has a 2600-year lifetime and a GWP of 9290. PFC-318, a by-product of fluorochemical production, has a 3200-year lifetime and a GWP of 10200. Daily means are shown in Figure 33 and the yearly averages at Zeppelin alongside global means in Figure 34.

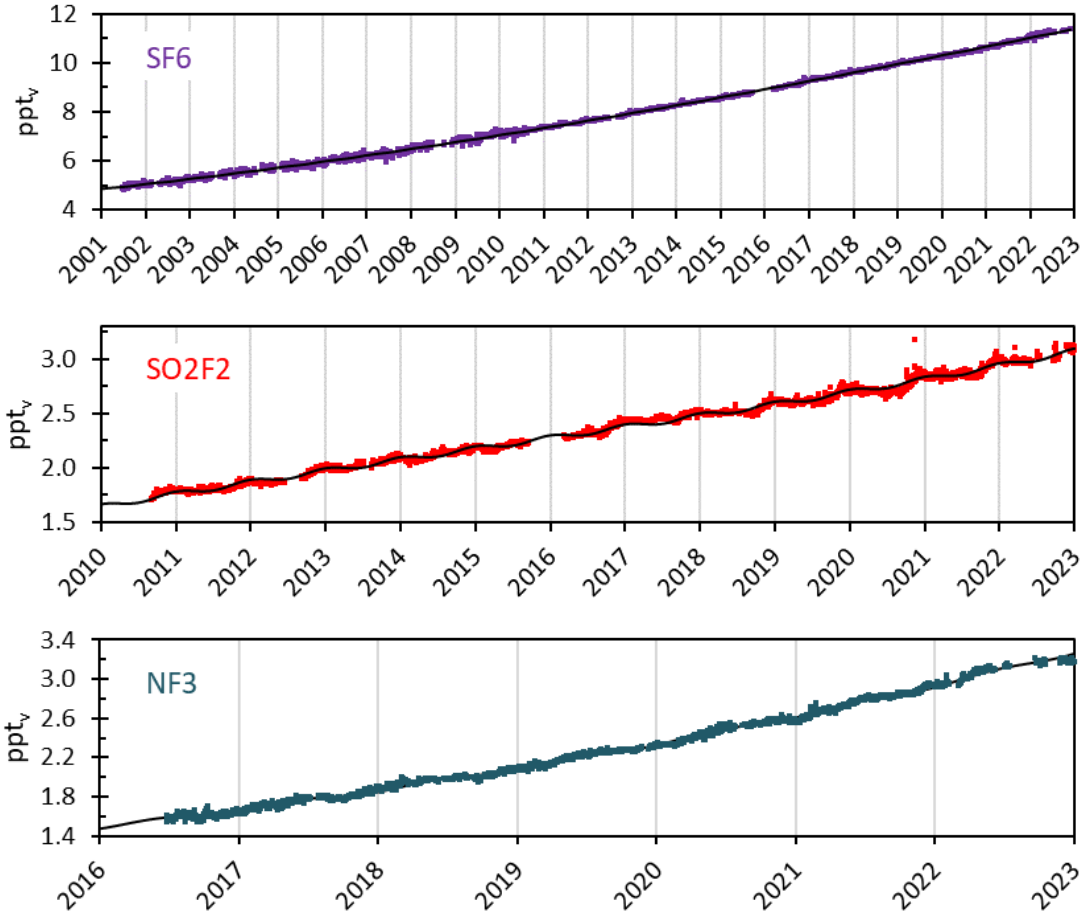

Figure 31: Daily averaged concentrations at the Zeppelin Observatory. Upper panel: SF_6 for the period 2001 to 2022. Middle panel: SO_2F_2 for the period 2010 to 2022. Lower panel: NF_3 from mid-2016 to 2022. The black solid lines are the empirical, fitted, mixing ratios, with fit coefficients yielding the trend. This trend calculation is described in Appendix II.

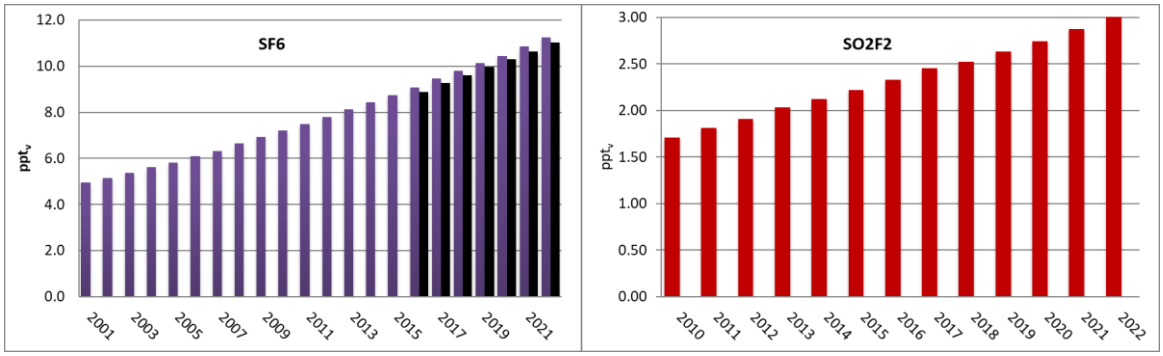

Figure 32: Annual means of SF_6 for the period 2001 to 2022 (left) and SO_2F_2 for the period 2010 to 2022 (right) at the Zeppelin observatory. The global annual means for SF_6 in 2016 to 2022 are included as black bars.

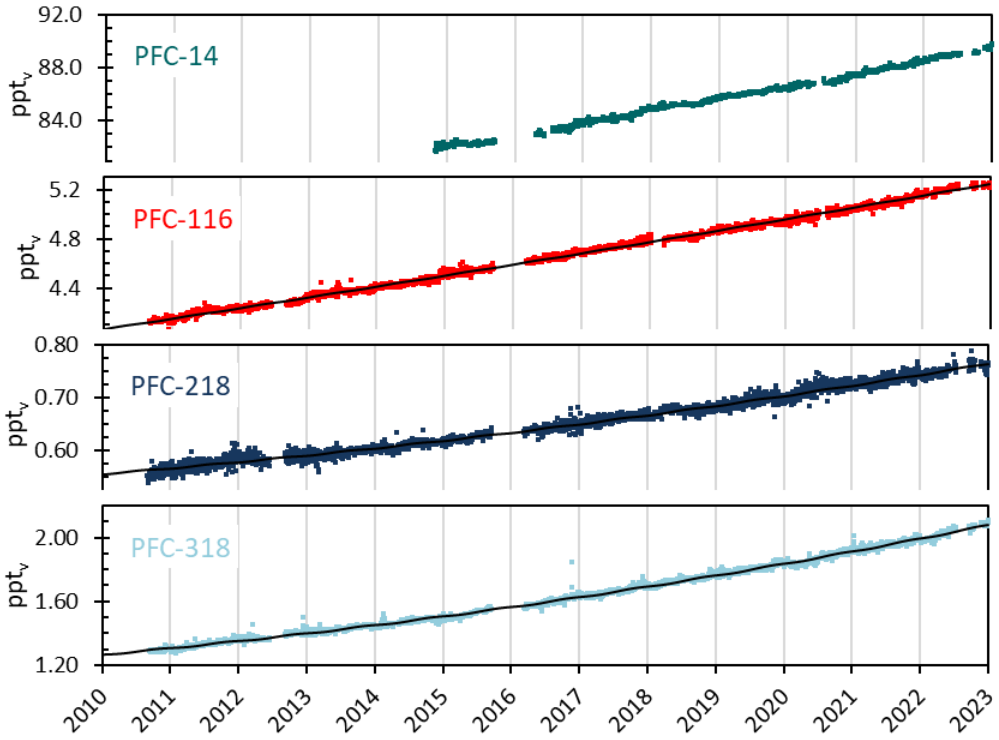

Figure 33: Daily averaged concentrations of perfluorocarbons at the Zeppelin observatory for the period 2010 to 2022: PFC-14 (green), PFC-116 (red), PFC-218 (dark blue), and PFC-318 (light blue). PFC-14 is only ranging back to autumn 2014. The black solid lines are the empirical, fitted, mixing ratios, with fit coefficients yielding the trend. This trend calculation is described in Appendix II.

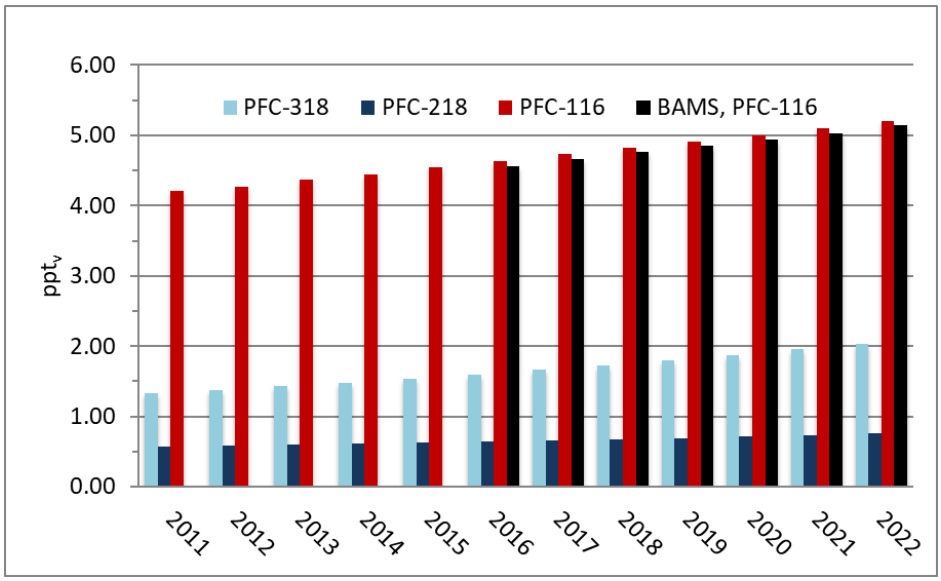

Figure 34: Annual mean concentrations of perfluorocarbons for the period 2010 to 2022 at the Zeppelin observatory: PFC-116 (red), PFC-218 (dark blue), and PFC-318 (light blue). The global annual means for PFC-116 in 2016 to 2022 are included as black bars.

2.2 Aerosol properties

The atmospheric aerosol is made of very small particles in the air. These particles affect the climate in two ways: directly, they can alter how sunlight travels through the atmosphere, either warming or cooling it (Figure 2). Indirectly, they influence clouds, which reflect sunlight and contribute to cooling.

Table 5 summarizes the aerosol optical and physical properties which are part of the monitoring program. We use 'aerosol optical depth (AOD)' measurements to evaluate the total direct impact on the atmosphere—combining absorption and scattering of light (= total extinction). This impact, whether warming or cooling, depends on how much light is absorbed or scattered. The balance between scattering and absorption is assessed using a parameter called 'single scattering albedo (SSA).' Purely scattering particles have an SSA of 1, while purely absorbing particles have an SSA of 0. Black carbon, which absorbs almost all visible light, has an SSA close to 0.

Figure 2 illustrates that uncertainties in understanding aerosol effects on climate since pre-industrial times are larger than estimated effects. This is due to challenges in modeling particle processes and uncertainties in emissions. By measuring direct effects at different wavelengths and providing a 'fingerprint', the so-called 'Ånsgstrøm exponent', of scattering and absorption, we can evaluate the particle sources and reduce uncertainties.

Lastly, we count the number of aerosol particles of different sizes (particle diameters) to calculate a particle number size distribution (PNSD). PNSD is a fundamental property of the aerosol. A higher total particle number (sum of particles at all sizes) means that all aerosol effects are larger. The shape of the PNSD influences cloud formation, aerosol scattering, and can also be used to interpret aerosol sources.

Table 5: Aerosol observations at Zeppelin, Birkenes and Troll Observatory. "X" mark funded by the Norwegian Environment Agency and Ministry of Climate and Environment. The rest, marked "O", is funded by NILU and other institutes. See also Appendix II for detailed methodology.

Parameter	Relevance	Zeppelin	Birkenes	Trollhaugen
Particle Number Size Distribution (PNSD)	**fundamental to all aerosol processes**	X	X	X
Number Size Distribution of Refractory Particles	**proxy for black carbon (BC) PNSD**	**X**	---	---
Aerosol Scattering Coefficient	**direct climate effect**	O	**X**	**X**
Aerosol Absorption Coefficient	**direct climate effect**	O, **X**	**X**	**X**
Aerosol Optical Depth	**direct climate effect**	**X**	**X**	**O**

2.2.1 Aerosol properties at Birkenes

Birkenes is a relatively clean site and aerosol number concentrations are typically low (Figure 36). Nevertheless, the relative proximity to settlements in Norway, even more polluted regions in Europe, and local vegetation means that emissions fall into one of four categories: 1) clean Arctic background aerosol; 2) Central and Eastern European aerosol; 3) biogenic aerosol, i.e., vegetation emitted precursor gases condensing to the particle phase by photooxidation; 4) wood combustion aerosol from domestic heating. Clean Arctic background is characterised by low absorption and particle number. Long-range transport of pollution from Central and Eastern Europe is characterised by the highest particle number. Biogenic aerosol is distinguished by the seasonal cycle of the Aitken mode particles Figure 35) which are due to secondary organic aerosol (SOA) formation from various gases emitted by plants and trees reacting with sunlight and the atmosphere. Residential heating is distinguishable by the seasonal cycle in total absorption (which peaks during the heating season) and the absorption Ångstrøm exponent (Figure 36) which is also generally higher in winter due the presence of light

absorbing compounds in wood smoke. The AOD total extinction measurements follow closely the Aitken and accumulation mode particles, peaking in Summer (Figure 37, Figure 38), i.e. the direct aerosol effect (Figure 2) peaks in Summer. Monthly mean AOD and Ångström coefficient, and number of observations, for all years are given in Appendix I.

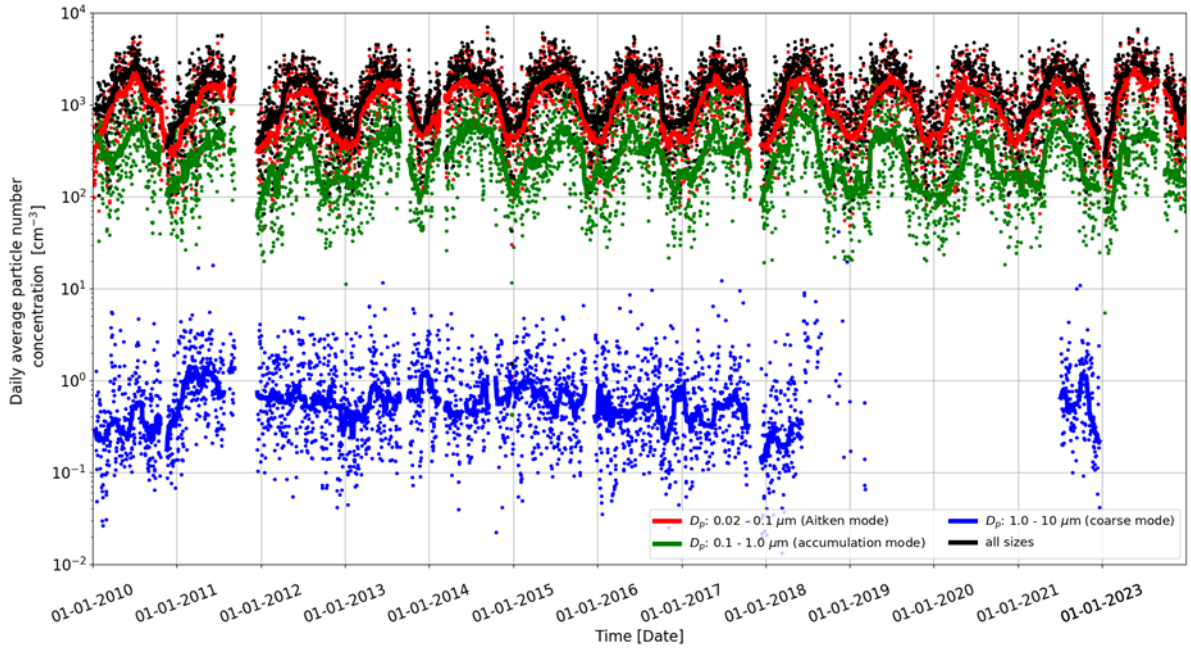

Figure 35: Birkenes 2010 to 2022 time series of binned particle number concentration integrated over selected size ranges. The dotted graphs represent daily averages of the respective size range, the lines the 55-day running median.

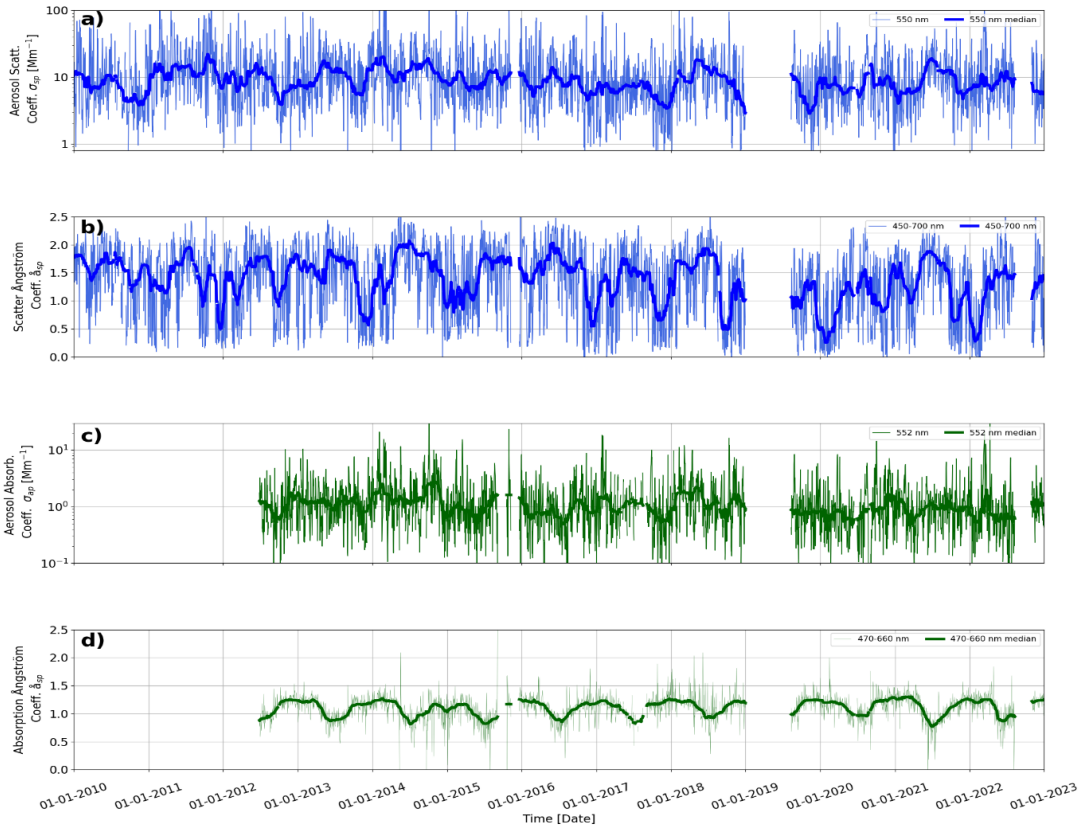

Figure 36: Optical properties measured at Birkenes from 2010 to 2022. a) daily means of aerosol scattering coefficient ($\sigma_{sp,\,at}$ 550 nm) from the integrating nephelometer; b) the scattering Ångstrøm coefficient; c) the aerosol absorption coefficient at 522 nm; d) Absorption Ångstrøm exponents. All plots include running 55-day medians to visualize seasonal variations. The data gap in 2019 is caused by a failure of the integrating nephelometer, measuring the particle scattering coefficient which also affected the particle absorption measurements since these depend on the nephelometer for bias corrections.

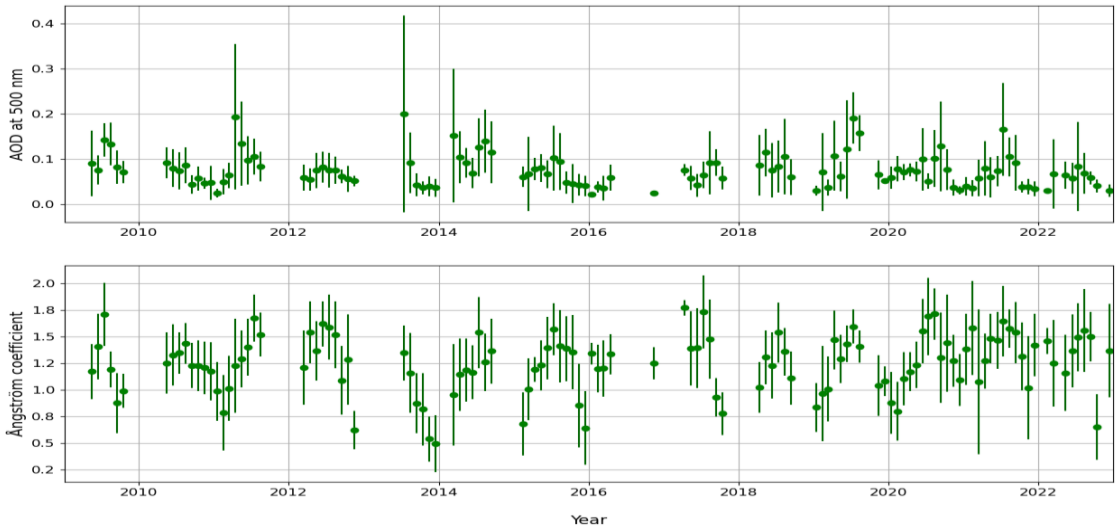

Figure 37: 2009 to 2022 time series of AOD (at 500 nm) in the atmospheric column above Birkenes (upper panel) and (470 nm, 800 nm) Ångström coefficient (lower panel). Monthly mean values and standard deviations are given.

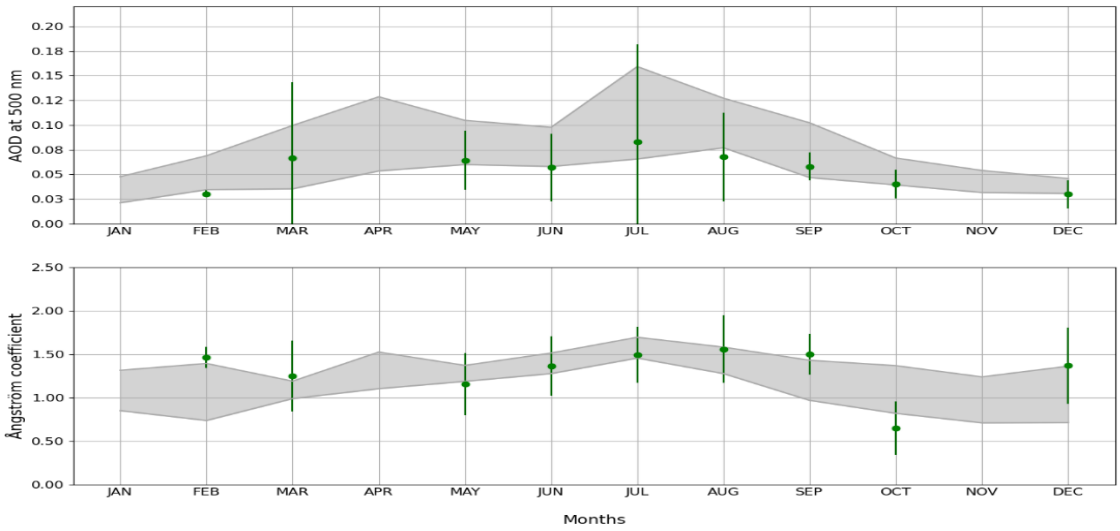

Figure 38: 2022 monthly mean AOD (at 500 nm) in the atmospheric column above Birkenes (upper panel) and (470, 800 nm) Ångström coefficient (lower panel). Mean values and standard deviations are given. Values marked in grey are the mean and standard deviations for the 2009 to 2022.

2.2.2 Aerosol properties at Zeppelin

Aerosol concentrations at Zeppelin are lower than at Birkenes due to its remote location. Meanwhile, a defining feature of the aerosol at Zeppelin is 'Arctic Haze' (AH). From late autumn to early spring air mass exchange between the Arctic and surrounding regions is considerably reduced. AH is then formed via chemical reactions in aerosol particles trapped under the winter Arctic vortex while the particle mass increases from any industrial emissions under the vortex (e.g., Law & Stohl, 2007). The AH onset is marked by an accumulation mode beginning in November (Figure 39) Outside the AH period such behaviour is typical for auto-processed aerosols and would normally only occur for shorter episodes of long range transported aerosols. What follows the onset of AH is then typically a long period with a stable, monomodal PNSD.

The late spring and summer PNSD at Zeppelin are somewhat more variable than in winter due to less stable atmospheric conditions. Particle formation events can be observed, with peak in the PNSD at particle diameters between 0.01 to 0.02 µm. These are triggered by photo-chemical production of chemical species that condense into the particle phase, and don't find enough existing particle surface to condense on, thus forming new particles (the same situation as for Birkenes). The refractory PNSD is almost exclusively mono-modal, with the single mode peaking in the Aitken-size range between 0.02-0.1 µm particle diameter Figure 40. It tends to be highest immediately before and after the AH period, when residential heating emissions may be transported to the region.

The AOD and Ångström exponent time series of monthly means and standard deviation since the start of measurements in 2002 are shown in Figure 41, while the 2022 values against the background of the average data and their standard deviation from the whole 20-year period (including 2022) are shown in Figure 42. Monthly mean values and standard deviations for all years are given in Appendix I.

In Ny-Ålesund, the solar elevation is less than 5° before 4th March and after 10th October, limiting the period with suitable sun-photometer observations to the spring-summer-early autumn period. To fill the long data gap during the Arctic winter, a PFR version making use of the moonlight around full moon (Lunar PFR) has been developed and tested by PMOD/WRC since 2015. In 2018, the Lunar PFR was integrated in the Svalbard Integrated Arctic Earth Observing Network (SIOS), and data are made available also for monitoring purposes. In principle, reliable measurements are possible from rising half-moon to waxing half-moon, but in Ny-Ålesund the period is further limited by the rapidly changing maximum elevation during the lunar cycle.

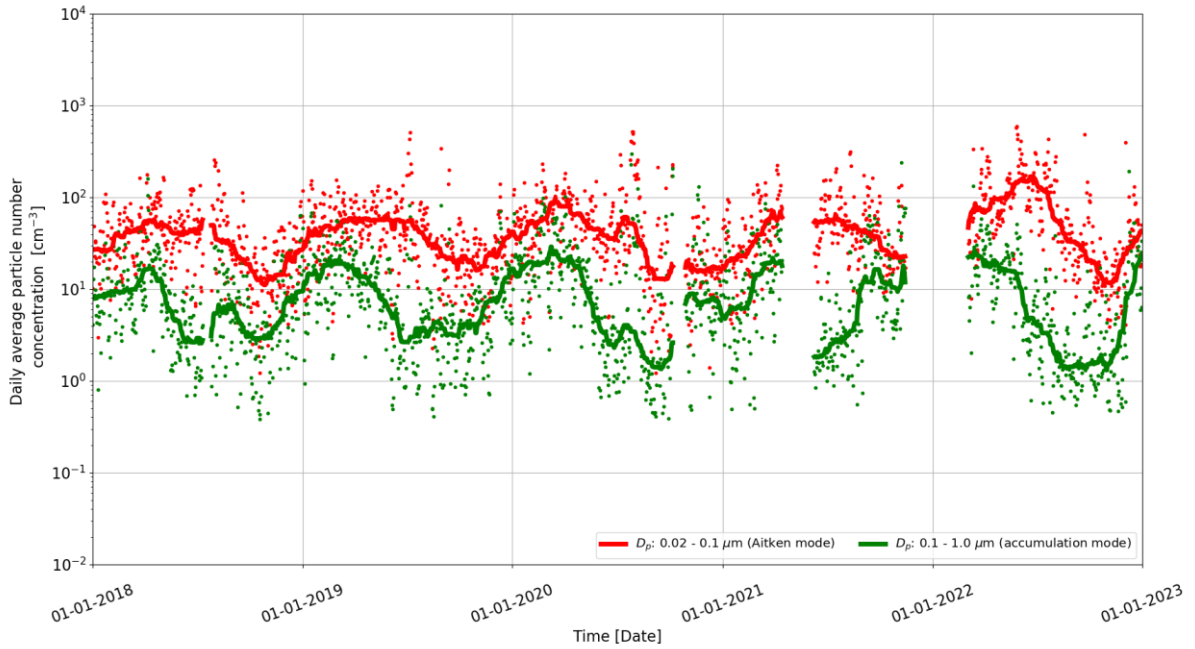

Figure 39: Zeppelin 2018 to 2022 size-binned refractory particle number concentration of the Aitken mode (0.02 µm< D_p < 0.1 µm, red) and accumulation mode (0.1 µm< D_p < 1 µm, green). The solid lines are the 55-day running median.

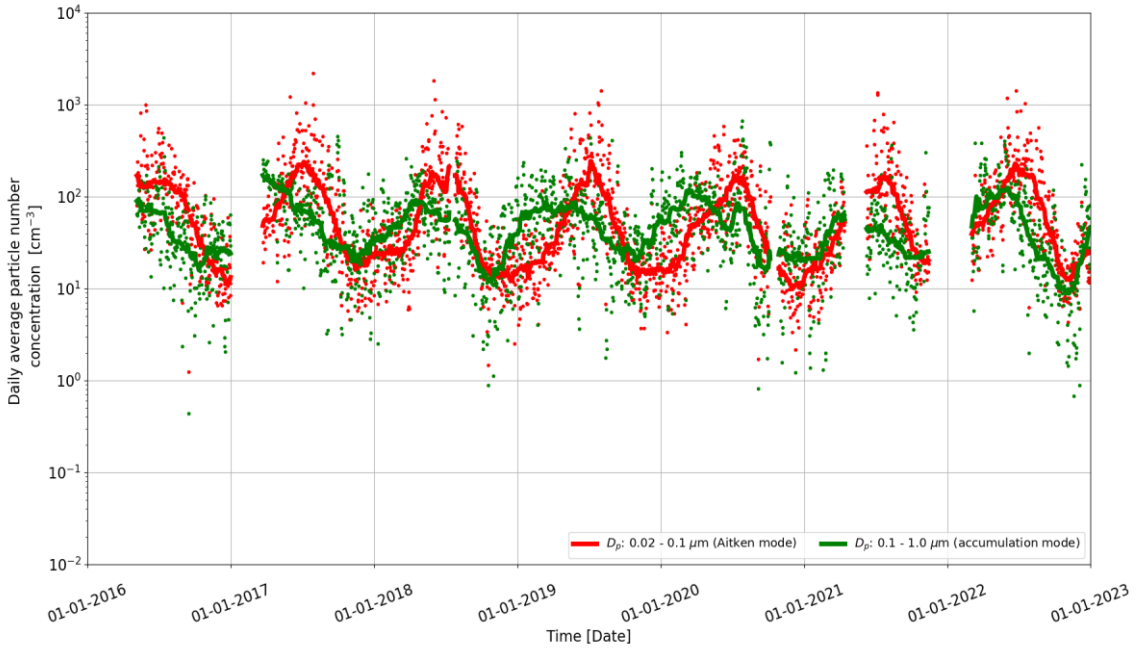

Figure 40: 2014 to 2022 time series of particle number concentration integrated over selected size ranges representing the different physical processes governing the atmospheric aerosol at Zeppelin. The data gap in 2021 was caused by a valve failure of the thermodenuder system, inducing a vacuum in the system and resulting in further damage.

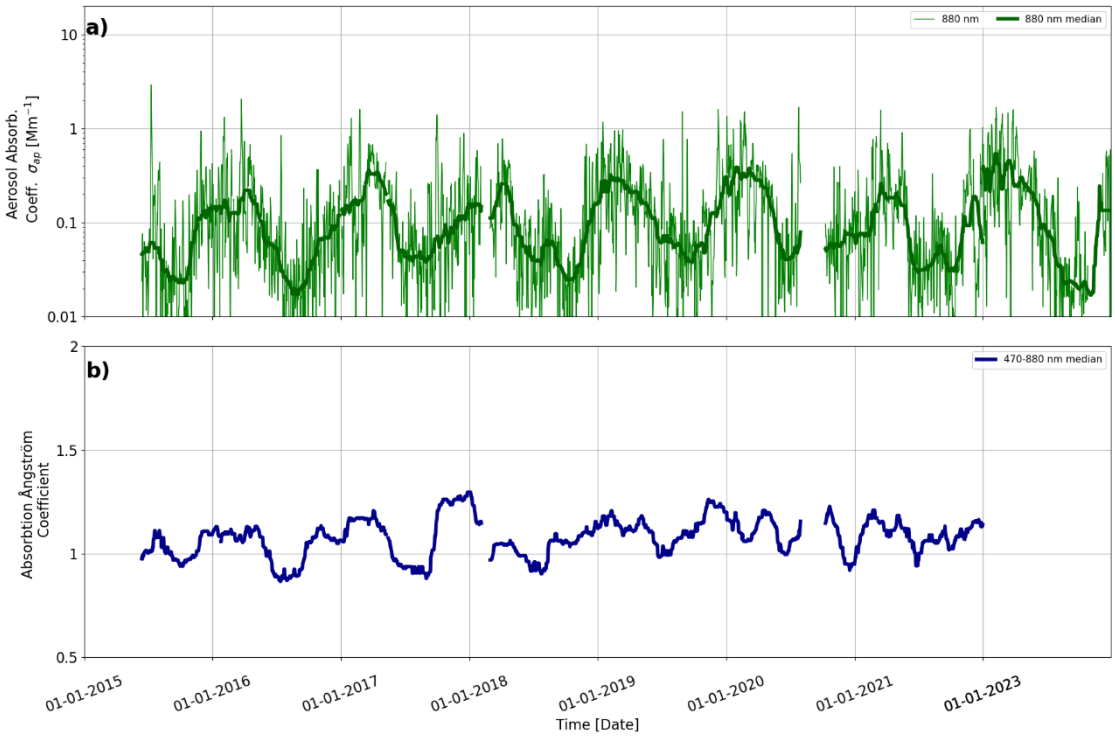

Figure 41: 2015 to 2022 time series graphs of data collected by the filter absorption photometer at Zeppelin Observatory since deployment in June 2015. Top: daily means of absorption coefficient at 880 nm, and 55-day running medians for top, middle and bottom of observed spectral range (heavy lines). Bottom: 55-day running medians of absorption Ångström coefficient, top, bottom, and whole observed spectral range.

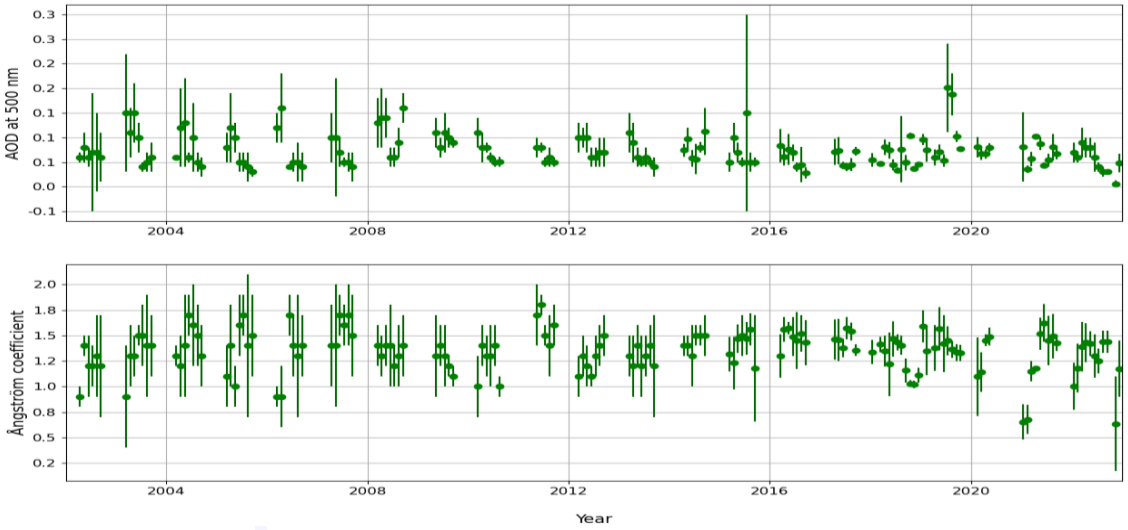

Figure 42: 2002 to 2022 time series of aerosol optical depth (AOD) at 500 nm wavelength in the atmospheric column above Ny-Ålesund (upper panel) and Ångström coefficient (lower panel). Monthly mean values and standard deviations are given.

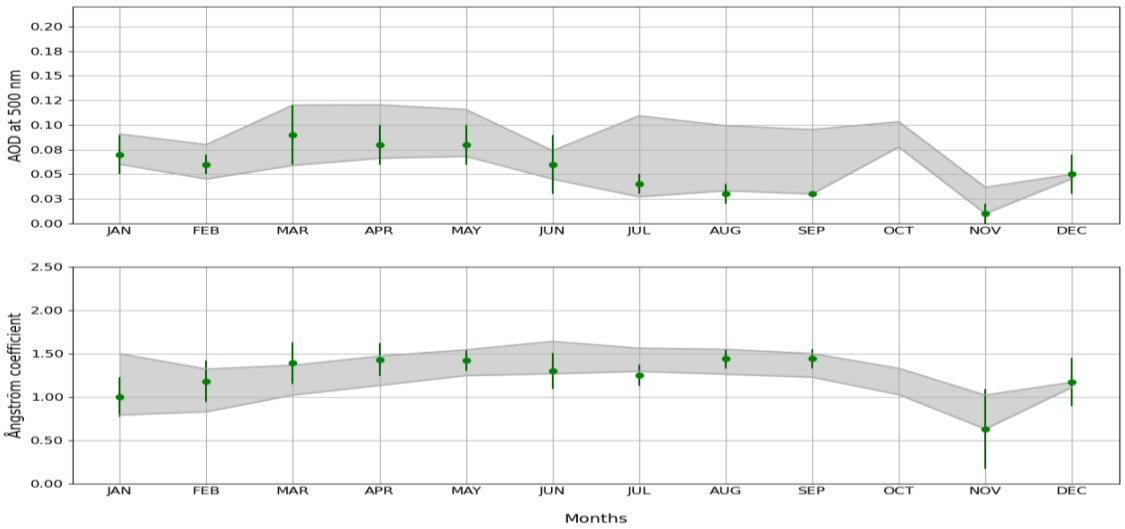

Figure 43: Seasonal variation of the aerosol optical depth (AOD) (upper panel) and Ångström coefficient (lower panel) observed in Ny-Ålesund in 2022. Values marked in grey are the mean and standard deviations for the time period 2002 to 2022; the 2022 monthly mean and standard deviations are shown in green.

2.2.3 Aerosol properties at Trollhaugen

Aerosol at Trollhaugen is distinguished by the extremely low levels, as expected since the region is remote and relatively free of human influence. As for the Arctic there is also a strong presence of a polar vortex phenomenon. Antarctic light absorbing aerosol is dominated by mid latitude emissions in winter (corresponding to summer in Antarctica, Figure 44). Furthermore, the time series of the single scattering albedo at Trollhaugen (Figure 44, panel e) shows the highest values close to 1, i.e., almost no particle absorption at all in Antarctic winter, coincident and consistent with the minimum in particle absorption.

Figure 47 shows the series of monthly means of both AOD at 500 nm and the multi-wavelength Ångström exponent while Figure 48 displays the 2022 monthly means on the background of the whole 8-year average and the total variability. In 2022 the AOD values returned to typical monthly mean values. Also, the Ångström exponents and their annual cycle with lowest values in austral winter and a maximum in summer follow mainly the 8-year mean, with March/April values slightly above the multi-annual mean.

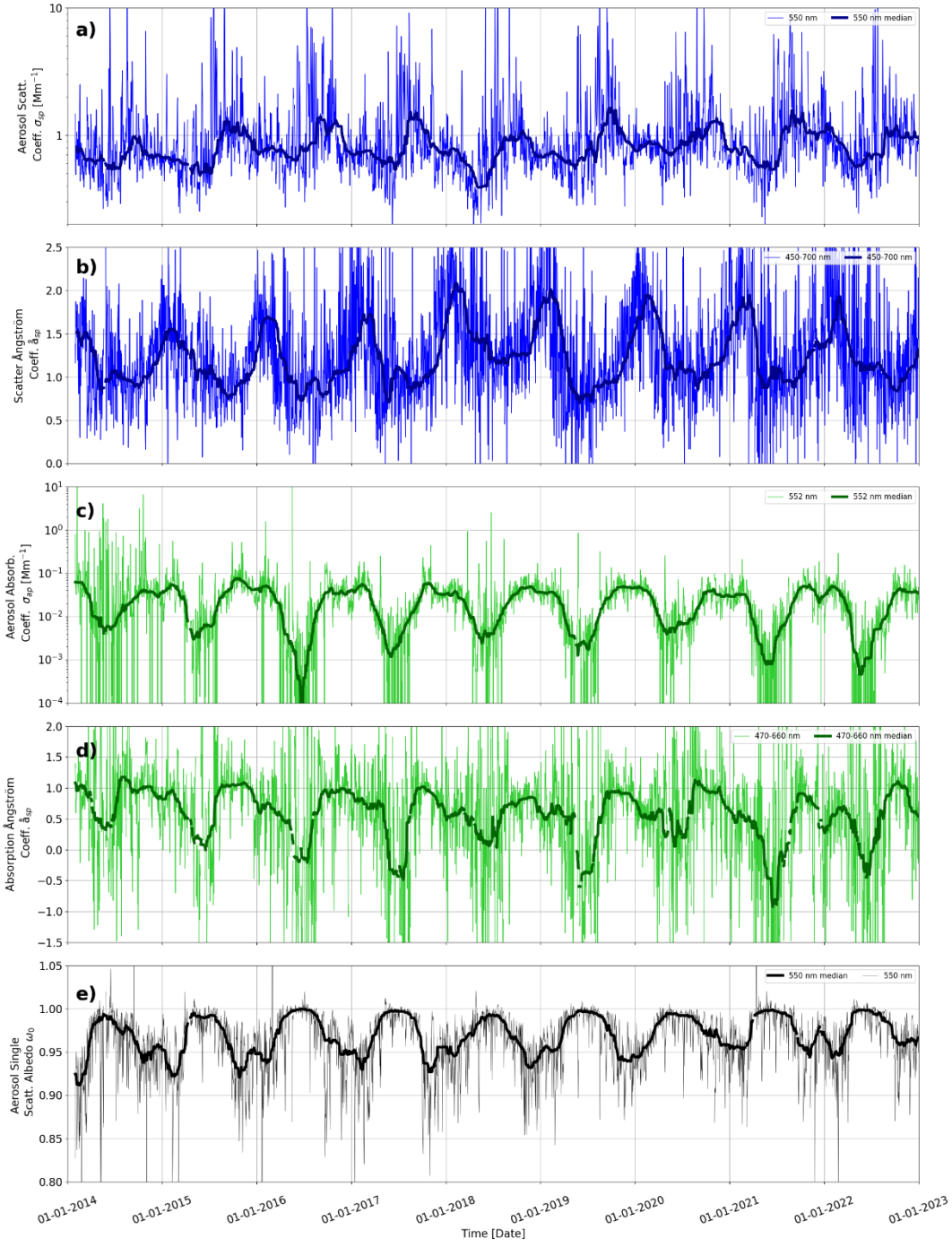

Figure 44: Time series of aerosol particle optical property daily means measured for 2014 to 2022 at Trollhaugen station. Panel a) shows the aerosol scattering coefficient σ_{sp} at 550 nm measured by integrating nephelometer. Panel c) the aerosol absorption coefficient σ_{ap} at 552 nm measured by filter absorption photometer. Panels b) and d) show the derived properties scattering and absorption Ångström coefficient $å_{sp}$ and $å_{ap}$, respectively, while Panel e) depicts the single scattering albedo ϖ_0. All plots also depict the running 55-day medians of the respective properties as heavy lines to visualize seasonal variations.

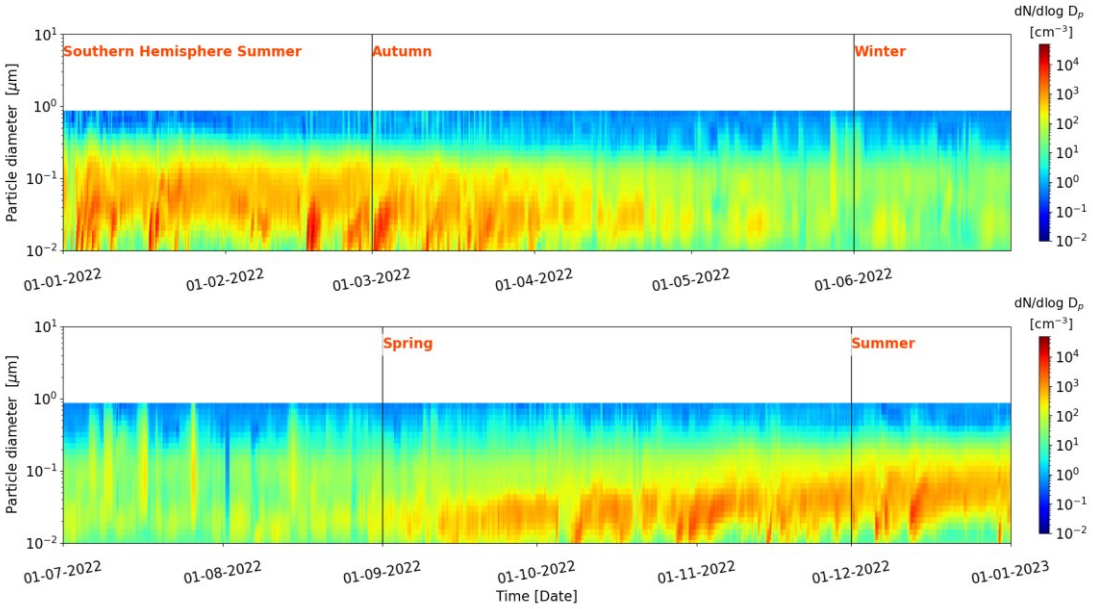

Figure 45: 2022 time series of particle number size distribution at Trollhaugen.

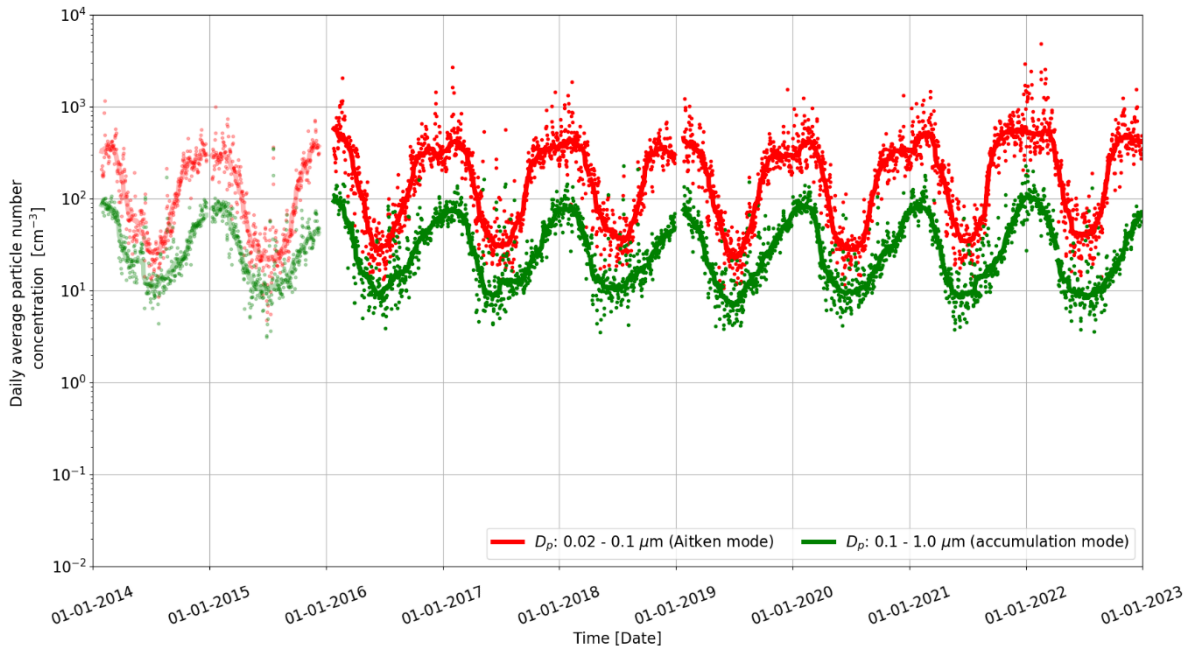

Figure 46: 2014 to 2022 time series of particle number concentration integrated over selected size ranges representing the different physical processes governing the atmospheric aerosol. The dotted graphs represent daily averages of the respective size range, the lines the 55-day running median. Data of the DMPS instrument prior to its upgrade are plotted in lighter colour as reminder that data before and after remodelling aren't directly comparable due to extension of the particle size range observed by the instrument.

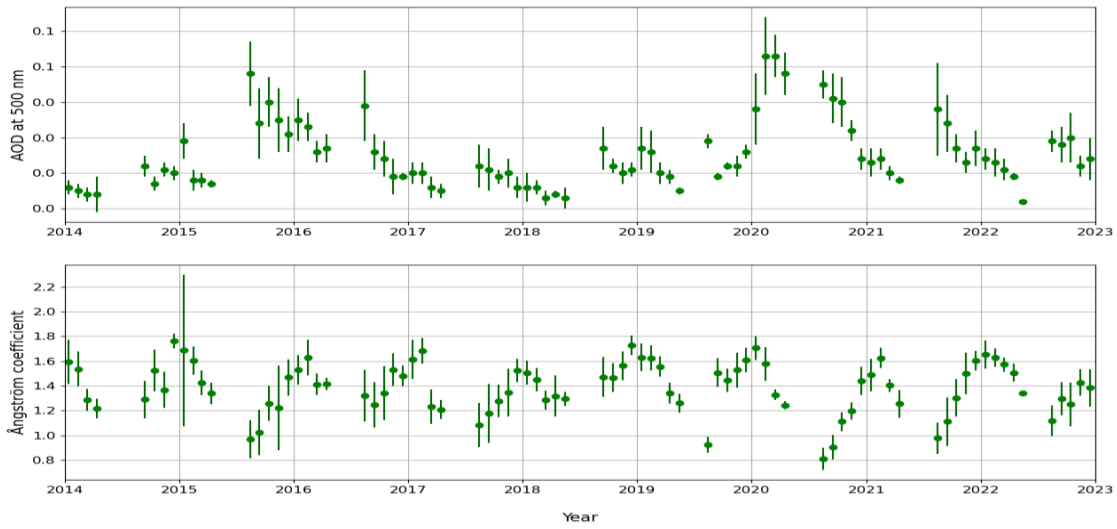

Figure 47: 2014 to 2022 time series of aerosol optical depth (AOD) at 500 nm wavelength in the atmospheric column above Trollhaugen Observatory, Antarctica (upper panel), Ångström coefficient (lower panel), and number of days per month with measurements. Monthly mean values and standard deviations are given.

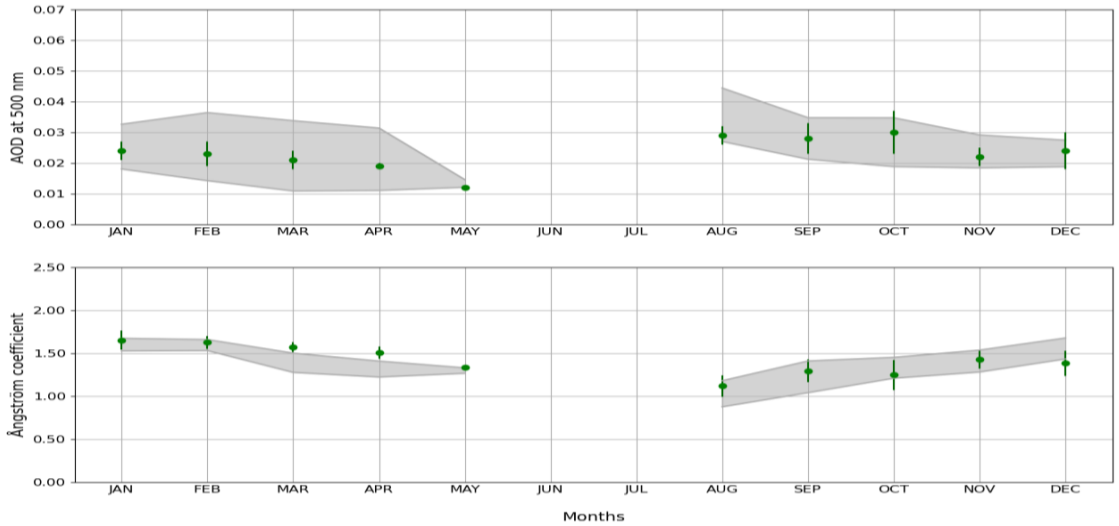

Figure 48: Seasonal variation of the aerosol optical depth (AOD) (upper panel) and Ångström coefficient (lower panel) observed at Troll Station, Antarctica. Values marked in grey are the mean and standard deviations for 2009 to 2022; the 2022 monthly mean and standard deviations are shown in green.

References

Aas, W., Berglen, T. F., Eckhardt, S., Fiebig, M., Solberg, S., Yttri, K.E. (2022) Monitoring of long-range transported air pollutants in Norway. Annual Report 2021. (NILU rapport 18/2022). Kjeller: NILU.

Asmi, A., Collaud Coen, M., Ogren, J. A., Andrews, E., Sheridan, P., Jefferson, A., Weingartner, E., Baltensperger, U., Bukowiecki, N., Lihavainen, H., Kivekäs, N., Asmi, E., Aalto, P. P., Kulmala, M., Wiedensohler, A., Birmili, W., Hamed, A., O'Dowd, C., G Jennings, S., Weller, R., Flentje, H., Fjaeraa, A. M., Fiebig, M., Myhre, C.E.L., Hallar, A. G., Swietlicki, E., Kristensson, A., Laj, P. (2013) Aerosol decadal trends - Part 2: In-situ aerosol particle number concentrations at GAW and ACTRIS stations. *Atmos. Chem. Phys.*, *13*, 895-916. https://doi.org/10.5194/acp-13-895-2013.

Baasandorj, M., Hall, B. D., Burkholder, J. B. (2012) Rate coefficients for the reaction of O(^{1}D) with the atmospherically long-lived greenhouse gases NF_3, SF_5CF_3, CHF_3, C_2F_6, c-C_4F_8, *n*-C_5F_{12}, and *n*-C_6F_{14}. *Atmos. Chem. Phys., 12,* 11753-11764. https://doi.org/10.5194/acp-12-11753-2012.

Blunden, J., T. Boyer, Bartow-Gillies, E. (Eds.) (2023) "State of the Climate in 2022". Bull. Amer. Meteor. Soc., 104 (9), Si–S501 https://doi.org/10.1175/2023BAMSStateoftheClimate.1.

Coen, M. Collaud., Andrews, E., Alastuey, A., Arsov, T. P., Backman, J., Brem, B. T., Bukowiecki, N., Couret, C., Eleftheriadis, K., Flentje, H., Fiebig, M., Gysel-Beer, M., Hand, J. L., Hoffer, A., Hooda, R., Hueglin, C., Joubert, W., Keywood, M., Kim, J. E., Kim, S.-W., Labuschagne, C., Lin, N.-H., Lin, Y., Lund Myhre, C., Luoma, K., Lyamani, H., Marinoni, A., Mayol-Bracero, O. L., Mihalopoulos, N., Pandolfi, M., Prats, N., Prenni, A. J., Putaud, J.-P., Ries, L., Reisen, F., Sellegri, K., Sharma, S., Sheridan, P., Sherman, J. P., Sun, J., Titos, G., Torres, E., Tuch, T., Weller, R., Wiedensohler, A., Zieger, P. and Laj, P. (2020) Multidecadal trend analysis of in situ aerosol radiative properties around the world. *Atmos. Chem. Phys., 20,* 8867-8908. https://doi.org/10.5194/acp-20-8867-2020.

Coen, M. C., Andrews, E., Asmi, A., Baltensperger, U., Bukowiecki, N., Day, D., Fiebig, M., Fjaeraa, A. M., Flentje, H., Hyvärinen, A., Jefferson, A., Jennings, S. G., Kouvarakis, G., Lihavainen, H., Myhre, C. L, Malm, W. C., Mihapopoulos, N., Molenar, J. V., O'Dowd, C., Ogren, J. A., Schichtel, B. A., Sheridan, P., Virkkula, A., Weingartner, E., Weller, R., Laj, P. (2013) Aerosol decadal trends - Part 1: In-situ optical measurements at GAW and IMPROVE stations. *Atmos. Chem. Phys., 13,* 869-894. https://doi.org/10.5194/acp-13-869-2013.

Coen, M.C., Weingartner, E., Apituley, A., Ceburnis, D., Fierz-Schmidhauser, R., Flentje, H., Henzing, J. S. (2010) Minimizing light absorption measurement artifacts of the Aethalometer: evaluation of five correction algorithms. *Atmos. Meas. Tech, 3,* 457–474. https://doi.org/10.5194/amt-3-457-2010.

Dalsøren, S. B., Myhre, C. L., Myhre, G., Gomez-Pelaez, A. J., Søvde, O. A., Isaksen, I. S. A., Weiss, R. F., Harth, C. M. (2016) Atmospheric methane evolution the last 40 years. *Atmos. Chem. Phys., 16,* 3099-3126. https://doi.org/10.5194/acp-16-3099-2016.

Dalsøren, S. D., Myhre, G., Hodnebrog, Ø., Myhre, C. L., Stohl, A., Pisso, I., Schwietzke, S., Höglund-Isaksson, L., Helmig, D., Reimann, S., Sauvage, S., Schmidbauer, N., Read, K. A., Carpenter, L. J., Lewis, A. C., Punjabi, S., Wallasch, M. (2018) Discrepancy between simulated and observed ethane and propane levels explained by underestimated fossil emissions. *Nature Geosci., 11,* 178-184. https://doi.org/10.1038/s41561-018-0073-0.

Delene, D.J., Ogren, J.A. (2002) Variability of aerosol optical properties at four North American surface monitoring sites. *J. Atmos. Sci., 59,* 1135-1150.

Dlugokencky, E.J., Hall, B. D., Montzka, S. A., Dutton, G., Mühle, J., Elkins, J. W. (2019) Long-lived greenhouse gases [in "State of the Climate in 2019"]. *Bull. Amer. Meteor. Soc.,* 101, No 8, S48–52. https://doi.org/10.1175/2020BAMSStateoftheClimate.1.

Dlugokencky, E.J., Hall, B. D., Montzka, S. A., Dutton, G., Mühle, J., Elkins, J. W. (2018) Long-lived greenhouse gases [in "State of the Climate in 2017"]. *Bull. Amer. Meteor. Soc.,* 99, S46-49. https://doi.org/10.1175/2018BAMSStateoftheClimate.1.

Drinovec, L., Močnik, G., Zotter, P., Prévôt, A. S. H., Ruckstuhl, C., Coz, E., Rupakheti, M., Sciare, J., Müller, T., Wiedensohler, A., Hansen, A. D. A. (2015) The "dual-spot" Aethalometer: an improved measurement of aerosol black carbon with real-time loading compensation. *Atmos. Meas. Tech, 8,* 1965-1979. https://doi.org/10.5194/amt-8-1965-2015.

Etiope, G., Ciccioli, P. (2009) Earth's Degassing: A Missing Ethane and Propane Source. *Science 323,* 478. https://doi.org/10.1126/science.1165904.

Etminan, M., Myhre, G., Highwood, E. J., Shine, K. P. (2016) Radiative forcing of carbon dioxide, methane, and nitrous oxide: A significant revision of the methane radiative forcing, *Geophys. Res. Lett*., 43, 12,614-12,623. https://doi.org/10.1002/2016GL071930.

Fiebig, M., Hirdman, D., Lunder, C. R., Ogren, J. A., Solberg, S., Stohl, A., Thompson, R. L. (2014) Annual cycle of Antarctic baseline aerosol: controlled by photooxidation-limited aerosol formation. *Atmos. Chem. Phys., 14,* 3083-3093. https://doi.org/10.5194/acp-14-3083-2014.

Fisher, R. E., France, J. L., Lowry, D., Lanoisellé, M., Brownlow, R., Pyle, J. A., Cain, M., Warwick, N., Skiba, U. M., Drewer, J., Dinsmore, K. J., Leeson, S. R., Bauguitte, S. J.-B., Wellpott, A., O'Shea, S. J., Allen, G., Gallagher, M. W., Pitt, J., Percival, C. J., Bower, K., George, C., Hayman, G. D., Aalto, T., Lohila, A., Aurela, M., Laurila, T., Crill, P. M., McCalley, C. K. and Nisbet, E. G. (2017) Measurement of the 13C isotopic signature of methane emissions from northern European wetlands. *Global Biogeochem. Cycles, 31,* 605-623. https://doi.org/10.1002/2016GB005504.

Forster, P., T. Storelvmo, K. Armour, W. Collins, J. L. Dufresne, D. Frame, D. J. Lunt, T. Mauritsen, M. D. Palmer, M. Watanabe, M. Wild, H. Zhang (2021) The Earth's Energy Budget, Climate Feedbacks, and Climate Sensitivity. In: *Climate Change 2021: The Physical Science Basis. Contribution of Working Group I to the Sixth Assessment Report of the Intergovernmental Panel on Climate Change* [Masson-Delmotte, V., P. Zhai, A. Pirani, S. L. Connors, C. Péan, S. Berger, N. Caud, Y. Chen, L. Goldfarb, M. I. Gomis, M. Huang, K. Leitzell, E. Lonnoy, J.B.R. Matthews, T. K. Maycock, T. Waterfield, O. Yelekçi, R. Yu and B. Zhou (eds.)]. Cambridge University Press.

France, J. L., Cain, M., Fisher, R. E., Lowry, D., Allen, G., O'Shea, S. J., Illingworth, S., Pyle, J., Warwick, N., Jones, B. T., Gallagher, M. W., Bower, K., Le Breton, M., Percival, C., Muller, J., Welpott, A., Bauguitte, S., George, C., Hayman, G. D., Manning, A. J., Myhre, C. L., Lanoisellé, M., Nisbet, E. G. (2016) Measurements of δ 13C in CH4 and using particle dispersion modeling to characterize sources of Arctic methane within an air mass. *J. Geophys. Res. Atmos., 121,* 14,257-14,270. https://doi.org/10.1002/2016JD026006.

Gliß, J., Mortier, A., Schulz, M., Andrews, E., Balkanski, Y., Bauer, S. E., Benedictow, A. M. K., Bian, H., Checa-Garcia, R., Chin, M., Ginoux, P., Griesfeller, J. J., Heckel, A., Kipling, Z., Kirkevåg, A., Kokkola, H., Laj, P., Le Sager, P., Lund, M. T., Lund Myhre, C., Matsui, H., Myhre, G., Neubauer, D., van Noije, T., North, P., Olivié, D. J. L., Sogacheva, L., Takemura, T., Tsigaridis, K. and Tsyro, S. G. (2020) Multi-model evaluation of aerosol optical properties in the AeroCom phase III Control experiment, using ground and space based columnar observations from AERONET, MODIS, AATSR and a merged satellite product as well as surface in-situ observations from GAW sites. *Atmos. Chem. Phys*. https://doi.org/10.5194/acp-2019-1214.

Groot Zwaaftink, C. D., Aas, W., Eckhardt, S., Evangeliou, N., Hamer, P., Johnsrud, M., Kylling, A., Platt, S. M., Stebel, K., Uggerud, H., and Yttri, K. E. (2022) What caused a record high PM10 episode in northern Europe in October 2020? *Atmos. Chem. Phys*., *22,* 3789-3810. https://doi.org/10.5194/acp-22-3789-2022.

Gulev, S. K., P. W. Thorne, J. Ahn, F. J. Dentener, C. M. Domingues, S. Gerland, D. Gong, D. S. Kaufman, H. C. Nnamchi, J. Quaas, J. A. Rivera, S. Sathyendranath, S. L. Smith, B. Trewin, K. von Shuckmann, R. S. Vose (2021) Changing State of the Climate System. In: *Climate Change 2021: The Physical Science Basis. Contribution of Working Group I to the Sixth Assessment Report of the Intergovernmental Panel on Climate Change* [Masson-Delmotte, V., P. Zhai, A. Pirani, S. L. Connors, C. Péan, S. Berger, N. Caud, Y. Chen, L. Goldfarb, M. I. Gomis, M. Huang, K. Leitzell, E. Lonnoy, J. B. R. Matthews, T. K. Maycock, T. Waterfield, O. Yelekçi, R. Yu and B. Zhou (eds.)]. Cambridge University Press.

Hall, B. D., Montzka, S. A., Dutton, G., Mühle, J., Elkins, J. W. (2017) Long-lived greenhouse gases [in "State of the Climate in 2016"]. *Bull. Amer. Meteor. Soc., 98* (8), S43-S46. https://doi.org/10.1175 /2017BAMSStateoftheClimate.1.

Hall, B. D., Montzka, S. A., Dutton, G., Miller, B. R., Elkins, J. W. (2020) Ozone-depleting substances [in "State of the Climate in 2019"]. *Bull. Amer. Meteor. Soc., 101* (8), S75-S76. https://doi.org/10.1175/BAMS-D-20-0104.1.

Hansen, K. M., Christensen, J. H., Geels, C., Silver, J. D., and Brandt, J. (2015) Modelling the impact of climate change on the atmospheric transport and the fate of persistent organic pollutants in the Arctic. *Atmos. Chem. Phys., 15*, 6549–6559, https://doi.org/10.5194/acp-15-6549-2015.

Hansen, G. H., Zielinski, T., Pakszys, P., Ritter, C., Gilardoni, S., Eleftheriadis, K., Kouremeti, N., Mateos, D., Herrero, S., Kazadzis, S., Mazzola, M., and Stebel, K. (2022) Re-evaluation and Homogenization of Aerosol Optical Depth Observations in Svalbard (ReHearsol). Annual report (NILU report 24/2023). Kjeller: NILU.

Hartmann, D.L., Klein Tank, A. M. G., Rusticucci, M., Alexander, L.V., Brönnimann, S., Charabi, Y., Dentener, F. J., Dlugokencky, E. J., Easterling, D. R., Kaplan, A., Soden, B. J., Thorne, P. W., Wild, M., Zhai, P. M. (2013) Observations: atmosphere and surface. In: *Climate Change 2013: The Physical Science Basis. Contribution of Working Group I to the Fifth Assessment Report of the Intergovernmental Panel on Climate Change*. Ed. by Stocker, T. F., Qin, D., Plattner, G.-K., Tignor, M., Allen, S. K., Boschung, J., Nauels, A., Xia, Y., Bex, V., Midgley, P.M. Cambridge, Cambridge University Press. pp. 159-254.

Heintzenberg, J. (1980) Particle size distribution and optical properties of Arctic haze. *Tellus, 32,* 251-260. https://doi.org/10.3402/tellusa.v32i3.10580.

Helmig, D., Rossabi, S., Hueber, J., Tans, P., Montzka, S. A., Masarie, K., Thoning, K., Plass-Duelmer, C., Claude, A., Carpenter, L. J., Lewis, A. C., Punjabi, S., Reimann, S., Vollmer, M. K., Steinbrecher, R., Hannigan, J. W., Emmons, L. K., Mahieu, E., Franco, B., Smale, D., Pozzer, A. (2016) Reversal of global atmospheric ethane and propane trends largely due to US oil and natural gas production. *Nature Geosci., 9,* 490-495. https://doi.org/10.1038/ngeo2721.

Hewitt, C. Nicholas (ed.) (1999) Reactive Hydrocarbons in the Atmosphere. San Diego, CA, Academic Press. P. 313.

Hodnebrog, Ø., Etminan, M., Fuglestvedt, J.S., Marston, G., Myhre, G., Nielsen, C.J., Shine, K.P., Wallington, T.J. (2013) Global warming potentials and radiative efficiencies of halocarbons and related compounds: A comprehensive review, (2013) *Reviews of Geophysics*, *51,* 300-378. https://doi.org/10.1002/rog.20013.

Hossaini, R., Chipperfield, M. P., Montzka, S. A., Leeson, A. A., Dhomse, S. and Pyle, J. A (2017) The increasing threat to stratospheric ozone from dichloromethane. *Nat. Commun., 8,* 15962, https://doi.org/10.1038ncomms15962.

IPCC (2021) Climate Change 2021: The Physical Science Basis. Contribution of Working Group I to the Sixth Assessment Report of the Intergovernmental Panel on Climate Change[Masson-Delmotte, V., P. Zhai, A. Pirani, S.L. Connors, C. Péan, S. Berger, N. Caud, Y. Chen, L. Goldfarb, M.I. Gomis, M. Huang, K. Leitzell, E. Lonnoy, J.B.R. Matthews, T.K. Maycock, T. Waterfield, O. Yelekçi, R. Yu, and B. Zhou (eds.)]. Cambridge University Press, Cambridge, United Kingdom and New York, NY, USA, https://doi.org/10.1017/9781009157896.

IPCC (2021b) Summary for Policymakers. In: *Climate Change 2021: The Physical Science Basis. Contribution of Working Group I to the Sixth Assessment Report of the Intergovernmental Panel on Climate Change* [Masson-Delmotte, V., P. Zhai, A. Pirani, S.L. Connors, C. Péan, S. Berger, N. Caud, Y. Chen, L. Goldfarb, M.I. Gomis, M. Huang, K. Leitzell, E. Lonnoy, J.B.R. Matthews, T.K. Maycock, T. Waterfield, O. Yelekçi, R. Yu, and B. Zhou (eds.)]. Cambridge University Press, Cambridge, United Kingdom and New York, NY, USA, pp. 3−32, https://doi.org/10.1017/9781009157896.001.

Isaksen, I. S. A., Hov, Ø. (1987) Calculation of trends in the tropospheric concentration of O_3, OH, CO, CH_4 and NO_x. *Tellus*, *39B*, 271-285.

Jackson, R.B., Saunois, M., Bousquet, P., Canadell, J.G., Poulter, B., Stavert, A.R., Bergamaschi, P., Niwa,Y., Segers, A., and Tsuruta, A. (2020) *Environ. Res. Lett., 15,* 071002. https://doi.org/10.1088/1748-9326/ab9ed2.

Laj, P., Bigi, A., Rose, C. Andrews, E. Lund Myhre, C. Collaud Coen, M. Lin, Y. Wiedensohler, A. Schulz, M. Ogren, J. A. Fiebig, M. Gliß, J. Mortier, A. Pandolfi, M. Petäja, T. Kim, S.-W. Aas, W. Putaud, J.-P. Mayol-Bracero, O. Keywood, M., Labrador, L. Aalto, P. Ahlberg, E. Alados Arboledas, L. Alastuey, A. Andrade, M. Artíñano, B. Ausmeel, S. Arsov, T. Asmi, E. Backman, J. Baltensperger, U., Bastian, S.,

Bath, O., Beukes, J. P., Brem, B. T., Bukowiecki, N., Conil, S., Couret, C., Day, D., Dayantolis, W., Degorska, A., Eleftheriadis, K., Fetfatzis, P., Favez, O., Flentje, H., Gini, M. I., Gregorič, A., Gysel-Beer, M., Hallar, A. G., Hand, J., Hoffer, A., Hueglin, C., Hooda, R. K., Hyvärinen, A., Kalapov, I., Kalivitis, N., Kasper-Giebl, A., Kim, J. E., Kouvarakis, G., Kranjc, I., Krejci, R., Kulmala, M., Labuschagne, C., Lee, H.-J., Lihavainen, H., Lin, N.-H., Löschau, G., Luoma, K., Marinoni, A., Martins Dos Santos, S., Meinhardt, F., Merkel, M., Metzger, J.-M., Mihalopoulos, N., Nguyen, N. A., Ondracek, J., Pérez, N., Perrone, M. R., Petit, J.-E., Picard, D., Pichon, J.-M., Pont, V., Prats, N., Prenni, A., Reisen, F., Romano, S., Sellegri, K., Sharma, S., Schauer, G., Sheridan, P., Sherman, J. P., Schütze, M., Schwerin, A., Sohmer, R., Sorribas, M., Steinbacher, M., Sun, J., Titos, G., Toczko, B., Tuch, T., Tulet, P., Tunved, P., Vakkari, V., Velarde, F., Velasquez, P., Villani, P., Vratolis, S., Wang, S.-H., Weinhold, K., Weller, R., Yela, M., Yus-Diez, J., Zdimal, V., Zieger, P., and Zikova, N. (2020) A global analysis of climate-relevant aerosol properties retrieved from the network of Global Atmosphere Watch (GAW) near-surface observatories. *Atmos. Meas Tech., 13*, 4353-4392. https://doi.org/10.5194/amt-13-4353-2020.

Lan, X., B. D. Hall, G. Dutton, J. Mühle, J. W. Elkins, and I. J. Vimon (2022) Long-lived greenhouse gases [in "State of the Climate in 2021"]. *Bull. Amer. Meteor. Soc., 103* (8), S81–S84. https://doi.org/10.1175/BAMS-D-22-0092.1

Lan, X., Tans, P., Hall, B. D., Dutton, G., Mühle, J., Elkins, J. W., Vimont, I. (2021) Long-lived greenhouse gases [in "State of the Climate in 2020"]. *Bull. Amer. Meteor., 102* (8), S53–S87. https://doi.org/10.1175/BAMS-D-21-0098.1.

Laturnus, F., Haselmann, K. F., Borch, T., Grøn, C (2002) Terrestrial natural sources of trichloromethane (chloroform, CHCl 3)–An overview. *Biogeochemistry* 60: 121-139.

Law, Kathy S., Stohl, A. (2007) Arctic air pollution: Origins and impacts. *science* 315, (5818), 1537-1540. https://doi.org/10.1126/science.1137695

Montzka, S. A., Dutton, G. S., Yu, P., Ray, E., Portmann, R. W., Daniel, J. S., Kuijpers, L., Hall, B. D., Mondeel, D., Siso, Nance, J. D., Rigby, M., Manning, A. J., Hu, L., Moore, F., Miller, B. R., Elkins, J. W. (2018) An unexpected and persistent increase in global emissions of ozone-depleting CFC-11. *Nature, 557,* 413-417.

Mortier, A., Gliss, J., Schulz, M., Aas, W., Andrews, E., Bian, H., Chin, M., Ginoux, P., Hand, J., Holben, B., Hua, Z., Kipling, Z., Kirkevåg, A., Laj, P., Lurton, T., Myhre, G., Neubauer, D., Olivié, D., von Salzen, K., Takemura, T. and Tilmes, S. (2020) Evaluation of climate model aerosol trends with ground-based observations over the last two decades -- an AeroCom and CMIP6 analysis. *Atmos. Chem. Phys., 20,* 13355-13378. https://doi.org/10.5194/acp-20-13355-2020.

Moskvitch, K. (2014) Mysterious Siberian crater attributed to methane. *Nature*. https://doi.org/10.1038/nature.2014.15649.

Myhre, C. L., Hermansen, O., Fiebig, M., Lunder, C., Fjæraa, A. M., Svendby, T., Platt, M., Hansen. G., Schmidbauer, N., Krognes, T. (2016) Monitoring of greenhouse gases and aerosols at Svalbard and Birkenes in 2015 - Annual report. Kjeller, NILU (Miljødirektoratet rapport, M-694/2016) (NILU report, 31/2016).

Myhre, C. L., Ferré, B., Platt, S. M., Silyakova, A., Hermansen, O., Allen, G., Pisso, I., Schmidbauer, N., Stohl, A., Pitt, J., Jansson, P., Greinert, J., Percival, C., Fjaeraa, A. M., O'Shea, S., Gallagher, M., Le Breton, M., Bower, K., Bauguitte, S., Dalsøren, S., Vadakkepuliyambatta, S., Fisher, R., Nisbet, E., Lowry, D., Myhre, G., Pyle, J., Cain, M., Mienert, J. (2016) Large methane release from the Arctic seabed west of Svalbard, but small release to the atmosphere. *Geophys. Res. Lett*., *43,* 4624–4631. https://doi.org/10.1002/2016GL068999.

Myhre, G., Myhre C. L., Forster, P. M., Shine, K. P. (2017) Halfway to doubling of CO2 radiative forcing. *Nature Geosci., 10,* 710-711. https://doi.org/10.1038/ngeo3036.

Myhre, G., Myhre, C. L., Samset, B. H., Storelvmo, T. (2013a) Aerosols and their relation to global climate and climate sensitivity. *Nature Education Knowledge, 4*(5), 7. http://www.nature.com/scitable/knowledge/library/aerosols-and-their-relation-to-global-climate-102215345.

Myhre, G., Shindell, D., Bréon, F.-M., Collins, W., Fuglestvedt, J., Huang, J., Koch, D., Lamarque, J.-F., Lee, D., Mendoza, B., Nakajima, T., Robock, A., Stephens, G., Takemura, T., Zhang, H. (2013b) Anthropogenic and natural radiative forcing. In: *Climate Change 2013: The Physical Science Basis. Contribution of Working Group I to the Fifth Assessment Report of the Intergovernmental Panel on Climate Change*. Ed. by Stocker, T.F., Qin, D., Plattner, G.-K., Tignor, M., Allen, S.K., Boschung, J., Nauels, A., Xia, Y., Bex, V., Midgley, P.M. Cambridge, Cambridge University Press. pp. 659-740.

Mühle, J., Trudinger, C. M., Western, L. M., Rigby, M., Vollmer, M. K., Park, S., Manning, A. J., Say, D., Ganesan, A., Steele, L. P., Ivy, D. J., Arnold, T., Li, S., Stohl, A., Harth, C. M., Salameh, P. K., McCulloch, A., O'Doherty, S., Park, M.-K., Jo, C. O., Young, D., Stanley, K. M., Krummel, P. B., Mitrevski, B., Hermansen, O., Lunder, C., Evangeliou, N., Yao, B., Kim, J., Hmiel, B., Buizert, C., Petrenko, V. V., Arduini, J., Maione, M., Etheridge, D. M., Michalopoulou, E., Czerniak, M., Severinghaus, J. P., Reimann, S., Simmonds, P. G., Fraser, P. J., Prinn, R. G., and Weiss, R. F. (2019) Perfluorocyclobutane (PFC-318, c-C4F8) in the global atmosphere. *Atmos. Chem. Phys., 19,* 10335–10359. https://doi.org/10.5194/acp-19-10335-2019.

Naik, V., S. Szopa, B. Adhikary, P. Artaxo, T. Berntsen, W. D. Collins, S. Fuzzi, L. Gallardo, A. Kiendler Scharr, Z. Klimont, H. Liao, N. Unger, P. Zanis, 2021, Short-Lived Climate Forcers. In: *Climate Change 2021: The Physical Science Basis. Contribution of Working Group I to the Sixth Assessment Report of the Intergovernmental Panel on Climate Change* [Masson-Delmotte, V., P. Zhai, A. Pirani, S. L. Connors, C. Péan, S. Berger, N. Caud, Y. Chen, L. Goldfarb, M. I. Gomis, M. Huang, K. Leitzell, E. Lonnoy, J. B. R. Matthews, T. K. Maycock, T. Waterfield, O. Yelekçi, R. Yu and B. Zhou (eds.)]. Cambridge University Press.

Ng, N. L., Kroll, J.H., Chan, A. W. H., Chhabra, P. S., Flagan, R. C., Seinfeld, J. H. (2007) Secondary organic aerosol formation from m-xylene, toluene, and benzene. *Atmos. Chem. Physics, 7,* 3909-3922.

Nicewonger, M. R., Verhulst, K. R., Aydin, M., Saltzman, E. S. (2016) Preindustrial atmospheric ethane levels inferred from polar ice cores: A constraint on the geologic sources of atmospheric ethane and methane. *Geophys. Res. Lett., 43,* 214-221. https://doi.org/10.1002/2015GL066854.

Oram, D. E., Mani, F. S., Laube, J. C., Newland, M. J., Reeves, C. E., Sturges, W. T., Penkett, S. A., Brenninkmeijer, C. A. M., Röckmann, T., and Fraser, P. J. (2012) Long-term tropospheric trend of octafluorocyclobutane (c-C_4F_8 or PFC-318), *Atmos. Chem. Phys., 12,* 261-269. https://doi.org/10.5194/acp-12-261-2012.

Pandolfi, M., Alados-Arboledas, L., Alastuey, A., Andrade, M., Angelov, C., Artiñano, B., Backman, J., Baltensperger, U., Bonasoni, P., Bukowiecki, N., Collaud Coen, M., Conil, S., Coz, E., Crenn, V., Dudoitis, V., Ealo, M., Eleftheriadis, K., Favez, O., Fetfatzis, P., Fiebig, M., Flentje, H., Ginot, P., Gysel, M., Henzing, B., Hoffer, A., Holubova Smejkalova, A., Kalapov, I., Kalivitis, N., Kouvarakis, G., Kristensson, A., Kulmala, M., Lihavainen, H., Lunder, C., Luoma, K., Lyamani, H., Marinoni, A., Mihalopoulos, N., Moerman, M., Nicolas, J., O'Dowd, C., Petäjä, T., Petit, J.-E., Pichon, J. M., Prokopciuk, N., Putaud, J.-P., Rodríguez, S., Sciare, J., Sellegri, K., Swietlicki, E., Titos, G., Tuch, T., Tunved, P., Ulevicius, V., Vaishya, A., Vana, M., Virkkula, A., Vratolis, S., Weingartner, E., Wiedensohler, A., and Laj, P. (2018) A European aerosol phenomenology – 6: scattering properties of atmospheric aerosol particles from 28 ACTRIS sites. *Atmos. Chem. Phys., 18*, 7877-7911. https://doi.org/10.5194/acp-18-7877-2018.

Park, S., Western, L. M., Saito, T., Redington, A., Henne, S., Fang, X., Prinn, R. G., Manning, A. J., Montzka, S. A., Fraser, P. J., Ganesan, A. L., Harth, C. M., Kim, J., Krummel, P. B., Liang, Q., Mühle, J., O'Doherty, S., Park, H., Park, M-K., Reimann, S., Salameh, P. K., Weiss, R. F., Rigby, M. (2021) A decline in emissions of CFC-11 and related chemicals from eastern China. *Nature, 590*(7846), 433-437. https://doi.org/10.1038/s41586-021-03277-w.

Peng, S., Lin, X., Thompson, R. L., Xi, Y., Liu, G., Hauglustaine, D., Lan, X., Poulter, B., Ramonet, M., Saunois, M., Yin, Y., Zhang, Z., Zheng, B., & Ciais, P. (2022) Wetland emission and atmospheric sink changes explain methane growth in 2020. Nature 612, 477–482. https://doi.org/10.1038/s41586-022-05447-w

Platt, S. M., Eckhardt, S., Ferré, B., Fisher, R. E., Hermansen, O., Jansson, P., Lowry, D., Nisbet, E. G., Pisso, I., Schmidbauer, N., Silyakova, A., Stohl, A., Svendby, T. M., Vadakkepuliyambatta, S., Mienert, J., and Lund Myhre, C. (2018) Methane at Svalbard and over the European Arctic Ocean. *Atmos. Chem. Phys., 18,* 17207-17224. https://doi.org/10.5194/acp-18-17207-2018.

Platt, S. M., Hov, Ø., Berg, T., Breivik, K., Eckhardt, S., Eleftheriadis, K., Evangeliou, N., Fiebig, M., Fisher, R., Hansen, G., Hansson, H.-C., Heintzenberg, J., Hermansen, O., Heslin-Rees, D., Holmén, K., Hudson, S., Kallenborn, R., Krejci, R., Krognes, T., Larssen, S., Lowry, D., Lund Myhre, C., Lunder, C., Nisbet, E., Nizetto, P. B., Park, K.-T., Pedersen, C. A., Aspmo Pfaffhuber, K., Röckmann, T., Schmidbauer, N., Solberg, S., Stohl, A., Ström, J., Svendby, T., Tunved, P., Tørnkvist, K., van der Veen, C., Vratolis, S., Yoon, Y. J., Yttri, K. E., Zieger, P., Aas, W., and Tørseth, K. (2022) Atmospheric composition in the European Arctic and 30 years of the Zeppelin Observatory, Ny-Ålesund. *Atmos. Chem. Phys., 22,* 3321-3369. https://doi.org/10.5194/acp-22-3321-2022.

Prather, M., Ehhalt, D., Dentener, F., Derwent, R. G., Dlugokencky, E., Holland, E., Isaksen, I. S. A., Katima, J., Kirchhoff, V., Matson, P., Midgley, P. M., Wang, M. (2001) Atmospheric chemistry and greenhouse gases. In: *Climate Change 2001: The Scientific Basis, Contribution of Working Group I to the Third Assessment Report of the Intergovernmental Panel on Climate Change.* Ed. by: Houghton, J. T., Ding, Y., Griggs, D. J., Noguer, M., van der Linden, P. J., Dai, X., Maskell, K., Johnson, C. A. Cambridge, Cambridge University Press. pp. 239-287.

Pisso, I., Myhre, C. L., Platt, S. M., Eckhardt, S., Hermansen, O., Schmidbauer, N., Mienert, J., Vadakkepuliyambatta, S., Bauguitte, S., Pitt, J., Allen, G., Bower, K.N., O'Shea, S., Gallagher, M. W., Percival, C.J., Pyle, J., Cain, M., Stohl, A. (2016) Constraints on oceanic methane emissions west of Svalbard from atmospheric in situ measurements and Lagrangian transport modelling. *J. Geophys. Res., 121,* 14188-14200. https://doi.org/10.1002/2016JD025590.

Putaud, J. P., Van Dingenen, R., Alastuey, A., Bauer, H., Birmili, W., Cyrys, J., Flentje, H., Fuzzi, S., Gehrig, R., Hansson, H. C., Harrison, R. M., Herrmann, H., Hitzenberger, R., Hüglin, C., Jones, A. M., Kasper-Giebl, A., Kiss, G., Kousa, A., Kuhlbusch, T. A. J., Löschau, G., Maenhaut, W., Molnar, A., Moreno, T., Pekkanen, J., Perrino, C., Pitz, M., Puxbaum, H., Querol, X., Rodriguez, S., Salma, I., Schwarz, J., Smolik, J., Schneider, J., Spindler, G., ten Brink, H., Tursic, J., Viana, M., Wiedensohler, A., & Raes, F. (2010) A European aerosol phenomenology – 3: Physical and chemical characteristics of particulate matter from 60 rural, urban, and kerbside sites across Europe. *Atmos. Environ., 44(*10), 1308-1320. https://doi.org/10.1016/j.atmosenv.2009.12.011.

R Core Team (2018) R: A language and environment for statistical computing. Vienna, Austria, R Foundation for Statistical Computing. https://www.R-project.org/.

Ramonet, M. , P. Ciais, F. Apadula, J. Bartyzal, Bartyzel, , A. Bastos, , P. Bergamaschi, P.E. Blanc, D. Brunner, L. C. di Torchiarolo, F. Calzolari, H. Chen, L. Chmura, A. Colomb, S. Conil, P. Cristofanelli, E. Cuevas, R. Curcoll, M. Delmotte1, A. di Sarra, L. Emmenegger, G. Forster, A. Frumau, C. Gerbig, F. Gheusi, S. Hammer, L. Haszpra12, J. Hatakka, L. Hazan, M. Heliasz, S. Henne, A. Hensen, O. Hermansen, P. Keronen, R.Kivi, K. Komínková, D. Kubistin, O. Laurent, T. Laurila, J.V. Lavric, I. Lehner, K.E.J. Lehtinen, A. Leskinen, M. Leuenberger, I. Levin, M. Lindauer, M. Lopez, C. LundMyhre, I. Mammarella, G. Manca, A. Manning, M.V. Marek, P. Marklund, D. Martin, F. Meinhardt, N. Mihalopoulos, M. Mölder, J.A. Morgui, J. Necki, S. O'Doherty, C. O'Dowd, M. Ottosson, C. Philippon, S. Piacentino, J.M. Pichon, C. Plass-Duelmer, A. Resovsky, L.Rivier, X. Rodó, M.K. Sha, H.A. Scheeren, D. Sferlazzo, T.G. Spain, K.M. Stanley, M. Steinbacher, P. Trisolino, A. Vermeulen, G. Vítková, D. Weyrauch, I. Xueref-Remy, K. Yala, C. Yver Kwok. The fingerprint of the summer 2018 drought in Europe on ground-based atmospheric CO2 measurements. *Phil.l Trans. R. Soc. B, 375,* 20190513. https://doi.org/10.1098/rstb.2019.0513

Repo, M. E., Susiluoto, S., Lind, S. E., Jokinen, S., Elsakov, V., Biasi, C., Virtanen, T., Pertti, J., Martikainen, P. J. (2009) Large N_2O emissions from cryoturbated peat soil in tundra. *Nature Geosci., 2*, 189-192. https://doi.org/10.1038/ngeo434.

Rigby, M., Park, S., Saito, T., Western, L. M., Redington, A. L., Fang, X. , Henne, S., Manning, A. J., Prinn, R. G., Dutton, G. S., Fraser, P. J., Ganesan, A. L., Hall, B. D., Harth, C. M., Kim, J., Kim, K.-R., Krummel, P. B., Lee, T., Li, S., Liang, Q., Lunt, M. F., Montzka, S. A., Mühle, J., O'Doherty, S., Park, M.-K., Reimann, S., Salameh, P. K., Simmonds, P., Tunnicliffe, R. L., Weiss, R. F., Yokouchi, Y. , Young, D. (2019) Increase in CFC-11 emissions from eastern China based on atmospheric observations. *Nature*, *569*, 546-550. https://doi.org/10.1038/s41586-019-1193-4 .

Saunois, M., Stavert, A. R., Poulter, B., Bousquet, P., Canadell, J. G., Jackson, R. B., Raymond, P. A., Dlugokencky, E. J., Houweling, S., Patra, P. K., Ciais, P., Arora, V. K., Bastviken, D., Bergamaschi, P., Blake, D. R., Brailsford, G., Bruhwiler, L., Carlson, K. M., Carrol, M., Castaldi, S., Chandra, N., Crevoisier, C., Crill, P. M., Covey, K., Curry, C. L., Etiope, G., Frankenberg, C., Gedney, N., Hegglin, M. I., Höglund-Isaksson, L., Hugelius, G., Ishizawa, M., Ito, A., Janssens-Maenhout, G., Jensen, K. M., Joos, F., Kleinen, T., Krummel, P. B., Langenfelds,

R. L., Laruelle, G. G., Liu, L., Machida, T., Maksyutov, S., McDonald, K. C., McNorton, J., Miller, P. A., Melton, J. R., Morino, I., Müller, J., Murguia-Flores, F., Naik, V., Niwa, Y., Noce, S., O'Doherty, S., Parker, R. J., Peng, C., Peng, S., Peters, G. P., Prigent, C., Prinn, R., Ramonet, M., Regnier, P., Riley, W. J., Rosentreter, J. A., Segers, A., Simpson, I. J., Shi, H., Smith, S. J., Steele, L. P., Thornton, B. F., Tian, H., Tohjima, Y., Tubiello, F. N., Tsuruta, A., Viovy, N., Voulgarakis, A., Weber, T. S., van Weele, M., van der Werf, G. R., Weiss, R. F., Worthy, D., Wunch, D., Yin, Y., Yoshida, Y., Zhang, W., Zhang, Z., Zhao, Y., Zheng, B., Zhu, Q., Zhu, Q., and Zhuang, Q. (2020) The Global Methane Budget 2000–2017. *Earth Syst. Sci. Data, 12,* 1561-1623. https://doi.org/10.5194/essd-12-1561-2020.

Simmonds, P. G., Manning, A. J., Cunnold, D. M., Fraser, P. J., McCulloch, A., O'Doherty, S., Krummel, P. B., Wang, R. H. J., Porter, L. W., Derwent, R. G., Greally, B., Salameh, P., Miller, B. R., Prinn, R. G., Weiss, R. F. (2006) Observations of dichloromethane, trichloroethene and tetrachloroethene from the AGAGE stations at Cape Grim, Tasmania, and Mace Head, Ireland. *J. Geophys. Res*., *111,* D18304. https://doi.org/10.1029/2006JD007082.

Stohl, A., Klimont, Z., Eckhardt, S., Kupiainen, K., Shevchenko, V. P., Kopeikin, V. M., and Novigatsky, A. N. (2013) Black carbon in the Arctic: the underestimated role of gas flaring and residential combustion emissions. *Atmos. Chem. Phys., 13,* 8833–8855, https://doi.org/10.5194/acp-13-8833-2013.

Svendby, T.M., Hansen, G.H., Bäcklund, A., Bernet, L., Nilsen, A.C., Schulze, D., Johnsen, B. (2022) Monitoring of the atmospheric ozone layer and natural ultraviolet radiation. Annual Report 2021. (NILU report 25/2022; Norwegian Environment Agency, M-2335|2022). Kjeller: NILU.

Thompson R.L. G. Broquet, C. Gerbig, T. Koch, M. Lang, G. Monteil, S. Munassar, A. Nickless, M. Scholze, M. Ramonet, U. Karstens, E. van Schaik, Z. Wu and C. Rödenbeck, (2020) Changes in net ecosystem exchange over Europe during the 2018 drought based on atmospheric observations. *Phil. Trans. R. Soc. B, 375,* 20190512. https://doi.org/10.1098/rstb.2019.0512

Thompson, R. L., Sasakawa, M., Machida, T., Aalto, T., Worthy, D., Lavric, J. V., Myhre, C. L., Stohl, A. (2017) Methane fluxes in the high northern latitudes for 2005–2013 estimated using a Bayesian atmospheric inversion. *Atmos. Chem. Phys.*, 17, 3553-3572. https://doi.org/10.5194/acp-2016-660.

Thompson, R. L., Dlugockenky, E., Chevallier, F., Ciais, P., Dutton, G., Elkins, J. W., Langenfelds, R. L., Prinn, R. G., Weiss, R. F., Tohjima, Y., Krummel, P. B., Fraser, P., Steele, L. P. (2013) Interannual variability in tropospheric nitrous oxide. *Geophys. Res. Lett, 40*, 4426-4431. https://doi.org/10.1002/grl.50721.

Tørseth, K., Aas, W., Breivik, K., Fjæraa, A. M., Fiebig, M., Hjellbrekke, A. G., Myhre, C. L., Solberg, S., Yttri, K. E. (2012) Introduction to the European Monitoring and Evaluation Programme (EMEP) and observed atmospheric composition change during 1972–200. *Atmos. Chem. Phys., 12,* 5447-5481. https://doi.org/10.5194/acp-12-5447-2012.

Umezawa, T., Baker, A. K., Oram, D., Sauvage, C., O'Sullivan, D., Rauthe-Schöch, A., Montzka, S. A., Zahn, A., Brenninkmeijer, C. A. M. (2014) Chloromethane in the upper troposphere observed by the CARIBIC passenger aircraft bservatory: Large-scale distributions and Asian summer monsoon outflow. *J. Geophys. Res. Atmos., 119,* 5542-5558. https://doi.org/10.1002/2013JD021396.

Vimont, I. J., B. D. Hall, G. Dutton, S. A. Montzka, J. Mühle, M. Crotwell, K. Petersen, S. Clingan, and D. Nance (2023): Ozone-depleting substances and their substitutes [in "State of the Climate in 2022"]. Bull. Amer. Meteor. Soc., 104 (9), S88–S90, https://doi.org/10.1175/2023BAMSStateoftheClimate_Intro.1.

Vollmer, M. K., Young, D., Trudinger, C. M., Muhle, J., Henne, S., Rigby, M., Park, S., Li, S., Guillevic, M., Mitrevski, B., Harth, C. M., Miller, B. R., Reimann, S., Yao, B., Steele, L. P., Wyss, S. A., Lunder, C. R., Arduini, J., McCulloch, A., Wu, S., Rhee, T. S., Wang, R. H. J., Salameh, P. K., Hermansen, O., Hill, M., Langenfelds, R. L., Ivy, D., O'Doherty, S., Krummel, P. B., Maione, M., Etheridge, D. M., Zhou, L., Fraser, P. J., Prinn, R. G.; Weiss, R. F., Simmonds, P. G. (2018) Atmospheric histories and emissions of chlorofluorocarbons CFC-13 (CClF3), ΣCFC-114 (C2Cl2F4), and CFC-115 (C2ClF5). *Atmos. Chem. Phys.*, *18*, 979-1002. https://doi.org/10.5194/acp-18-979-2018.

Wiedensohler, A., Birmili, W., Nowak, A., Sonntag, A., Weinhold, K., Merkel, M., Wehner, B., Tuch, T., Pfeifer, S., Fiebig, M., Fjäraa, A. M., Asmi, E., Sellegri, K., Depuy, R., Venzac, H., Villani, P., Laj, P., Aalto, P., Ogren, J. A., Swietlicki, E., Williams, P., Roldin, P., Quincey, P., Hüglin, C., Fierz-Schmidhauser, R., Gysel, M., Weingartner, E., Riccobono, F., Santos, S., Grüning, C., Faloon, F., Beddows, D., Harrison, R., Monahan, C., Jennings, S. G., O'Dowd, C. D., Marinoni, A., Horn, H.-G., Keck, L., Jiang, J., Scheckman, J., McMurry, P.H., Deng, Z., Zhao, C. S., Moerman, M., Henzing, B., de Leeuw, G., Löschau, G., Bastian, S. (2012) Mobility particle size spectrometers: harmonization of technical standards and data structure to facilitate high quality long-term observations of atmospheric particle number size distributions. *Atmos. Meas. Tech.*, *5,* 657-685. https://doi.org/10.5194/amt-5-657-2012.

Wilkinson, M. D., Dumontier, M., Aalbersberg, I. J., Appleton, G., Axton, M., Baak, A., Blomberg, N., Boiten, J. W., Santos, L. B. D., Bourne, P. E., Bouwman, J., Brookes, A. J., Clark, T., Crosas, M., Dillo, I., Dumon, O., Edmunds, S., Evelo, C. T., Finkers, R., Gonzalez-Beltran, A., Gray, A. J. G., Groth, P., Goble, C., Grethe, J. S., Heringa, J., Hoen, P. A. C., Hooft, R., Kuhn, T., Kok, R., Kok, J., Lusher, S. J., Martone, M. E., Mons, A., Packer, A. L., Persson, B., Rocca-Serra, P., Roos, M., van Schaik, R., Sansone, S. A., Schultes, E., Sengstag, T., Slater, T., Strawn, G., Swertz, M. A., Thompson, M., van der Lei, J., van Mulligen, E., Velterop, J., Waagmeester, A., Wittenburg, P., Wolstencroft, K., Zhao, J., and Mons, B. (2016) The FAIR Guiding Principles for scientific data management and stewardship. *Sci. Data, 3,* 160018. https://doi.org/https://doi.org//10.1038/sdata.2016.18.

WMO (2023) Greenhouse Gas Bulletin. The State of Greenhouse Gases in the Atmosphere Based on Global Observations through 2022. Geneva, World Meteorological Organization (GHG Bulletin No. 19, 15 November 2023).

WMO (2022) Greenhouse Gas Bulletin. The State of Greenhouse Gases in the Atmosphere Based on Global Observations through 2021. Geneva, World Meteorological Organization (GHG Bulletin No. 18, 26 October 2022).

WMO (2021) Greenhouse Gas Bulletin. The State of Greenhouse Gases in the Atmosphere Based on Global Observations through 2020. Geneva, World Meteorological Organization (GHG Bulletin No. 17, 25 October 2021).

WMO (2020) Greenhouse Gas Bulletin. The state of greenhouse gases in the atmosphere using global observations through 2019. Geneva, World Meteorological Organization (GHG Bulletin No. 16, 23 November 2020). https://library.wmo.int/doc_num.php?explnum_id=10437.

WMO (2019) Greenhouse Gas Bulletin. The state of greenhouse gases in the atmosphere using global observations through 2018. Geneva, World Meteorological Organization (GHG Bulletin No. 15, 25 November 2019). https://library.wmo.int/index.php?lvl=notice_display&id=21620#.X1i3NN7VI2w

WMO (2018) Scientific assessment of ozone depletion: 2018. Geneva, World Meteorological Organization (Global Ozone Research and Monitoring Project-Report No. 58). https://www.esrl.noaa.gov/csd/assessments/ozone/2018/.

WMO (2017) Greenhouse Gas Bulletin. The state of greenhouse gases in the atmosphere using global observations through 2016. Geneva, World Meteorological Organization (GHG Bulletin No. 13, 30 October 2017). https://library.wmo.int/opac/doc_num.php?explnum_id=4022.

WMO (2016) Greenhouse Gas Bulletin. The state of greenhouse gases in the atmosphere using global observations through 2015. Geneva, World Meteorological Organization (GHG Bulletin No. 12, 24 October 2016). http://library.wmo.int/pmb_ged/ghg-bulletin_12_en.pdf.

WMO (2015) Greenhouse Gas Bulletin. The state of greenhouse gases in the atmosphere using global observations through 2014. Geneva, World Meteorological Organization (GHG Bulletin No. 11, 9 November 2015). http://library.wmo.int/pmb_ged/ghg-bulletin_11_en.pdf.

WMO (2014) Greenhouse Gas Bulletin. The state of greenhouse gases in the atmosphere using global observations through 2013. Geneva, World Meteorological Organization (GHG Bulletin No. 10, 9th September 2014). http://library.wmo.int/opac/index.php?lvl=notice_display&id=16396#.VGHPz5-gQtK.

WMO (2014b) Scientific assessment of ozone depletion: 2014. Geneva, World Meteorological Organization (Global ozone research and monitoring project, Report No. 55). https://www.esrl.noaa.gov/csd/assessments/ozone/2014/chapters/2014OzoneAssessment.pdf.

WMO (2013) Greenhouse Gas Bulletin. The state of greenhouse gases in the atmosphere using global observations through 2012. Geneva, World Meteorological Organization (GHG Bulletin No. 9, 6 November 2013). http://www.wmo.int/pages/prog/arep/gaw/ghg/documents/GHG_Bulletin_No.9_en.pdf.

WMO (2012) Greenhouse Gas Bulletin. The state of greenhouse gases in the atmosphere using global observations through 2011. Geneva, World Meteorological Organization (GHG Bulletin No. 8, 19 November 2012). http://www.wmo.int/pages/prog/arep/gaw/ghg/documents/GHG_Bulletin_No.8_en.pdf.

WMO (2011) Scientific assessment of ozone depletion: 2010. Geneva, World Meteorological Organization (Global ozone research and monitoring project, Report No. 52).

Xian, P., Zhang, J., O'Neill, N.T., Reid, J.S., Toth, T.D., Sorenson, B., Hyer, E.J., Campbell, J.R., and K. Ranjbar (2022) Arctic spring and summertime aerosol optical depth baseline from long-term observations and model reanalyses – Part 2: Statistics of extreme AOD events, and implications for the impact of regional biomass burning processes. *Atmos. Chem. Phys., 22,* 9949-9967, https://doi.org/10.5194/acp-22-9949-2022.

Xu, Y., Zaelke, D., Velders, G.J.M., Ramanathan, V. (2013) The role of HFCs in mitigating 21st century climate change. *Atmos. Chem. Phys., 13,* 6083-6089. https://doi.org/10.5194/acp-13-6083-2013.

Zanatta, M., Gysel, M., Bukowiecki, N., Müller, T., Weingartner, E., Areskoug, H., Fiebig, M., Yttri, K. E., Mihalopoulos, N., Kouvarakis, G., Beddows, D., Harrison, R. M., Cavalli, F., Putaud, J. P., Spindler, G., Wiedensohler, A., Alastuey, A., Pandolfi, M., Sellegri, K., Swietlicki, E., Jaffrezo, J. L., Baltensperger, U., Laj, P. (2016) A European aerosol phenomenology-5: Climatology of black carbon optical properties at 9 regional background sites across Europe. *Atmos. Environ., 145,* 346-364. https://doi.org/10.1016/j.atmosenv.2016.09.035.

Zeileis A. (2004) Econometric Computing with HC and HAC Covariance Matrix Estimators. *J. Stat. Software*, *11,* 1-17. https://doi.org/https://doi.org/10.18637/jss.v011.i10.

Zeileis, A. (2006) Object-oriented computation of sandwich estimators. *J. Stat. Software*, *16,* 1-16. https://doi.org/10.18637/jss.v016.i09.

Appendix A

Data Tables

Table A 1: Annual mean concentration for all greenhouse gases included in the programme at Zeppelin and Birkenes. All concentrations are mixing ratios in ppt, except for methane and carbon monoxide (ppb) and carbon dioxide (ppm). The annual means are based on a combination of the measurements and the fitted values; during periods with lacking observations we have used the fitted mixing ratios in the calculation of the annual mean. All underlying measurement data are open and accessible and can be downloaded directly from the database: http://ebas.nilu.no/

Component	*2001*	2002	2003	2004	2005	2006	2007	2008	2009	2010	2011	2012	2013	2014	2015	2016	2017	2018	2019	2020	2021	2022
Carbon dioxide - Zeppelin												394.8	397.4	399.6	401.0	404.4	408.0	409.3	411.9	414.2	417.4	419.6
Carbon dioxide - Birkenes									391.4	394.1	396.6	397.9	400.7	402.8	405.2	409.8	411.2	415.2	416.1	418.8	421.3	423.9
Methane - Zeppelin	*1845.1*	1843.2	1855.5	1853.0	1852.0	1853.2	1863.3	1873.2	1888.2	1880.0	1879.8	1891.9	1898.0	1910.0	1920.2	1931.8	1938.9	1938.5	1953.1	1968.8	1981.9	1999.6
Methane - Birkenes									1881.2	1887.2	1895.6	1900.5	1902.5	1917.3	1926.1	1941.9	1945.3	1953.0	1961.2	1975.3	1991.7	2005.5
Carbon monoxide	*130.3*	126.1	140.3	130.4	128.7	126.2	120.3	120.1	117.9	128.8	115.5	120.7	113.1	113.4	112.8	112.4	114.3	113.6	115.6	117.6	128.0	115.0
Nitrous oxide										323.6	324.2	325.1	326.1	327.2	328.0	329.0	330.0	331.3	332.1	333.4	334.4	335.8
Chlorofluorocarbons																						
CFC-11	259.3	257.2	254.9	253.2	251.0	249.2	246.5	244.6	242.7	240.8	238.6	237.4	235.9	234.2	233.0	231.5	230.1	229.1	227.3	224.9	222.6	220.7
CFC-12	547.4	547.6	547.6	545.6	546.7	546.2	542.2	541.5	537.7	534.5	531.6	529.0	526.2	522.9	519.4	516.2	512.4	509.1	505.4	501.6	498.0	494.3
CFC-113	81.4	80.8	80.0	79.4	78.8	77.9	77.5	76.8	76.2	75.5	74.7	74.1	73.5	73.0	72.3	71.7	71.1	70.6	70.0	69.5	69.1	68.7
CFC-115	8.22	8.18	8.22	8.28	8.41	8.39	8.37	8.40	8.43	8.42	8.42	8.44	8.43	8.46	8.51	8.53	8.59	8.66	8.73	8.75	8.81	8.90
Hydrochlorofluorocarbons																						
HCFC-22	158.4	164.1	170.7	175.9	181.5	189.2	196.4	204.6	212.4	219.7	225.8	231.0	236.4	241.2	245.3	248.8	252.2	255.2	257.6	258.2	258.6	258.0
HCFC-141b	16.8	17.9	18.7	19.3	19.5	20.0	20.5	21.2	21.6	22.2	23.1	24.0	24.6	25.3	25.5	25.9	25.8	25.6	25.8	26.1	26.2	26.0
HCFC-142b	14.3	15.0	15.9	16.7	17.3	18.3	19.3	20.3	21.3	22.0	22.7	22.9	23.2	23.3	23.5	23.5	23.5	23.3	23.2	22.9	22.7	22.1
Hydrofluorocarbons																						
HFC-125	2.2	2.6	2.9	3.3	4.0	4.9	5.8	6.9	8.0	9.6	11.8	13.5	15.6	17.9	20.3	22.9	25.8	28.9	32.3	35.6	39.4	43.5
HFC-134a	21.1	26.0	30.7	35.4	39.8	44.1	48.5	53.4	57.8	63.6	68.6	73.7	79.0	84.6	90.2	96.5	103.1	108.4	114.6	120.0	125.9	132.1
HFC-152a	2.6	3.4	4.3	5.1	5.8	6.8	7.8	8.6	9.0	9.5	10.0	10.2	10.2	10.1	10.1	10.2	10.3	10.3	10.6	10.5	10.7	10.8
HFC-23										23.8	24.7	25.6	26.7	27.7	28.7	29.6	30.7	31.9	33.2	34.5	35.6	36.6
HFC-365mfc										0.72	0.79	0.87	0.93	1.02	1.10	1.19	1.24	1.29	1.32	1.33	1.34	1.36
HFC-227ea										0.70	0.79	0.88	0.99	1.10	1.21	1.34	1.47	1.59	1.75	1.90	2.08	2.26

Component	*2001*	2002	2003	2004	2005	2006	2007	2008	2009	2010	2011	2012	2013	2014	2015	2016	2017	2018	2019	2020	2021	2022
HFC-236fa										0.09	0.10	0.11	0.13	0.14	0.15	0.16	0.17	0.19	0.21	0.22	0.23	0.24
HFC-245fa										1.64	1.80	1.98	2.19	2.39	2.58	2.80	3.04	3.26	3.53	3.70	3.83	3.97
HFC-32										5.68	6.57	7.66	9.28	10.93	12.89	15.23	18.26	21.54	25.22	28.70	32.74	37.72
HFC-4310mee										0.21	0.22	0.24	0.25	0.26	0.27	0.28	0.29	0.29	0.30	0.31	0.32	0.32
HFC-143a										11.86	13.18	14.58	16.03	17.63	19.09	20.73	22.51	23.92	25.57	27.11	28.79	30.49
Perfluorinated compounds																						
PFC-14															82.43	83.32	84.27	85.25	86.11	86.94	87.98	88.99
PFC-116										4.11	4.20	4.27	4.37	4.45	4.55	4.64	4.74	4.82	4.91	5.00	5.10	5.20
PFC-218										0.56	0.57	0.59	0.60	0.61	0.63	0.64	0.66	0.67	0.69	0.71	0.73	0.75
PFC-318										1.28	1.33	1.38	1.43	1.47	1.53	1.59	1.66	1.73	1.80	1.87	1.95	2.04
Sulphurhexafluoride	4.95	5.14	5.37	5.61	5.82	6.09	6.31	6.64	6.93	7.19	7.50	7.78	8.11	8.43	8.75	9.09	9.46	9.80	10.14	10.45	10.84	11.24
Nitrogen trifluoride																1.61	1.76	1.98	2.21	2.48	2.78	3.10
Sulfuryl fluoride										1.71	1.81	1.91	2.03	2.12	2.22	2.33	2.45	2.52	2.63	2.74	2.88	3.01
Halons																						
H-1211	4.39	4.43	4.48	4.53	4.52	4.48	4.43	4.39	4.33	4.26	4.18	4.09	3.97	3.87	3.77	3.65	3.55	3.45	3.37	3.27	3.18	3.09
H-1301	2.99	3.07	3.13	3.17	3.21	3.22	3.24	3.28	3.29	3.32	3.33	3.35	3.36	3.37	3.39	3.38	3.39	3.38	3.39	3.39	3.39	3.39
H-2402										0.47	0.46	0.45	0.44	0.44	0.43	0.42	0.41	0.41	0.41	0.40	0.40	0.39
Other halocarbons																						
Chloromethane	506.6	521.1	526.5	522.7	519.1	520.7	523.3	525.2	526.3	520.7	509.6	515.5	519.2	514.3	512.6	521.4	516.7	514.2	507.7	508.6	511.1	515.0
Bromomethane	9.17	9.14	8.87	8.86	8.52	8.57	8.31	7.76	7.37	7.29	7.20	7.07	6.99	6.88	6.70	6.74	6.56	6.54	6.71	6.66	6.75	6.61
Dichloromethane	31.19	31.44	32.49	32.51	32.28	33.53	35.58	37.62	38.61	42.17	42.05	44.85	53.57	54.24	53.67	56.46	61.23	60.75	59.18	63.22	68.82	71.38
Trichloromethane	11.12	10.68	10.70	10.35	10.38	10.43	10.62	10.44	10.87	11.52	11.99	12.19	12.75	13.48	13.66	14.22	15.32	14.80	12.31	13.13	12.72	12.28
Carbon tetrachloride										86.73	85.27	84.43	83.48	82.53	81.76	80.64	79.48	78.88	78.03	77.16	76.15	74.96
Trichloroethane	37.69	31.94	27.29	22.92	19.23	15.97	13.38	11.12	9.23	7.74	6.47	5.33	4.47	3.76	3.26	2.79	2.36	2.01	1.72	1.55	1.37	0.97
Trichloroethene	0.71	0.66	0.57	0.53	0.51	0.49	0.34	0.38	0.54	0.53	0.55	0.49	0.55	0.49	0.44	0.42	0.41	0.42	0.38	0.31	0.31	0.21

Component	*2001*	2002	2003	2004	2005	2006	2007	2008	2009	2010	2011	2012	2013	2014	2015	2016	2017	2018	2019	2020	2021	2022
Tetrachloroethene	4.63	4.21	4.07	3.89	3.39	2.91	3.14	2.72	2.97	3.13	2.82	2.67	2.55	2.57	2.58	2.55	2.48	2.31	2.29	2.12	2.14	2.00
Volatile Organic Compounds (VOC)																						
Ethane										1487.1	1472.3	1584.9	1567.7	1643.5	1634.5	1572.9	1577.1	1525.9	1603.8	1522.6	1541.8	1487.5
Propane										531.0	528.8	571.4	578.3	567.8	530.4	551.1	583.0	497.3	455.4	344.9	355.0	462.7
Butane										197.5	187.6	200.5	203.8	192.1	175.2	162.2	193.0	143.5	140.3	121.2	117.0	169.7
Pentane										67.7	61.8	63.3	67.4	63.8	59.2	56.1	60.9	39.2	44.0	42.2	42.2	55.7
Benzene										84.5	72.7	74.6	69.6	71.4	68.3	67.3	62.7	63.8	62.3	63.0	68.2	60.3
Toluene										35.4	29.3	28.6	26.6	28.6	25.7	25.4	18.1	20.9	19.1	19.6	20.2	18.4

*Trichloroethene: Larger uncertainties in the numbers due to low concentrations, memory effects and blanks in the instrument. The reference numbers (scale UB-98) have also larger uncertainties for the same reasons.
**Tetrachloroethene: Larger uncertainties in the 2001-2010 numbers due to larger variability in the measurements with the ADS-GCMS instrument.

Table A 2: All calculated trends per year, error and regression coefficient for the fit. The trends are all in ppt per year, except for CH_4, N_2O, and CO which are in ppb and CO_2 is in ppm. The negative trends are in blue, and the positive trends are shown in red.

Component	Formula	Trend/yr	Error	R^2
Carbon dioxide - Zeppelin	CO_2	2.49	0.03	0.97
Carbon dioxide - Birkenes		2.53	0.04	0.83
Methane - Zeppelin	CH_4	7.05	0.09	0.94
Methane - Birkenes		9.36	0.17	0.78
Carbon monoxide	CO	-0.79	0.21	0.76
Nitrous oxide	N_2O	1.03	0.01	0.99
Chlorofluorocarbons				
CFC-11	CCl_3F	-1.77	0.012	0.99
CFC-12	CF_2Cl_2	-2.71	0.019	0.99
CFC-113	CF2ClCFCl2	-0.62	0.002	1.00
CFC-115	CF_3CF_2Cl	0.03	0.001	0.82
Hydrochlorofluorocarbons				
HCFC-22	$CHClF_2$	5.20	0.032	0.997
HCFC-141b	$C_2H_3FCl_2$	0.47	0.014	0.973
HCFC-142b	CH_3CF_2Cl	0.41	0.012	0.981
Hydrofluorocarbons				
HFC-125	CHF_2CF_3	1.93	0.005	0.999
HFC-134a	CH_2FCF_3	5.28	0.012	0.999
HFC-152a	CH_3CHF_2	0.36	0.009	0.964
HFC-23	CHF_3	1.08	0.006	0.998
HFC-365mfc	$CH_3CF_2CH_2CF_3$	0.06	0.0005	0.981
HFC-227ea	CF_3CHFCF_3	0.13	0.0003	0.999
HFC-236fa	$CF_3CH_2CF_3$	0.01	0.00005	0.988
HFC-245fa	$CHF_2CH_2CF_3$	0.20	0.001	0.996
HFC-32	CH_2F_2	2.65	0.009	0.999
HFC-4310mee	$C_5H_2F_{10}$	0.01	0.000	0.965
HFC-143a	CH_3CF_3	1.56	0.003	0.998
Perfluorinated compounds				
PFC-14	CF_4	0.929	0.0353	0.997
PFC-116	C_2F_6	0.090	0.0002	0.997
PFC-218	C_3F_8	0.016	0.0001	0.987
PFC-318	$c\text{-}C_4F_8$	0.062	0.0002	0.997
Sulphurhexafluoride	SF_6	0.301	0.0004	0.999
Nitrogen trifluoride	NF_3	0.250	0.0266	0.998
Sulfuryl fluoride	SO_2F_2	0.106	0.0006	0.994
Halons				
H-1211	$CBrClF_2$	-0.072	0.0003	0.997

Component	Formula	Trend/yr	Error	R^2
H-1301	$CBrF_3$	0.016	0.0003	0.789
H-2402	$CBrF_2CBrF_2$	-0.006	0.00004	0.969
Halogenated compounds				
Chloromethane	CH_3Cl	-0.447	0.1685	0.869
Bromomethane	CH_3Br	-0.136	0.0059	0.878
Dichloromethane	CH_2Cl_2	2.016	0.0631	0.937
Trichloromethane	$CHCl_3$	0.179	0.0149	0.680
Carbon tetrachloride	CCl_4	-0.940	0.0094	0.969
Trichloroethane	CH_3CCl_3	-1.509	0.0090	0.999
Trichloroethene*	$CHClCCl_2$	-0.014	0.0029	0.410
Tetrachloroethene**	CCl_2CCl_2	-0.102	0.0063	0.544
Volatile Organic Compounds (VOC)				
Ethane***	C_2H_6	-0.29	3.60	0.87
Propane***	C_3H_8	-15.18	3.36	0.78
Butane***	C_4H_{10}	-6.28	1.46	0.71
Pentane***	C_5H_{12}	-2.05	0.48	0.66
Benzene***	C_6H_6	-1.40	0.38	0.85
Toluene***	$C_6H_5CH_3$	-1.28	0.24	0.70

**Trichloroethene: Larger uncertainties in the numbers due to low concentrations, memory effects and blanks in the instrument. The reference numbers (scale UB-98) have also larger uncertainties for the same reasons.*

***Tetrachloroethene: Larger uncertainties in the 2001-2010 numbers due to larger variability in the measurements with the ADS-GCMS instrument.*

**** Larger uncertainty for VOC due to shorter timeseries*

Table A 3: 2010 to 2022 seasonal and annual means of integral particle concentrations in the ultrafine (0.002 to 0.01 µm), fine (0.01 to 1 µm) and coarse (1 to 10 µm) particle size range for Birkenes, Trollhaugen, and Zeppelin stations.

		Birkenes				Trollhaugen[1]		Zeppelin	
Year	Season	N_{ait}/ cm^{-3}	N_{acc}/ cm^{-3}	N_{coa}/ cm^{-3}	N_{tot}/ cm^{-3}	N_{ait} / cm^{-3}	$^{2}N_{acc}$/ cm^{-3}	N_{ait}/ cm^{-3}	$^{2}N_{acc}$/ cm^{-3}
2009/10	Winter	467	433	0.296	967				
2010	Spring	1249	372	0.704	1633				
2010	Summer	1807	555	0.643	2381				
2010	Autumn	912	343	0.562	1358				
2010	Whole Year	1101	412	0.575	1593				
2010/11	Winter	544	320	0.974	863				
2011	Spring	1341	422	1.620	1765				
2011	Summer	1661	497	1.250	2161				
2011	Autumn	1908	560	1.844	2470				
2011	Whole Year	1215	417	1.427	1644				
2011/12	Winter	433	217	0.927	664				
2012	Spring	1179	303	0.982	1523				
2012	Summer	1447	435	1.041	1892				
2012	Autumn	722	169	0.918	898				
2012	Whole Year	951	288	0.912	1258				
2012/13	Winter	421	203	0.550	626				
2013	Spring	1314	392	1.012	1711				
2013	Summer	1680	497	0.951	2182				
2013	Autumn	785	183	0.952	968				
2013	Whole Year	1107	335	0.951	1454				
2013/14	Winter	737	342	1.246	1079				
2014	Spring	1569	429	0.823	1998	183	32		
2014	Summer	1717	642	0.757	2358	43	19		
2014	Autumn	1286	532	0.950	1818	207	28		
2014	Whole Year	1333	488	0.859	1821	183	34		
2014/15	Winter	567	203	1.038	770	368	67		
2015	Spring	1571	360	1.030	1931	134	25		
2015	Summer	2198	614	0.866	2812	38	23		
2015	Autumn	1081	378	0.766	1459	221	28		
2015	Whole Year	1363	395	0.963	1758	171	32		
2015/16	Winter	594	245	0.867	839				
2016	Spring	1471	483	0.848	1954	170	26		
2016	Summer	1608	535	0.876	2143	47	18	156	64
2016	Autumn	983	319	0.707	1302	262	35	47	31
2016	Whole Year	1167	391	0.804	1558	231	37	---	---
2016/17	Winter	585	219	0.717	804	473	74	---	---
2017	Spring	1474	476	0.564	1950	157	31	96	126
2017	Summer	1599	537	1.013	2136	51	20	282	70
2017	Autumn	1291	440	0.734	1731	265	27	56	63
2017	Whole Year	1256	424	0.721	1679	238	38	---	---
2017/18	Winter	517	275	0.399	792	482	78	27	44
2018	Spring	1511	649	---	2159	170	24	107	85
2018	Summer	1948	617	---	2565	45	18	225	66
2018	Autumn	986	300	---	1286	273	28	30	25
2018	Whole Year	1255	460	---	1715	233	35	92	55
2018/19	Winter	578	229	---	806	427	64	18	60
2019	Spring	1406	500	---	1906	183	25	78	95
2019	Summer	1867	509	---	2376	34	14	224	68
2019	Autumn	805	185	---	990	233	29	29	28
2019	Whole Year	1163	356	---	1519	202	31	87	64
2019/20	Winter	567	133	---	700	398	78	25	78
2020	Spring	1480	291	---	1770	187	27	90	88
2020	Summer	1570	554	---	2125	36	13	148	96
2020	Autumn	907	251	---	1158	237	28	34	38
2020	Whole Year	1133	306	---	1439	219	37	77	75
2020/2021	Winter	503	160	---	721	395	72	16	23
2021	Spring	1107	255	---	1490	213	29	38	54

Year	Season	Birkenes				Trollhaugen[1]		Zeppelin	
		N_{ait}/ cm^{-3}	N_{acc}/ cm^{-3}	N_{coa}/ cm^{-3}	N_{tot}/ cm^{-3}	N_{ait} / cm^{-3}	$^{2}N_{acc}$/ cm^{-3}	N_{ait}/ cm^{-3}	$^{2}N_{acc}$/ cm^{-3}
2021	Summer	1560	548	0.608	2217	46	11	127	39
2021	Autumn	977	195	0.703	1236	429	33	35	23
2021	Whole Year	1062	294	---	1445	289	38	61	34
2021/2022	Winter	457	97	---	593	528	91	---	---
2022	Spring	1664	308	---	2185	251	29	77	93
2022	Summer	1860	457	---	2512	49	10	164	61
2022	Autumn	1061	184	---	1319	360	24	28	13
2022	Whole Year	1298	273	---	1711	285	36	83	53

[1] Cells shaded in grey mark values obtained with an older instrument version that can't be compared directly with later values. Numbers
given for the time when the respective season is present in the Northern hemisphere. Actual seasons in Southern hemisphere are shifted by 6 months. In 2020, numbers for Birkenes have been reprocessed for all years since 2010 taking into account recent intercalibrations.
[2]The accumulation mode integral particle concentration N_{acc} at Trollhaugen and Zeppelin extends only up to 0.8 µm particle diameter due to lack of an instrument covering larger particles. For Birkenes, N_{acc} includes particles up to 1 µm diameter

Table A 4: 2010 - 2022 seasonal and annual means of optical aerosol properties scattering coefficient, absorption coefficient, and single scattering albedo (all at 550 nm) for Birkenes, Trollhaugen, and Zeppelin stations, as far as available.

		Birkenes			Trollhaugen[1]			Zeppelin		
Year	Season	σ_{sp} Mm^{-1}	σ_{ap} Mm^{-1}	v_0	σ_{sp} Mm^{-1}	σ_{ap} Mm^{-1}	v_0	σ_{sp} Mm^{-1}	σ_{ap} Mm^{-1}	v_0
2009/10	Winter	16.82	3.09	0.88						
2010	Spring	12.33	0.78	0.93						
2010	Summer	11.30	0.70	0.94						
2010	Autumn	7.26	0.71	0.90						
2010	Whole Year	11.52	1.24	0.91						
2010/11	Winter	16.96	2.18	0.89						
2011	Spring	18.67	1.26	0.93						
2011	Summer	15.43	0.74	0.95						
2011	Autumn	29.74	2.87	0.92						
2011	Whole Year	20.26	1.69	0.93						
2011/12	Winter	11.29	1.00	0.91						
2012	Spring	15.10	0.86	0.93						
2012	Summer	12.62	0.67	0.95						
2012	Autumn	9.80	0.65	0.92						
2012	Whole Year	12.22	0.83	0.92						
2012/13	Winter	12.48	1.84	0.84						
2013	Spring	17.03	1.48	0.90						
2013	Summer	13.81	1.15	0.92						
2013	Autumn	8.89	1.25	0.85						
2013	Whole Year	13.73	1.40	0.88						
2013/14	Winter	22.89	2.64	0.87						
2014	Spring	12.95	2.09	0.87	0.74	-0.05	0.95			
2014	Summer	15.85	1.26	0.92	1.39	0.04	0.98			
2014	Autumn	18.76	3.41	0.82	1.02	0.15	0.93			
2014	Whole Year	16.99	2.30	0.87	1.01	0.09	0.95			
2014/15	Winter	13.98	1.30	0.89	0.74	0.04	0.94			
2015	Spring	12.72	1.48	0.89	0.65	0.02	0.97			
2015	Summer	12.45	1.46	0.90	2.44	0.02	0.98			0.30
2015	Autumn	15.69	2.45	0.95	1.32	0.07	0.94			0.14
2015	Whole Year	14.36	1.56	0.90	1.32	0.04	0.96			
2015/16	Winter	13.59	1.24	0.88	0.87	0.05	0.94			0.38
2016	Spring	14.86	1.10	0.91	0.78	0.17	0.97			0.39
2016	Summer	11.93	0.77	0.94	2.01	0.00	0.99			0.09
2016	Autumn	11.47	1.46	0.85	1.54	0.04	0.95			0.12
2016	Whole Year	12.26	1.12	0.89	1.31	0.06	0.97			0.24
2016/17	Winter	12.27	2.24	0.81	0.82	0.05	0.94			0.40
2017	Spring	8.71			0.76	0.02	0.97			0.48
2017	Summer	8.58			1.57	0.01	0.99			0.10
2017	Autumn	8.09	1.21	0.85	1.22	0.05	0.94			0.29
2017	Whole Year	9.07			1.10	0.03	0.96			0.33
2017/18	Winter	13.56	1.66	0.83	0.72	0.04	0.95			0.34
2018	Spring	17.10	2.45	0.87	0.60	0.03	0.97			0.32
2018	Summer	13.62	1.23	0.91	1.78	0.06	0.98			0.12
2018	Autumn	14.08	2.04	0.86	1.31	0.04	0.95			0.10
2018	Whole Year	14.54	1.90	0.86	1.10	0.04	0.96			0.21
2018/19	Winter	---	---	---	0.73	0.04	0.94			0.45
2019	Spring	---	---	---	0.81	0.03	0.97			0.46
2019	Summer	---	---	---	1.81	0.01	0.99			0.19
2019	Autumn	6.26	0.93	0.85	1.61	0.04	0.96			0.13
2019	Whole Year	---	---	---	1.26	0.03	0.97			0.33
2019/20	Winter	10.15	0.96	0.87	0.88	0.04	0.95			0.73
2020	Spring	10.84	1.03	0.90	0.89	0.02	0.98			0.36
2020	Summer	11.28	1.07	0.91	1.43	0.01	0.99			0.24
2020	Autumn	12.63	1.53	0.88	1.60	0.04	0.97			0.13
2020	Whole Year	11.62	1.21	0.89	1.19	0.03	0.97			0.36
2020/21	Winter	9.81	1.76	0.80	0.80	0.11	0.95			0.17
2021	Spring	8.38	0.76	0.87	0.66	0.02	0.98			0.50
2021	Summer	17.36	1.08	0.93	1.88	0.02	0.99			0.08
2021	Autumn	12.23	1.21	0.86	1.27	0.14	0.95			0.20
2021	Whole Year	11.42	1.14	0.86	1.23	0.07	0.97			0.25
2021/22	Winter	8.74	1.11	0.85	1.14	0.13	0.95			
2022	Spring	15.63	2.12	0.89	0.76	0.04	0.98			
2022	Summer	12.9	0.9	0.94	1.59	0.02	0.99			
2022	Autumn	12.43	1.41	0.87	1.15	0.12	0.96			
2022	Whole Year	12.43	1.4	0.89	1.12	0.08	0.97			

Table A 5: Monthly means and standard deviation of AOD at 500 nm in Ny-Ålesund.

Month/ Year	Jan	Feb	Mar	Apr	May	Jun	Jul	Aug	Sep	Oct	Nov	Dec
Aerosol optical depth (AOD)												
2002				0.06 ±0.01	0.08 ±0.03	0.06 ±0.02	0.07 ±0.12	0.07 ±0.08	0.06 ±0.05			
2003			0.15 ±0.12	0.11 ±0.05	0.15 ±0.06	0.10 ±0.03	0.04 ±0.01	0.05 ±0.02	0.06 ±0.03			
2004			0.06 ±0.00	0.12 ±0.08	0.13 ±0.09	0.06 ±0.01	0.10 ±0.07	0.05 ±0.02	0.04 ±0.02			
2005			0.08 ±0.03	0.12 ±0.07	0.10 ±0.03	0.05 ±0.02	0.05 ±0.02	0.04 ±0.03	0.03 ±0.01			
2006			0.12 ±0.03	0.16 ±0.07		0.04 ±0.00	0.05 ±0.02	0.05 ±0.04	0.04 ±0.03			
2007				0.10 ±0.05	0.10 ±0.12	0.07 ±0.03	0.05 ±0.01	0.05 ±0.02	0.04 ±0.03			
2008			0.13 ±0.05	0.14 ±0.06	0.14 ±0.04	0.06 ±0.02	0.06 ±0.02	0.09 ±0.03	0.16 ±0.03			
2009					0.11 ±0.03	0.08 ±0.02	0.11 ±0.04	0.10 ±0.02	0.09 ±0.01			
2010			0.11±0.03	0.08 ±0.03	0.08 ±0.01	0.06 ±0.01	0.05 ±0.01	0.05 ±0.01				
2011					0.08 ±0.02	0.08 ±0.01	0.05 ±0.01	0.06 ±0.02	0.05 ±0.01			
2012			0.10 ±0.03	0.10 ±0.02	0.10 ±0.03	0.06 ±0.02	0.06 ±0.02	0.07 ±0.03	0.07 ±0.03			
2013			0.11 ±0.04	0.09 ±0.04	0.06 ±0.02	0.05 ±0.01	0.06 ±0.02	0.05 ±0.01	0.04 ±0.02			
2014				0.07 ±0.01	0.10 ±0.02	0.06 ±0.02	0.06 ±0.03	0.08 ±0.01	0.11 ±0.05			
2015			0.05 ±0.02	0.10 ±0.03	0.07 ±0.02	0.05 ±0.01	0.15 ±0.20	0.05 ±0.02	0.05 ±0.01			
2016			0.08 ±0.03	0.06 ±0.02	0.08 ±0.03	0.07 ±0.02	0.04 ±0.01	0.05 ±0.04	0.03 ±0.01			
2017				0.07 ±0.03	0.07 ±0.03	0.04 ±0.01	0.04 ±0.01	0.05 ±0.01	0.07 ±0.01			
2018	0.05 ±0.01		0.05 ±0.01	0.08 ±0.02	0.07 ±0.02	0.04 ±0.01	0.03 ±0.01	0.08 ±0.07	0.05 ±0.02	0.10 ±0.01	0.04 ±0.00	0.05 ±0.01
2019	0.10 ±0.01	0.07 ±0.02		0.06 ±0.02	0.07 ±0.02	0.05 ±0.01	0.20 ±0.09	0.19 ±0.04	0.10 ±0.01	0.08 ±0.00		
2020		0.08 ±0.02	0.07 ±0.04	0.07 ±0.01	0.08 ±0.01							
2021		0.03 ±0.00	0.07 ±0.08		0.06 ±0.03	0.06 ±0.03	0.08 ±0.10	0.07 ±0.04	0.06 ±0.01	0.04 ±0.01		0.03 ±0.01
2022	0.07 ±0.02	0.06 ±0.01	0.09 ±0.03	0.08 ±0.02	0.08 ±0.02	0.06 ±0.03	0.04 ±0.01	0.03 ±0.01	0.03 ±0.00		0.01 ±0.01	0.05 ±0.02
Mean 2009-2022	0.08 ±0.02	0.06 ±0.02	0.09 ±0.03	0.09 ±0.03	0.09 ±0.02	0.06 ±0.01	0.07 ±0.04	0.07 ±0.03	0.06 ±0.03	0.09 ±0.01	0.02 ±0.01	0.05 ±0.00

[1]Numbers given for the time when the respective season is present in the Northern hemisphere. Actual seasons in Southern hemisphere are shifted by 6 months.

Table A 6: Monthly means and standard deviation of the Ångström coefficient (Å) in Ny-Ålesund.

Month/ Year	Jan	Feb	Mar	Apr	May	Jun	Jul	Aug	Sep	Oct	Nov	Dec
Ångström Exponent												
2002				0.9 ±0.1	1.4 ±0.1	1.2 ±0.3	1.2 ±0.2	1.3 ±0.4	1.2 ±0.5			
2003			0.9 ±0.5	1.3 ±0.3	1.3 ±0.2	1.5 ±0.1	1.5 ±0.3	1.4 ±0.5	1.4 ±0.3			
2004			1.3 ±0.1	1.2 ±0.3	1.4 ±0.5	1.7 ±0.2	1.6 ±0.4	1.5 ±0.3	1.3 ±0.3			
2005			1.1 ±0.3	1.4 ±0.4	1.0 ±0.2	1.6 ±0.3	1.7 ±0.2	1.4 ±0.7	1.5 ±0.4			
2006			0.9 ±0.1	0.9 ±0.3		1.7 ±0.2	1.4 ±0.3	1.3 ±0.6	1.4 ±0.3			
2007				1.4 ±0.4	1.4 ±0.6	1.7 ±0.2	1.6 ±0.2	1.7 ±0.3	1.5 ±0.4			
2008			1.4 ±0.2	1.3 ±0.2	1.4 ±0.2	1.4 ±0.4	1.2 ±0.2	1.3 ±0.3	1.4 ±0.3			
2009					1.3 ±0.4	1.4 ±0.2	1.3 ±0.3	1.2 ±0.1	1.1 ±0.1			
2010			1.0 ±0.3	1.4 ±0.2	1.3 ±0.2	1.3 ±0.3	1.4 ±0.2	1.0 ±0.1				
2011					1.7 ±0.3	1.8 ±0.1	1.5 ±0.1	1.4 ±0.3	1.6 ±0.2			
2012			1.1 ±0.2	1.3 ±0.2	1.2 ±0.2	1.1 ±0.1	1.3 ±0.2	1.4 ±0.2	1.5 ±0.2			
2013			1.3 ±0.2	1.2 ±0.3	1.4 ±0.2	1.6 ±0.3	1.3 ±0.2	1.4 ±0.2	1.2 ±0.5			
2014				1.4 ±0.1	1.4 ±0.1	1.3 ±0.3	1.5 ±0.1	1.5 ±0.1	1.5 ±0.2			
2015			1.32 ±0.17	1.23 ±0.26	1.47 ±0.14	1.50 ±0.20	1.47 ±0.16	1.56 ±0.16	1.18 ±0.52			
2016			1.30 ±0.21	1.56 ±0.12	1.57 ±0.06	1.49 ±0.19	1.45 ±0.28	1.52 ±0.18	1.43 ±0.22			
2017				1.46 ±0.20	1.46 ±0.21	1.38 ±0.09	1.57 ±0.11	1.54 ±0.09	1.36 ±0.06			
2018	1.34 ±0.12		1.41 ±0.08	1.35 ±0.15	1.22 ±0.31	1.47 ±0.17	1.43 ±0.08	1.41 ±0.10	1.16 ±0.12	1.03 ±0.03	1.02 ±0.03	1.11 ±0.07
2019	1.59 ± 0.16	1.35 ± 0.23		1.25 ± 0.27	1.47 ± 0.23	1.35 ± 0.23	1.38± 0.18	1.30 ± 0.10	1.28 ± 0.06	1.19 ± 0.12		
2020		1.10 ± 0.39	1.14 ±0.19	1.45 ± 0.06	1.49 ± 0.09							
2021		1.46 ±0.12	1.25 ±0.41		1.16 ± 0.36	1.36 ± 0.34	1.49 ± 0.32	1.56 ± 0.39	1.50 ±0.23	0.65 ±0.31		1.37 ±0.44
2022	1.00 ±0.23	1.18 ±0.24	1.39 ±0.24	1.43 ±0.19	1.42 ±0.12	1.30 ±0.21	1.25 ±0.12	1.44 ±0.11	1.44 ±0.11		0.63 ±0.46	1.17 ±0.28
Mean 2009-2022	1.15 ±0.35	1.08 ±0.25	1.19 ±0.17	1.30 ±0.17	1.40 ±0.15	1.45 ±0.19	1.43 ±0.13	1.41 ±0.14	1.36 ±0.14	1.18 ±0.15	0.83 ±0.20	1.14 ±0.03

Table A 7: Number of days with AOD observations in Ny-Ålesund made within the months.

Month/Year	Jan	Feb	Mar	Apr	May	Jun	Jul	Aug	Sep	Oct	Nov	Dec
Number of days with cloud-free and quality assured observations												
2002				4	15	11	6	9	14			
2003			3	12	16	8	15	17	12			
2004			2	8	13	9	5	12	12			
2005			12	17	24	15	10		11			
2006			6	12		5	12	4	13			
2007				16	9	12	17	10	9			
2008			15	12	14	20	16	13	2			
2009					7	10	17	8	8			
2010			7	18	7	10	12	3	1			
2011					2	2	7	4	6			
2012			6	18	12	15	16	11	4			
2013			5	13	10	10	8	7	9			
2014				13	9	9	9	14	4			
2015			5	17	15	9	17	13	6			
2016			6	14	8	7	12	10	7			
2017				13	19	11	12	6	3			
2018	7		3	10	5	12	9	11	5	2	2	2
2019	9	3		10	19	18	9	16	7	1		
2020		11	5	6	7							
2021		3	17		14	22	19	17	4	6		9
2022	4	10	8	22	22	10	10	12	4		3	6
Total 2002-2022	26	25	84	236	251	217	236	189	145	9	5	17

Table A 8: Monthly means and standard deviation of AOD at 500 nm at Birkenes.

Month/Year	Jan	Feb	Mar	Apr	May	Jun	Jul	Aug	Sep	Oct	Nov	Dec
Aerosol optical depth (AOD)												
2009				0.29 ±0.00	0.09 ±0.05	0.09 ±0.05	0.18 ±0.06	0.17 ±0.07	0.10 ±0.04	0.08 ±0.03		
2010					0.10 ±0.04	0.09 ±0.04	0.10 ±0.07	0.10 ±0.05	0.05 ±0.02	0.07 ±0.03	0.04 ±0.01	
2011	0.02 ±0.01	0.03 ±0.01	0.07 ±0.02	0.21 ±0.19	0.13 ±0.07	0.10 ±0.04	0.13 ±0.06	0.09 ±0.05				
2012			0.07 ±0.05	0.05 ±0.02	0.08 ±0.04	0.09 ±0.04	0.07 ±0.03	0.08 ±0.03	0.07 ±0.01	0.06 ±0.03	0.04 ±0.00	
2013							0.17 ±0.17	0.12 ±0.09	0.05 ±0.03	0.05 ±0.03		
2014			0.15 ±0.14	0.11 ±0.06	0.10 ±0.03	0.08 ±0.03	0.13 ±0.06	0.15 ±0.07	0.14 ±0.06			
2015			0.04 ±0.02	0.07 ±0.02	0.07 ±0.03	0.06 ±0.02	0.10 ±0.07	0.09 ±0.06	0.04 ±0.02	0.03 ±0.03	0.04 ±0.01	
2016	0.01 ±0.00	0.03 ±0.01	0.03 ±0.02	0.05 ±0.03							0.02 ±0.00	
2017*				0.08 ±0.01	0.06 ±0.03	0.04 ±0.03	0.06 ±0.03	0.09 ±0.07	0.09 ±0.03	0.06 ±0.03		
2018*				0.09 ±0.07	0.11 ±0.05	0.07 ±0.06	0.08 ±0.06	0.10 ±0.08	0.06 ±0.04			
2019	0.03 ±0.01	0.07 ±0.09	0.04 ±0.02	0.11 ±0.08	0.06 ±0.03	0.12 ±0.11	0.19 ±0.06	0.16 ±0.04			0.07 ±0.03	0.05 ±0.00
2020	0.06 ±0.02	0.08 ±0.07	0.07 ±0.02	0.08 ±0.01	0.07 ±0.02	0.10 ±0.07	0.06 ±0.02	0.11 ±0.06	0.14 ±0.10	0.08 ±0.04	0.04 ±0.02	0.03 ±0.01
2021	0.04 ±0.02	0.04 ±0.02	0.06 ±0.04	0.08 ±0.06	0.06 ±0.04	0.07 ±0.03	0.17 ±0.10	0.10 ±0.06	0.09 ±0.06	0.04 ±0.01	0.04 ±0.02	0.03 ±0.02
2022		0.03 ±0.00	0.07 ±0.08		0.06 ±0.03	0.06 ±0.03	0.08 ±0.10	0.07 ±0.04	0.06 ±0.01	0.04 ±0.01		0.03 ±0.01
Mean 2009 -2022	0.03 0.01	0.05 ±0.02	0.07 ±0.03	0.09 ±0.04	0.08 ±0.02	0.08 ±0.02	0.11 ±0.04	0.10 ±0.03	0.07 ±0.03	0.05 ±0.01	0.04 ±0.01	0.04 ±0.01

* version 3 data analysis (Aeronet)

Table A 9: Monthly means and standard deviation of the Ångström coefficient (Å) at Birkenes

Month/Year	Jan	Feb	Mar	Apr	May	Jun	Jul	Aug	Sep	Oct	Nov	Dec
Ångström coefficient (Å)												
2009				1.5 ±0.0	1.2 ±0.3	1.4 ±0.3	1.4 ±0.4	1.1 ±0.2	1.0 ±0.2	1.1 ±0.2		
2010					1.3 ±0.3	1.4 ±0.3	1.4 ±0.2	1.4 ±0.2	1.3 ±0.3	1.3 ±0.3	1.3 ±0.23	
2011	1.0 ±0.2	1.0 ±0.1	1.0 ±0.3	1.2 ±0.5	1.3 ±0.3	1.5 ±0.3	1.6 ±0.3	1.6 ± 0.1				
2012			1.1 ±0.4	1.6 ±0.3	1.4 ±0.4	1.7 ±0.1	1.6 ±0.3	1.5 ±0.3	1.1 ±0.3	1.4 ±0.4	0.8 ±0.3	
2013							1.3 ± 0.2	1.2 ±0.3	0.8 ±0.2	0.8 ±0.3		
2014			0.87 ±0.48	1.04 ±0.33	1.07 ±0.27	1.02 ±0.24	1.38 ±0.33	1.14 ±0.25	1.19 ±0.16			
2015			0.93 ±0.16	1.06 ±0.13	1.11 ±0.20	1.30 ±0.20	1.49 ±0.20	1.37 ±0.26	1.30 ±0.23	1.23 ±0.25	0.84 ±0.33	
2016	0.68 ±0.07	1.00 ±0.2	0.90 ±0.3	1.13 ±0.2							1.11 ±0.08	
2017*				1.77 ±0.07	1.39 ±0.35	1.39 ±0.37	1.73 ±0.34	1.48 ±0.37	0.93 ±0.18	0.78 ±0.20		
2018				1.02 ± 0.24	1.31 ± 0.25	1.23 ± 0.31	1.54 ± 0.28	1.36 ± 0.23	1.11 ±0.25			
2019	0.83 ±0.23	0.96 ±0.45	1.01 ±0.31	1.47 ± 0.28	1.29 ± 0.23	1.43 ± 0.17	1.60 ± 0.16	1.41 ± 0.15			1.04 ±0.29	1.08 ±0.14
2020	0.88 ±0.29	0.80 ±0.28	1.10 ±0.25	1.17 ± 0.18	1.18 ± 0.24	1.39 ± 0.28	1.41 ± 0.21	1.51 ± 0.21	1.16 ±0.35	1.24 ±0.38	1.05 ±0.18	0.94 ±0.22
2021	1.38 ±0.34	1.58 ±0.44	1.07 ±0.68	1.27 ± 0.26	1.48 ± 0.23	1.47 ± 0.27	1.65 ± 0.33	1.58 ± 0.18	1.54 ±0.29	1.31 ±0.32	1.02 ±0.49	1.42 ±0.29
2022		1.46 ±0.12	1.25 ±0.41		1.16 ± 0.36	1.36 ± 0.34	1.49 ± 0.32	1.56 ± 0.39	1.50 ±0.23	0.65 ±0.31		1.37 ±0.44
Mean 2009-2022	1.08 ±0.23	1.07 ±0.33	1.09 ±0.10	1.31 ±0.21	1.28 ±0.09	1.40 ±0.12	1.58 ±0.12	1.42 ±0.15	1.20 ±0.23	1.09 ±0.27	0.98 ±0.26	1.04 ±0.32

* version 3 data analysis (Aeronet)

Table A 10: Number of days with AOD observations at Birkenes made within the months.

Month/Year	Jan	Feb	Mar	Apr	May	Jun	Jul	Aug	Sep	Oct	Nov	Dec
Number of days with cloud-free and quality assured observations (lev 2; lev 1.5 for 2013)												
2009*						20	23	10	12	13	13	
2010*						13	16	17	19	16	10	11	13
2011*	13	4	19	22	19	23	15	15				
2012*			11	14	11	8	17	23	10	13	3	
2013*							27	21	14	7	14	6
2014*			12	19	17	26	22	14	19			
2015*		7	10	3	21	25	27	19	12	11	10	4
2016*	5	13	11	10							2	
2017*				2	19	17	21	16	6	9		
2018*				8	29	24	27	18	12			
2019	6	9	14	23	24	15	5	11			4	3
2020*	13	12	7	3	11	21	22	22	17	11	9	3
2021*	10	11	9	27	15	26	23	27	18	9	12	1
2022*		3	17		14	22	19	17	4	6		9
Total	47	59	110	131	213	246	252	234	141	89	65	39

Table A 11: Monthly means and standard deviation of aerosol optical depth (AOD) at 500 nm at Trollhaugen Observatory

Month/ Year	Jan	Feb	Mar	Apr	May	Jun	Jul	Aug	Sep	Oct	Nov	Dec
Aerosol optical depth (AOD)												
2014	0.016 ±0.002	0.015 ±0.002	0.014 ±0.002	0.014 ±0.005					0.022 ±0.003	0.017 ±0.002	0.021 1±0.002	0.020 ±0.002
2015	0.029 ±0.003	0.018 ±0.003	0.018 ±0.002	0.017 ±0.001				0.048 ±0.009	0.034 ±0.010	0.040 ±0.007	0.035 ±0.009	0.031 ±0.005
2016	0.035 ±0.006	0.033 ±0.004	0.026 ±0.003	0.027 ±0.004				0.039 ±0.010	0.026 ±0.005	0.024 ±0.005	0.019 ±0.005	0.019 ±0.001
2017	0.020 ±0.003	0.020 ±0.003	0.016 ±0.003	0.015 ±0.002				0.022 ±0.006	0.021 ±0.006	0.019 ±0.002	0.020 ±0.004	0.016 ±0.003
2018	0.016 ±0.004	0.016 ±0.002	0.013 ±0.002	0.014 ±0.001	0.013 ±0.003				0.027 ±0.006	0.022 ±0.002	0.020 ±0.003	0.021 ±0.002
2019	0.027 ±0.006	0.026 ±0.006	0.020 ±0.003	0.019 ±0.002	0.015 ±0.001			0.029 ±0.002	0.019 ±0.001	0.022 ±0.001	0.022 ±0.003	0.026 ±0.002
2020	0.038 ±0.01	0.053 ±0.01	0.053 ±0.01	0.048 ±0.01				0.045 ±0.004	0.041 ±0.007	0.040 ±0.007	0.032 ±0.003	0.024 ±0.003
2021	0.023 ±0.004	0.024 ±0.003	0.020 ±0.002	0.018 ±0.001				0.038 ±0.013	0.034 ±0.008	0.027 ±0.004	0.023 ±0.003	0.027 ±0.003
2022	*0.024 ±0.003*	*0.023 ±0.004*	*0.021 ±0.003*	*0.019 ±0.001*	*0.012 ±0.000*			*0.029 ±0.003*	*0.028 ±0.005*	*0.030 ±0.007*	*0.022 ±0.003*	*0.024 ±0.006*
Mean 2014-2022	*0.025 ±0.007*	*0.025 ±0.011*	*0.022 ±0.011*	*0.021 ±0.01*	*0.013 ±0.001*			*0.036 ±0.009*	*0.028 ±0.007*	*0.027 ±0.008*	*0.024 ±0.005*	*0.023 ±0.004*

* version 3 data analysis (Aeronet) – all data have been re-analyzed

Table A 12: Monthly means and standard deviation of the Ångström coefficient (Å) at Trollhaugen.

Month/Year	Jan	Feb	Mar	Apr	May	Jun	Jul	Aug	Sep	Oct	Nov	Dec
Ångström coefficient (Å)												
2014	1.59 ±0.18	1.54 ±0.14	1.29 ±0.09	1.22 ±0.08					1.29 ±0.15	1.52 ±0.17	1.37 ±0.15	1.76 ±0.06
2015	1.69 ±0.61	1.60 ±0.12	1.43 ±0.10	1.34 ±0.09				0.97 ±0.15	1.03 ±0.18	1.26 ±0.14	1.22 ±0.34	1.47 ±0.15
2016	1.53 ±0.12	1.63 ±0.14	1.41 ±0.09	1.42 ±0.05				1.32 ±0.21	1.25 ±0.18	1.34 ±0.22	1.53 ±0.13	1.48 ±0.09
2017	1.61 ±0.16	1.68 ±0.10	1.23 ±0.14	1.21 ±0.08				1.08 ±0.18	1.18 ±0.24	1.28 ±0.13	1.35 ±0.19	1.53 ±0.10
2018	1.51 ±0.10	1.45 ±0.09	1.29 ±0.08	1.32 ± 0.17	1.30 ± 0.06				1.47 ±0.16	1.47 ±0.11	1.56 ±0.12	1.73 ±0.08
2019	1.63 ±0.11	1.63 ±0.10	1.56 ±0.08	1.34 ± 0.08	1.26 ± 0.08			0.92 ±0.07	1.51 ±0.12	1.44 ±0.09	1.53 ±0.14	1.61 ±0.10
2020	1.71 ± 0.10	1.58 ± 0.14	1.33 ± 0.04	1.24 ± 0.03				0.81 ± 0.09	0.91 ± 0.10	1.11 ± 0.08	1.20 ± 0.07	1.44 ± 0.11
2021	1.49 ± 0.10	1.63 ± 0.08	1.40 ± 0.05	1.25 ± 0.11				0.98 ± 0.13	1.11 ± 0.20	1.30 ± 0.15	1.50 ± 0.17	1.60 ± 0.08
2022	1.65± 0.11	1.63± 0.07	1.57± 0.06	1.51± 0.07	1.34± 0.00			1.12± 0.12	1.30± 0.13	1.30± 0.18	1.43± 0.11	1.38± 0.15
Mean 2014-2022	1.60 ±0.07	1.60 ±0.06	1.39 ±0.11	1.32 ±0.09	1.30 ±0.03			1.03 ±0.15	1.23 ±0.19	1.33 ±0.12	1.41 ±0.13	1.56 ±0.12

Table A 13: Number of days with AOD observations at Trollhaugen made per month.

Month/Year	Jan	Feb	Mar	Apr	May	Jun	Jul	Aug	Sep	Oct	Nov	Dec
Number of days with cloud-free and quality assured observations (lev 2; lev 1.5 for 2013)												
2014	15	22	13	21					4	10	13	11
2015	7	21	11	12				5	14	12	10	25
2016	20	15	15	13				8	10	15	21	21
2017	24	15	24	9				11	11	15	15	10
2018	22	12	13	19	3				11	18	21	18
2019	12	21	21	11	5			1	7	17	9	20
2020	12	21	11	7				7	17	17	10	12
2021	16	17	8	6				9	17	20	17	17
2022	18	19	22	10	1			11	15	14	22	14
Total	146	163	138	108	9			52	106	138	138	148

Appendix B

Description of instruments and methodologies

On the instrumental methods used for the measurements of the various greenhouse gases at Birkenes and Zeppelin Observatories

In this section of the appendix, the instrumental methods used for the measurements of the various greenhouse gases are presented, see also Platt et al., 2022 for more details and historical development of Zeppelin. Additionally, we explain the theoretical methods used in calculation of the trends.

The next table provides details about greenhouse gas measurements and recent improvement and extensions.

Table B 1: Instrumental details for greenhouse gas measurements at Zeppelin and Birkenes.

Component		Instrument and method	Time res.	Calibration procedures	Start - End	Comment
Methane (Birkenes)	CH_4	Picarro CRDS G1301 CO2/CH4/H2O	1 h 5 s	Working std. calibrated against GAW stds at EMPA	19th May 2009 – Jan 2018	
Methane (Birkenes)	CH_4	Picarro CRDS G2401 CO2/CH4/CO	1 h 5 s	ICOS reference standards	1st Jan 2018 ->	Data coverage in 2022: 92%
Methane (Zeppelin)	CH_4	GC-FID	1h	NOAA reference standards	Aug 2001-Apr 2012	
Methane (Zeppelin)	CH_4	Picarro CRDS	1 h 5 sec	ICOS reference standards	20th Apr. 2012 ->	Data coverage 2022: 96%
Nitrous oxide (Zeppelin)	N_2O	GC-ECD	30 min	NOAA reference standards	27th Mar 2010 – 31st Dec 2017	
Nitrous oxide (Zeppelin)	N_2O	Picarro CRDS	1 h 5 sec	ICOS reference standards	1st Jan 2018 ->	Data coverage 2020 88%
Carbon monoxide (Zeppelin)	CO	GC-HgO/UV	20 min	Every 20 min, working std. calibrated vs. GAW std.	Sep. 2001 - 2012	
Carbon monoxide (Zeppelin)	CO	Picarro CRDS	1 h 5 sec	ICOS reference standards.	20th Apr 2012 ->	Data coverage 2022: 96%
Carbon monoxide (Birkenes)	CO	Picarro CRDS G2401 CO2/CH4/CO	1 h 5 sec	ICOS reference standards.	1st Jan 2018 ->	Data coverage in 2022: 94%
Carbon dioxide (Zeppelin)	CO_2	Li-Cor	1 h	NOAA reference standards	1989 - 2012	CO_2 measured by ITM Stockholm University (SU) until 2012
Carbon dioxide (Zeppelin)	CO_2	Picarro CRDS	1 h 5 sec	ICOS reference standards	20th Apr. 2012 ->	Data coverage 2022: 96%
Carbon dioxide (Birkenes)	CO_2	Picarro CRDS G1301 CO2/CH4/H2O	1 h 5 s	Working std. calibrated against GAW stds at EMPA	19th May 2009 -– Jan 2018>	Data coverage in 2019: 95%
Carbon dioxide (Birkenes)	CO_2	Picarro CRDS G2401 CO2/CH4/CO	1 h 5 s	ICOS reference standards	1st Jan 2018 ->	Data coverage in 2022: 94%
CFC-11 CFC-12 CFC-113 CFC-115 HFC-125 HFC-134a HFC-152a HFC-365mfc HCFC-22 HCFC-141b HCFC-142b H-1301 H-1211 H-2402	$CFCl_3$ CF_2Cl_2 $CF_2ClCFCl_2$ CF_3CF_2Cl CHF_2CF_3 CH_2FCF_3 CH_3CHF_2 $CF_3CH_2CHF_2CH_3$ CHF_2Cl CH_3CFCl_2 CH_3CF_2Cl CF_3Br CF_2ClBr	ADS-GCMS	4 h	Every 4 hours, working std. calibrated vs. AGAGE std.	4th Jan 2001-2010	The measurements of the CFCs, TCE and PCE have higher uncertainty and are not within the required precision of AGAGE. See next section for details.

TComponent		Instrument and method	Time res.	Calibration procedures	Start - End	Comment
Chloromethane	CH_3Cl	ADS-GCMS	4h	Every 4 hours, working std. calibrated vs. AGAGE std.	4th Jan 2001-2010	
Bromomethane	CH_3Br					
Dichloromethane	CH_2Cl_2					
Trichloromethane	$CHCl_3$					
Trichloroethane	CH_3CCl_3					
Trichloroethene	$CHClCCl_2$					
Tetrachloroethene	CCl_2CCl_2					
Sulphurhexafluoride	SF_6					
Nitrogen trifluoride	NF_3	Medusa-GCMS No. 19	2 h	Every 2 hours, working std. calibrated vs. AGAGE std	1st September 2010	Data coverage 2022: 60%
PFC-14	CF_4					
PFC-116	C_2F_6					
PFC-218	C_3F_8					
PFC-318	c-C_4F_8					
Sulphurhexafluoride	SF_6					
Sulfuryl fluoride	SO_2F_2					
HFC-23	CHF_3					
HFC-32	CH_2F_2					
HFC-125	CHF_2CF_3					
HFC-134a	CH_2FCF_3					
HFC-143a	CH_3CF_3					
HFC-152a	CH_3CHF_2					
HFC-227ea	CF_3CHFCF_3					
HFC-236fa	$CF_3CH_2CF_3$					
HFC-245fa	$CF_3CH_2CHF_2$					
HFC-365mfc	$CH_3CF_2CH_2CF_3$					
HFC-43-10mee	$CF_3(CHF)_2CF_2CF_3$					
HCFC-22	$CHClF_2$					
HCFC-141b	CH_3CCl_2F					
HCFC-142b	CH_3CClF_2					
CFC-11	CCl_3F					
CFC-12	CCl_2F_2					
CFC-113	CCl_2FCClF_2					
CFC-115	$CClF_2CF_3$					
H-1211	$CBrClF_2$					
H-1301	$CBrF_3$					
H-2402	$C_2Br_2F_4$					
Chloromethane	CH_3Cl					
Bromomethane	CH_3Br					
Dichloromethane	CH_2Cl_2					
Trichloromethane	$CHCl_3$					
Trichloroethane	CH_3CCl_3					
Dibromomethane	CH_2Br_2					
Trichloroethene	$CHClCCl_2$					
Tetrachloroethene	CCl_2CCl_2					
Carbon tetrachloride	CCl_4					
Ethane	C_2H_6					
Propane	C_3H_8					
Butane	C_4H_{10}					
Pentane	C_5H_{12}					
Benzene	C_6H_6					
Toluene	$C_6H_5CH_3$					
Ozone	O_3		5 min			

The overall data coverage for 2022 was 60%. The relatively low data coverage is due to several break downs of different critical parts that had long delivery times. Some of them, the sample trap, is not commercially available, and is an instrument part that the whole AGAGE network is working continuously with to find a better product and a commercial supplier to make and sell.

DATA QUALITY AND UNCERTAINTIES

HALOCARBONS

In 2001 – 2010 measurements of a wide range of hydrochlorofluorocarbons, hydrofluorocarbons (HCFC-141b, HCFC-142b, HFC-134a etc.), methyl halides (CH_3Cl, CH_3Br, CH_3I) and the halons (e.g. H-1211, H-1301) were measured with good scientific quality by using ADS-GCMS. The system also measured other compounds like the chlorofluorocarbons (CFCs), but the quality and the precision of these measurements were not at the same level. Table B 2 shows a list over those species measured with the ADS-GCMS at Zeppelin Observatory from 2001 - 2010. The species that are in blue are of acceptable scientific quality and in accordance with recommendations and criteria of the AGAGE network for measurements of halogenated greenhouse gases in the atmosphere. Those listed in red have higher uncertainties and are not within the required precision of AGAGE. There are various reasons for these increased uncertainties; unsolved instrumental problems e.g. possible electron overload in detector (for the CFC's), influence from other species, detection limits (CH_3I, $CHClCCl_2$) and unsolved calibration problems ($CHBr_3$) or instrumental issues (CCl_2CCl_2). On 1st September 2010, the ADS-GCMS was replaced by a Medusa-GCMS system. The uncertainties improved for almost all species (Table A 11 for details), but there are periods where measurements of the CFC's were still not satisfactory due to a failure in the detector and still high blank values and memory effects in the instruments leads to higher uncertainties in the CHClCCl2 (TCE) measurements.

Table B 2: ADS-GCMS measured species at Zeppelin from 4th January 2001 to 1st September 2010. Good scientific quality data in Blue; Data with reduced quality data in Red. The data are available through http://ebas.nilu.no. Please read and follow the stated data policy upon use.

Compound	Typical precision (%)	Compound	Typical precision (%)
SF_6	1.5	H1301	1.5
HFC134a	0.4	H1211	0.4
HFC152a	0.6	CH_3Cl	0.6
HFC125	0.8	CH_3Br	0.8
HFC365mfc	1.7	CH_3I	5.1
HCFC22	0.2	CH_2Cl_2	0.4
HCFC141b	0.5	$CHCl_3$	0.3
HCFC142b	0.5	$CHBr_3$	15
HCFC124	2.3	CCl_4	0.5
CFC11	0.3	CH_3CCl_3	0.6
CFC12	0.3	$CHClCCl_2$	1.2
CFC113	0.2	CCl_2CCl_2	0.7
CFC115	0.8		

Table below gives an overview over the species measured with the Medusa-GCMS systems at the AGAGE stations and the typical precision with the different instruments. The Medusa-GCMS instrument at the Zeppelin Observatory has the same precision as shown in the Table B 3.

Table B 3: AGAGE measured species.

Compound	Typical precision (%)	Compound	Typical precision (%)
NF_3	1	CFC-11	0.15
CF_4	0.15	CFC-12	0.05
C_2F_6	1	CFC-113	0.2
C_3F_8	3	CFC-115	0.8
c-C4F8	1.5	H-1301	1.7
SF_6	0.6	H-1211	0.4
SO_2F_2	2	H-2402	2
HFC-23	0.7	CH_3Cl	0.2
HFC-32	3	CH_3Br	0.6
HFC-134a	0.5	CH_2Cl_2	0.5
HFC-152a	1.4	CH_2Br_2	1.5
HFC-125	0.7	CCl_4	1
HFC-143a	1	CH_3CCl_3	0.7
HFC-227ea	2.2	$CHClCCl_2$	3
HFC-236fa	10	CCl_2CCl_2	0.5
HFC-245fa	3	C_2H_6	0.3
HFC-365mfc	5	C_3H_8	0.6
HFC-43-10mee	3	C_4H_{10}	0.6
HCFC-22	0.3	C_6H_6	0.3
HCFC-141b	0.5	C_7H_8	0.6
HCFC-142b	0.4		

METHANE Methane is measured at both Birkenes and Zeppelin using a Picarro CRDS (Cavity Ring-Down Spectrometer) monitor which is calibrated against ICOS reference standards (NOAA scale). The instrument participates in ring tests and applies to the ICOS system for calibration and measurement control. The continuous data are also compared to weekly flask samples sent to NOAA CMDL, Boulder Colorado. All data are available for download from EBAS database http://ebas.nilu.no.

$\delta^{13}C_{CH4}$ Air samples from Zeppelin are collected in 1 L steel or aluminium canisters at the same air inlet as CH_4. Two samples per week are sent to the Greenhouse Gas Laboratory at Royal Holloway University of London. Methane mole fraction was measured using a Picarro 1301 cavity ring down spectrometer (CRDS). δ13C analysis is carried out using a modified gas chromatography isotope ratio mass spectrometry system for all samples (Trace Gas and Isoprime mass spectrometer, Isoprime Ltd.) with 0.05‰ repeatability. All measurements for the canisters are made in triplicate. See Fischer et al., 2017 and Myhre et al., 2016 for more details.

N_2O MEASUREMENTS N_2O at Zeppelin is measured using a mid-IR Cavity Ring Down instrument (since December2017) which is calibrated against ICOS reference standards (NOAA scale). The instrument participates in ring tests and applies to the ICOS system for calibration and measurement control. The continuous data are also compared to weekly flask samples sent to NOAA CMDL, Boulder Colorado. This instrument is doing continuous measurements with improved precision and higher measurement frequency (< 1 min). The instrument had to be sent back to the instrument maker for repair in December 2021.

CO_2 MEASUREMENTS Carbon dioxide (CO_2) at Birkenes and Zeppelin is monitored using a Picarro Cavity Ring-Down Spectrometer for continuous measurements, calibrated against a set of ICOS reference standards (NOAA scale). The instrument participates in ring tests and applies to the ICOS system for calibration and measurement control. The continuous data are also compared to weekly flask samples sent to NOAA CMDL, Boulder Colorado. All data will be available for download from the EBAS database http://ebas.nilu.no.

CO MEASUREMENTS Carbon monoxide (CO) at Birkenes and Zeppelin is monitored using a Picarro Cavity Ring-Down Spectrometer for continuous measurements, calibrated against a set of ICOS reference standards (NOAA scale). The instrument participates in yearly ring tests and applies to the ICOS system for calibration and measurement control. The continuous data are also compared to weekly flask samples sent to NOAA CMDL, Boulder Colorado. All data will be available for download from the EBAS database http://ebas.nilu.no.

IMPLEMENTATION OF MEASUREMENTS FROM BIRKENES AND ZEPPELIN INTO ICOS RESEARCH INFRASTRUCTURE

The Integrated Carbon Observation System (ICOS) is a European research infrastructure forming an observation system that will measure and assess the global carbon budget, including atmospheric CO_2, CH_4 and CO concentrations, while ensuring independent and reliable measurements. ICOS-Norway (https://no.icos-cp.eu) contributes to the network of atmospheric measurements with two observatories, Birkenes and Zeppelin.

ICOS has divided their sites into two labels Class 1 and Class 2, dependent on instrumental setup. At Class 1 sites a wider range of measurements of different species are required. Whilst for Class 2 fewer parameters are mandatory. The labelling process evaluates the site set up, the instrumentation with its calibration set-up and data handling, as a quality certificate of the data output from the ICOS site (Figure 49). The labelling process is time consuming as the instrument (Picarro) needs to be evaluated for minimum 1 month at the central ICOS lab, ICOS Atmospheric Thematic Centre (ATC) in France. Another central ICOS lab, ICOS Central Analytical Laboratories (CAL) in Germany, provides calibration cylinders and it takes 4 months to produce them. The same lab provides calibration cylinders and it takes 4 months to produce them. After having the instrument and calibration routines established at the site, the measurements will have to go through a 6 month evaluation period before approval as an ICOS site. In total it typically takes about 1.5 years to get an ICOS certificate.

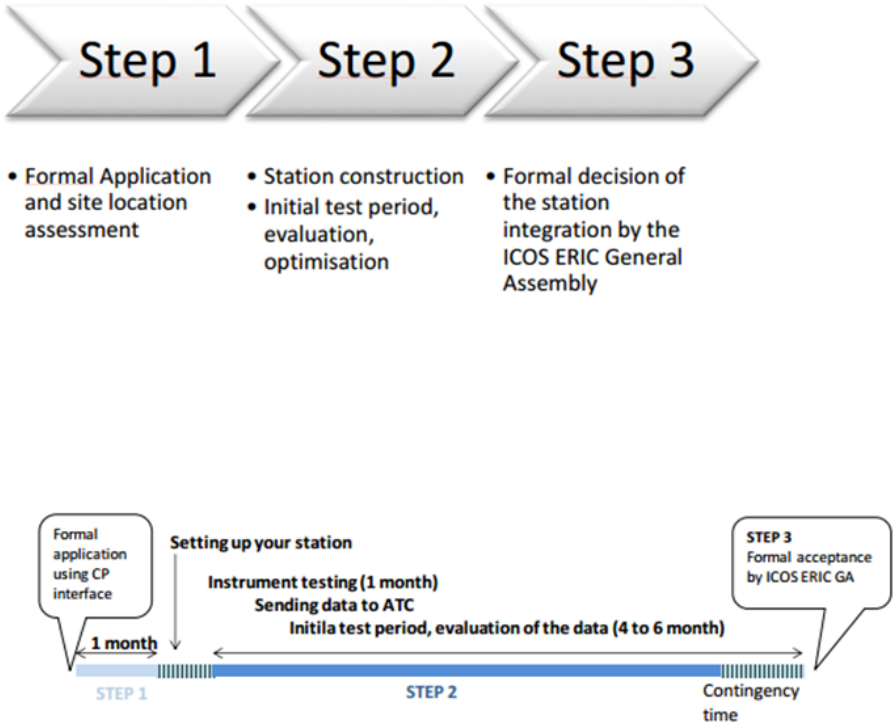

Figure 49: Outline of the labelling process for ICOS stations according to the atmosphere thematic centre (ATC).

The ATC has established the following recommended parameters for ICOS Class 1 and Class 2 sites:

Category	Gases, continuous	Gases, periodical	Meteorology, continuous	Eddy Fluxes
Class 1 Mandatory parameters	• **CO_2, CH_4, CO** : at each sampling height	• **CO_2, CH_4, N_2O, SF_6, CO, H_2, ^{13}C and ^{18}O in CO_2**: weekly sampled at highest sampling height† • **^{14}C** (radiocarbon integrated samples): at highest sampling height	• **Air temperature, relative humidity, wind direction, wind speed**: at highest and lowest sampling height* • **Atmospheric Pressure** • **Planetary Boundary Layer Height**** †	
Class 2 Mandatory parameters	• **CO_2, CH_4** : at each sampling height		• **Air temperature, relative humidity, wind direction, wind speed**: at highest and lowest sampling height* • **Atmospheric Pressure**	
Recommended parameters***	• **^{222}Rn, N_2O, O_2/N_2 ratio** • **CO** for Class 2 stations	• **CH_4 stable isotopes, O_2/N_2 ratio** for Class 1 stations: weekly sampled at highest sampling height		• **CO_2** : at one sampling height

* Atmospheric temperature and relative humidity recommended at all sampling heights
** Only required for continental stations.
*** Recommended for its scientific value but support from ATC in terms of protocols, data base, spare analyzer will not be ensured as long as the parameters are not mandatory.

The Zeppelin Observatory was labelled as an ICOS Class 1 site in 2018. Meanwhile, for sites such as Birkenes, classed as a 'continental site' by ICOS, the ATC requires that measurements are from air sampled at 100 m above ground or higher, typically using sampling inlets installed on a mast, with additional sampling at 10 m, and between 40-70 m. The purpose of this is to minimise the influence of vegetation (i.e. photosynthesis) on CO_2 measurements. For Zeppelin, a mountain top site, the only requirement was that sampling is 'sufficiently high to avoid contamination e.g. by local sources'.

Due to the location of the Birkenes Observatory on a small hill at 40 m, construction of foundations for a 100 m would be challenging and expensive. Thus, NILU initiated negotiations with ATC to lower the required sampling height on the basis that the Observatory is already elevated by 40 m. The ATC agreed to lower the required sampling height to 75 m, a more feasible mast height requiring less extensive foundations, stating in writing: "The Birkenes Observatory location and site infrastructure fulfil the ICOS requirements and recommendations specified in the latest ICOS Atmospheric Station Specifications document (version 1.3, November 2017) when the tower will be installed."

As of 28th August 2020 construction of the 75 m mast was complete (Figure 50) and the installation of equipment on the mast (meteorological equipment, sample inlets etc.) were mostly done by the second week of September. The very first measurements from the 75-meter mast were performed on 14th September. The finalization of the installation is scheduled to the beginning of October. Note that the new mast has also required changes to the station infrastructure i.e. changing the location of the station entrance, upgraded protection from lightning strikes and falling ice, as well as changes in health and safety procedures (the station may no longer be accessed if there is a risk of thunder storms).

Figure 50: Birkenes Observatory with the new 75 m mast installed August-September 2020 to comply with the ICOS requirements.

Status of the labelling process for Birkenes and Zeppelin Observatories:

- The Zeppelin Observatory has achieved Class 1 status and is fully integrated in the network
- The Birkenes Observatory has achieved class 2 status as of May 2021

At class 1 sites an automatic flask sampler (comprising several evacuated steel flasks which are filled at pre-set intervals using electronically operated valves) is mandatory and has been installed at the Zeppelin station. The flask sampler currently runs one sample every 10 days. The flask sampling program is developed by ICOS but there are some issues with the automatic flask sampler. Work in progress for fixing this to enable an increased flask sampling frequence.

On 25th May 2021, The ICOS General Assembly unanimously accepted labelling of Birkenes Observatory as a Class 2 Atmosphere Station.

AIR INLET AT ZEPPELIN

In 2011 the air inlet for the GHG measurements at Zeppelin were improved to reduce possible influence from the station and visitors at the station. The inlet was moved away from the station and installed in a 15 m tower nearby for the following components:

- N_2O
- CH_4
- CO_2
- CO
- Halogenated compounds
- NOAA flasks sampling program
- Isotope flask sampling of CO_2 and CH_4

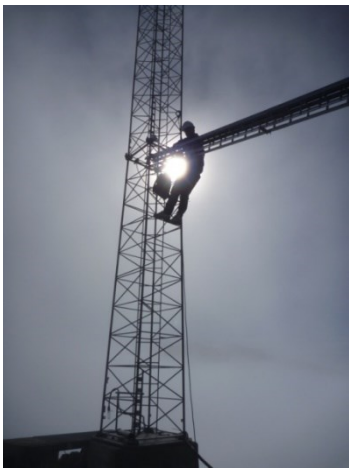

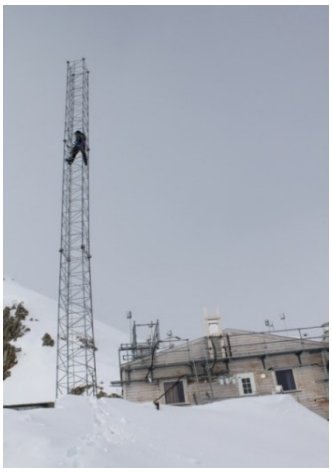

DETERMINATION OF BACKGROUND DATA

Based on the daily mean concentrations an algorithm is selected to find the values assumed as clean background air. If at least 75% of the trajectories within +/- 12 hours of the sampling day are arriving from a so-called clean sector, defined below, one can assume the air for that specific day to be non-polluted. The remaining 25% of the trajectories from European, Russian or North American sector are removed before calculating the background.

CALCULATION OF TRENDS FOR GREENHOUSE GASES AND VOCS

To calculate the annual trends the observations have been fitted as described in Simmonds et al. (2006) by an empirical equation of Legendre polynomials and harmonic functions with linear, quadratic, and annual and semi-annual harmonic terms:

$$f(t) = a + b\left(\frac{N}{12}\right)\cdot P_1\left(\frac{t}{N}-1\right) + \frac{1}{3}\cdot d\left(\frac{N}{12}\right)^2 \cdot P_2\left(\frac{t}{N}-1\right) + c_1\cdot\cos\left(\frac{2\pi t}{12}\right) + s_1\sin\left(\frac{2\pi t}{12}\right) + c_2\cos\left(\frac{4\pi t}{12}\right) + s_2\sin\left(\frac{4\pi t}{12}\right)$$

The observed *f* can be expressed as functions of time measures from the 2N-months interval of interest. The coefficient *a* defines the average mole fraction, *b* defines the trend in the mole fraction and *d* defines the acceleration in the trend. The *c* and *s* define the annual and inter-annual cycles in mole fraction. N is the mid-point of the period of investigation. P_i are the Legendre polynomials of order *i*.

This equation is used for all GHGs except for the halocarbons, where the fit between the empirical equation and observations improves if the semi-annual harmonic terms are replaced by an additional Legendre polynomial.

We are applying a new and improved method for estimating the *uncertainties* in the estimated annual trends from the time series regression modelling. In previous years, these uncertainties were estimated using a standard method from ordinary linear regression, where it was implicitly assumed that the residuals of the fitted regression models were uncorrelated. However, the use of such standard methods is known to often underestimate the true uncertainties in the estimated parameters if these assumptions are not true, i.e. if the residuals are autocorrelated, which to a large extent is the case for the regression models being fitted here.

In the current report we have replaced the standard method with a new method for estimation of uncertainties in the estimated annual trend that takes into account the presence of autocorrelated errors in the fitted model residuals. The new method also takes into account possible presence of heteroscedasticity, which means that the variances of the residuals might vary with the level of the time series, which also affects the uncertainties of the estimated trend. To this end we use the routine vcovHAC in the sandwich package in R (R Core Team, 2018) as described in Zeileis (2006; 2004), to estimate standard deviation of all estimated parameters of the time series regression models. Here HAC is short for Heteroscedastic and Autocorrelation Consistent.

It is important to emphasize that the new method only alters the estimated *uncertainties* of the annual trend estimates. The annual trend estimates themselves are not influenced by this update and have been correctly estimated using standard linear regression also in previous year's reports.

ON THE SURFACE IN SITU OBSERVATIONS OF AEROSOL MICROPHYSICAL AND OPTICAL PROPERTIES AT BIRKENES, ZEPPELIN AND TROLLHAUGEN OBSERVATORY

Table B 4: Overview of atmospheric aerosol parameters measured by surface in situ observations operated at which station

	Birkenes	Trollhaugen	Zeppelin
Particle Number Size Distribution (fine size range D_p < 0.8 µm)	X	X	X
Particle Number Size Distribution (coarse size range D_p > 0.8 µm)	X (OPS)		X (APS)
Particle Number Size Distribution, refractory particle fraction (fine size range D_p < 0.8 µm)			X
Aerosol Scattering Coefficient (spectral)	X	X	
Aerosol Absorption Coefficient (spectral)	X	X	X

Concerning surface in situ observations of microphysical and optical properties of atmospheric aerosol, the table on the left gives an overview over the parameters observed at Birkenes, Trollhaugen, and Zeppelin stations and operated by NILU.

To achieve high quality data with appropriate uncertainty and precision, this requires networked instruments to participate in inter-comparisons at ACTRIS aerosol calibration centre in Leipzig, Germany, in regular intervals. This activity has proven to be necessary in order to ensure comparable measurements within the distributed infrastructure. The frequency of these inter-comparisons, once every 2-3 years, is balanced with minimising the downtime associated with these quality assurance measures. In 2016, instruments targeting the direct aerosol climate effect were in the focus of inter-comparisons. Both the integrating nephelometer and the newer filter absorption photometer, measuring the spectral aerosol particle scattering and absorption coefficients respectively, were scheduled for being inter-compared, with satisfactory outcome in both cases. Between inter-comparisons, instruments are field calibrated regularly to ensure internal consistency of the time series.

With respect to microphysical aerosol properties, the particle number size distribution (PNSD) at surface-level is observed at all 3 stations covered in this report, at least over parts of the relevant range in particle size. The relevant particle sizes cover a range of 0.01 µm – 10 µm in particle diameter. The diameter range of 1.0 µm – 10 µm is commonly referred to as coarse mode, the range D_p < 1.0 µm as fine mode. The fine mode is separated further into Aitken-mode (0.01 µm < D_p < 0.1 µm) and accumulation mode (0.1 µm < D_p < 1 µm). The distinction of these modes is justified by different predominant physical processes as function of particle size. In the Aitken-mode, particles grow by condensation of precursor gases from the gas-phase and coagulate among themselves or with accumulation mode particles. Accumulation mode particles grow by taking up Aitken-mode particles or by mass uptake while being activated as cloud droplets, and they are removed by precipitation. Coarse mode particles in turn are formed by break-up of biological or crustal material, including pollen, bacteria, and fungus spores, and removed by gravitational settling and wet removal. The PNSD of an aerosol is needed for quantifying any interaction or effect of the aerosol since all of them depend strongly on particle size.

To measure the PNSD over the full relevant size range, several measurement principles need to be combined. A Differential Mobility Particle Spectrometer (DMPS) measures the particle number size distribution, now in the range of 0.01 – 0.8 µm particle diameter after several improvements of the instruments at all three stations, i.e. almost the full fine mode. In a DMPS, the particles in the sample air stream are put into a defined state of charge by exposing them to an ionised atmosphere in thermal equilibrium. The DMPS uses a cylindrical capacitor to select a narrow size fraction of the particle phase. The particle size of the selected size fraction is determined by the voltage applied to the capacitor. The particle number concentration in the selected size fraction is then counted by a Condensation Particle

Counter (CPC). A mathematical inversion that considers charge probability, diffusional losses of particles in the system, transfer function of the capacitor, and counting efficiency of the CPC is then used to calculate the particle number size distribution.

The PNSD of particles with diameters 0.25 µm < D_p < 30 µm can be measured with 2 device types: 1) an Optical Particle Spectrometer (OPS); 2) an Aerodynamic Particle Spectrometer (APS). In the OPS, the particles in the sample stream are focussed through a laser beam. The instrument registers number and amplitude of the pulses of light scattered by the particles. The particle pulses are sorted into a histogram by their amplitude, where the pulse amplitude yields the particle diameter and the pulse number the particle concentration, i.e. together the PNSD. Particle sizing in an OPS depends on the particle refractive index, particularly its imaginary part which determines particle absorption. In an APS, particles are exposed to an air flow passage where the particles are accelerated. The time needed for the particle to pass the passage depends on the amount of acceleration, and thus its aerodynamic diameter. The time needed to pass the passage is measured by laser beams at start and end of the passage. Together with counting the number of particles per time, this yields the particle number size distribution.

Both, the DMPS, the OPS, and the APS, yield method specific measures of the particle diameter, the electrical mobility, the optical, and the aerodynamic particle diameter, respectively. When related to the spherical equivalent geometric particle diameter commonly referred to, all particle size measures depend on particle shape (causing a 5% systematic uncertainty in particle diameter), the optical particle diameter in addition on particle refractive index (causing a 20% systematic uncertainty in particle diameter), and the aerodynamic particle diameter on particle density (causing a 15% systematic uncertainty in particle diameter). Where possible, the PNSDs provided by DMPS and OPS/APS are joined into a common PNSD, in this report. To quality assure this process, PNSDs are accepted only if DMPS and OPS/APS PNSD agree within 25% in particle diameter in their overlap size range. Together, both instruments provide a PNSD that spans over 3 orders of magnitude in particle diameter, and over 6 orders of magnitude in particle concentration.

Optical aerosol parameters quantify the direct aerosol climate effect. The observation programme at Birkenes includes the spectral particle scattering coefficient $\sigma_{sp}(\lambda)$ and the spectral particle absorption coefficient $\sigma_{ap}(\lambda)$. The scattering coefficient quantifies the amount of light scattered by the aerosol particle population in a sample per distance a light beam travels through the sample. The absorption coefficient is the corresponding property quantifying the amount of light absorbed by the particle population in the sample. An integrating nephelometer is used for measuring $\sigma_{sp}(\lambda)$ at 450, 550, and 700 nm wavelength. In this instrument, the optical sensors look down a blackened tube that is filled with aerosol sample. The tube is illuminated by a light source with a perfect cosine intensity characteristic perpendicularly to the viewing direction. It can be shown mathematically that this setup integrates the scattered light seen by the optical sensors over all scattering angles. The nephelometer at Birkenes has successfully undergone quality assurance by intercomparison within the EU research infrastructure ACTRIS in 2015. In 2017 we detected drift in the older filter absorption photometer operated at Birkenes since 2009 through carefully implemented quality control within ACTRIS. The drift was detected by operating the older filter absorption photometer in parallel with a newer, more stable make and model in order to ensure a continuous, rupture-free aerosol absorption time series at Birkenes. In addition, the newer instrument was sent to an inter-comparison within the European research infrastructure for short-lived climate forcers ACTRIS. These exercises connect individual instruments to a network-wide primary standard, ensuring traceability and comparability of observations at stations in the network. The old instrument exhibiting the drift has since been decommissioned.

For the nephelometer at Trollhaugen, such intercomparisons are impossible because of the remote Antarctic location and associated logistical challenges. However, the Trollhaugen instrument undergoes the same regular on-site quality assurance as the Birkenes instrument, including regular calibration verification traceable to physical first principles (calibration with high-purity carbon dioxide,

where scattering coefficient of carbon dioxide can be calculated from fundamental quantum mechanics).

The spectral particle absorption coefficient $\sigma_{ap}(\lambda)$ is measured by filter absorption photometers. A filter absorption photometer infers $\sigma_{ap}(\lambda)$ by measuring the decrease in optical transmissivity of a filter while the filter is loaded with the aerosol sample. The transmissivity time series is subsequently translated into an absorption coefficient time series by using Lambert-Beer's law, the same law also used in optical spectroscopy. The filter absorption photometers deployed at Birkenes have been a custom-built 1 wavelength Particle Soot Absorption Photometer (PSAP), a commercial 3-wavelength PSAP, and a modern AE33 aethalometer. The 1-wavelength PSAP received quality assurance by intercomparison within ACTRIS in 2013 discovering calibration stability issues. The 3-wavelength PSAP has undergone ACTRIS intercalibration successfully in 2015, i.e. without discovering any issues. Thus, both instruments are interpreted in combination to benefit from both, quality assurance in a research network and spectral capabilities. For 2013 and later, the data of the 3-wavelength PSAP are used, for 2010-2012, the data of the older 1-wavelength are used after being corrected by comparison with the newer instrument during the overlap period. For comparison with the nephelometer, the PSAP data has been transferred to a wavelength of 550 nm using the measured spectral dependence (3-wavelength PSAP), or by assuming an absorption Ångström coefficient $å_{ap}$ of -1 (1-wavelength PSAP, adding 2% systematic uncertainty to the data). The AE33 aethalometer has been deployed at Birkenes in late 2017. It extends the spectral range of the $\sigma_{ap}(\lambda)$ measurements to 370 – 950 nm (UV to near IR) with a resolution of 7 wavelengths. Previous aethalometer models suffered from high systematic uncertainties due to uncorrected dependencies on filter loading (e.g. Collaud Coen et al.,2010). Comparisons and calibrations within ACTRIS have shown that this systematic uncertainty has been reduced significantly in the AE33 model by an internal loading compensation (Drinovec et al., 2015).

The same AE33 aethalometer instrument type has been operated at Zeppelin since 2015.

Figure 51 compares the particle absorption coefficient between the Particle Absorption Photometer (PSAP) deployed at Birkenes in 2012, and the AE33 aethalometer deployed there in 2017 with a scatter plot including regression line. The analysis shows a correlation coefficient R^2 of 0.97 for the whole range of values, i.e. 97% of the variation in the data of one instrument is explained by the respective variation of the other instrument. This result ensures that the new instrument will continue the time series consistently. The slope of the regression line deviates from 1. Corresponding calibration factors are currently being established by the ACTRIS Research Infrastructure.

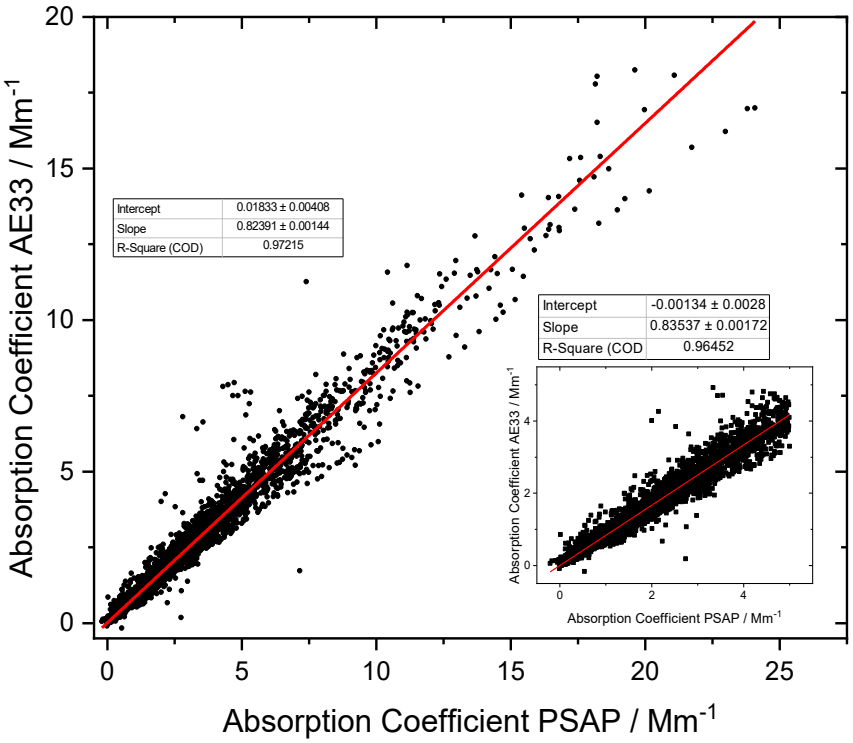

Figure 51: Comparison of particle absorption coefficient data measured the Particle Absorption Photometer (PSAP) deployed at Birkenes in 2012, and the AE33 aethalometer deployed there in 2017. The wavelength of the absorption coefficient has been interpolated to 550 nm for both instruments. The data are compared as scatter plot with regression line (red), large panel for the total range of values, small panel for values ≤ 5 Mm^{-1}.

Even though the oldest filter absorption photometer in operation at Birkenes underwent quality assurance by off-site intercomparison within ACTRIS in 2013, a drift of the reading of the older compared to the newer instrument can be observed between 2013 – 2015. These stability issues of the older filter absorption photometer were discovered already during the 2013 intercomparison. Consequently, also the newer filter absorption photometer was subjected to an ACTRIS intercomparison in 2015. The intercomparison discovered no issues with the newer instrument and confirmed stability of calibration. As a result, the whole σ_{ap} time series obtained with the old filter absorption photometer has been corrected with the 2012 instrument as reference, yielding a consistent aerosol absorption time series for Birkenes for the years since 2010. In 2017, the 2012 absorption photometer experienced problems related to an unstable measurement of the sample flow, leading to low data coverage in summer 2017. Due to the importance of the aerosol absorption measurement in relation to emissions from biomass combustion for domestic heating, it was decided to install the new 7-wavelength version in parallel, and keep both instruments running as mutual backup.

All in situ observations of aerosol properties representing the ground-level are conducted for the aerosol at dry-state (RH < 40%) for obtaining inter-comparability across the network.

DETAILS ABOUT AEROSOL OPTICAL DEPTH MEASUREMENTS

AERONET - Cimel C-318

- Sun (9 channels) and sky radiances
- Wavelength range: 340-1640 nm
- 15 min sampling
- No temperature stabilization
- AOD uncertainty: 0.01-0.02

PFR-GAW- Precision Filter Radiometer

- Direct sun measurements (4 channels)
- Wavelength range: 368 - 862 nm
- 1 min averages
- Temperature stabilized
- AOD uncertainty: 0.01

Figure 52: Photos and typical features of the standard instrument of the AERONET (left panel) and GAW PFR network instruments (right panel).

In 2002, Physikalisch-Meteorologisches Observatorium Davos/World Radiation Center (PMOD/WRC), in collaboration with NILU, started AOD observations in Ny-Ålesund (at the Sverdrup station, 46 m a.s.l.) as part of the global AOD network on behalf of the WMO GAW program. A precision filter radiometer (PFR) measures the extinction in four narrow spectral bands at 368 nm, 415 nm, 500 nm and 862 nm. Data quality control includes instrumental control like detector temperature and solar pointing control as well as objective cloud screening. Ångström coefficients are derived for each set of measurements using all four PFR channels. Calibration is performed annually at PMOD/WRC. Quality assured data are available at the World Data Centre of Aerosols (WDCA), hosted at NILU (see https://ebas.nilu.no). In order to calculate a daily average, at least 50 single measurements are required.

The sun-photometer measurements in Ny-Ålesund are part of the global network of aerosol optical depth (AOD) observations, which started in 1999 on behalf of the WMO GAW program. The instrument is located on the roof of the Sverdrup station, Ny-Ålesund, close to the EMEP station on the Zeppelin Mountain (78.9°N, 11.9°E, 474 m a.s.l.). The Precision Filter Radiometer (PFR) has been in operation since May 2002. In Ny-Ålesund, the sun is below 5° of elevation from 10th October to 4th March, limiting the period with sufficient sunlight to the spring-early autumn season. However, during the summer months it is possible to measure day and night if the weather conditions are satisfactory. The instrument measures direct solar radiation in four narrow spectral bands centred at 862 nm, 501 nm, 411 nm, and 368 nm. Data quality control includes instrumental control like detector temperature and solar pointing control as well as objective cloud screening. Measurements made at full minutes are averages of 10 samples for each channel made over a total duration of 1.25 seconds. SCIAMACHY TOMSOMI and OMI ozone columns as well as meteorological data from Ny-Ålesund are used for the retrieval of aerosol optical depth (AOD).

At Birkenes Observatory, aerosol optical depth measurements started in spring 2009, utilizing an automatic sun and sky radiometer (CIMEL type CE-318) of the global Aerosol Robotic Network (AERONET) at NASA-GSFC, with spectral interference filters centred at selected wavelengths: 340 nm, 380 nm, 440 nm, 500 nm, 675 nm, 870 nm, 1020 nm, and 1640 nm. The measurement frequency is approximately 15 minutes (this depends on the air-mass and time of day). Calibration is performed about once per year, at the Atmospheric Optics Group at the University of Valladolid (GOA-UVa), Spain. GOA manages the calibration for the AERONET sun photometers of the European sub-network of AERONET. Raw data are processed and quality assured centrally by AERONET. Data reported for 2009 - 2017 are quality-assured AERONET level 2.0 data, which means they have been pre- and post-field-calibrated, automatically cloud cleared and have been manually inspected by AERONET.

From 2017, only the new analysis algorithm (version 3) is used at the central AERONET analysis unit at NASA GSFC. In this version, the data quality control, including cloud screening, has been improved and a temperature correction has been applied to all wavelength channels. A comparison between the data from all years of operations at Birkenes (2019 – 2016) analysed with version 3 and version 2 revealed an increase of 25% in number of usable data, especially in the winter half-year. While during the summer months, the agreement between the two versions is better than 2% for both AOD and (470, 870nm) Ångström coefficient, there are significant deviations (>10%) in the months with less than 1000 observations over the whole period (November – February). A comprehensive analysis of the differences between the two versions and possible effects on trend studies is in progress; a paper by the NASA GSFC team will be published in the near future.

Due to the large gaps in data acquisition caused by the obligatory annual calibrations at the University of Valladolid combined with technical problems and occasionally unfavourable weather conditions at Birkenes, NILU decided to purchase a second Cimel instrument which will be operated alternately with the current instrument. It will be taken into operation in fall 2018.

Outlook on observations of aerosol optical depth in Ny-Ålesund

A major obstacle to obtaining a year-round AOD climatology in the Arctic arises from the long polar night. To fill gaps in the aerosol climatology at Ny-Ålesund, a lunar photometer will be operated on a quasi-permanent basis in the frame of the SIOS infrastructure project. This is a collaborative initiative between NILU, PMOD/WRC and ISAC-CNR. Seasonal deployments of a lunar photometer owned by PMOD/WRC were already made in the winters of 2014/15 and 2016/17. The multiple-season deployment started in autumn 2018.

Figure 53: Moon PFR on the Kipp & Zonen tracker during the day (left, parking position) and during night-time measurements (right).

The PFR instrument modified by PMOD-WRC was installed on a tracker model Kipp & Zonen provided usually hosting a sun photometer. Figure 53 shows the instrument on the tracker during daytime and night-time. Six lunar cycles were monitored: the first during February 2014, while the other 5 during winter 2014-2015. We collected data on 66 measurement periods, from Moon-rise to Moon-set or from minimum-to-minimum elevation as in Polar Regions no set-rise events are possible. Among these, we obtained 17 distinct good measurement periods, due to the frequent occurrence of clouds. For further details see, e.g., Mazzola at al., 2015.

Appendix C

Abbreviations

Abbreviation	Full name
ACSM-ToF	Aerosol Chemical Speciation Monitor
ACTRIS	Aerosols, Clouds, and Trace gases Research InfraStructure Network
ADS-GCMS	Adsorption-Desorption System – Gas Chromatograph Mass Spectrometer
AeroCom	Aerosol Comparisons between Observations and Models
AERONET	Aerosol Robotic Network
AGAGE	Advanced Global Atmospheric Gases Experiment
AIRS	Atmospheric Infrared Sounder
AMAP	Arctic Monitoring and Assessment
AOD	Aerosol optical depth
AWI	Alfred Wegener Institute
BC	Black carbon
CAMP	Comprehensive Atmospheric Monitoring Programme
CCN	Cloud Condensation Nuclei
CCNC	Cloud Condensation Nucleus Counter
CFC	Chlorofluorocarbons
CICERO	Center for International Climate and Environmental Research – Oslo
CIENS	Oslo Centre for Interdisciplinary Environmental and Social Research
CLTRAP	Convention on Long-range Transboundary Air Pollution
CO	Carbon monoxide
CPC	Condensation Particle Counter
DMPS	Differential Mobility Particle
EMEP	European Monitoring and Evaluation Programme
ENVRI^{plus}	Environmental Research Infrastructures Providing Shared Solutions for Science and Society
EOS	Earth Observing System
ERF	Effective radiative forcing ERF
ERFaci	ERF due to aerosol–cloud interaction
EU	European Union
EUSAAR	European Supersites for Atmospheric Aerosol Research
FLEXPART	FLEXible PARTicle dispersion model
GAW	Global Atmosphere Watch
GB	Ground based
GHG	Greenhouse gas
GOA-UVA	Atmospheric Optics Group of Valladolid University
GOSAT	Greenhouse Gases Observing Satellite

Abbreviation	Full name
GOSAT-IBUKI	Greenhouse Gases Observing Satellite "IBUKI"
GWP	Global Warming Potential
HCFC	Hydrochlorofluorocarbons
HFC	Hydrofluorocarbons
ICOS	*Integrated Carbon Observation System*
InGOS	Integrated non-CO2 Greenhouse gas Observing System
IPCC	Intergovernmental Panel on Climate Change
ISAC-CNR	Institute of Atmospheric Sciences and Climate (ISAC) of the Italian National Research Council
ITM	Stockholm University - Department of Applied Environmental Science
JAXA	Japan Aerospace Exploration Agency
LLGHG	Well-mixed greenhouse gases
MOCA	Methane Emissions from the Arctic OCean to the Atmosphere: Present and Future Climate Effects
MOE	Ministry of the Environment
NARE	Norwegian Antarctic Research Expeditions
MP	Montreal Protocol
NASA	National Aeronautics and Space Administration
NEOS-ACCM	Norwegian Earth Observation Support for Atmospheric Composition and Climate Monitoring
NIES	National Institute for Environmental Studies
NOAA	National Oceanic and Atmospheric Administration
NRS	Norsk Romsenter
OC	Organic Carbon
ODS	Ozone-depleting substances
OH	Hydroxyl radical
OPS	Optical Particle Spectrometer
OSPAR	Convention for the Protection of the marine Environment of the North-East Atlantic
PFC	Perflueorinated compounds
PFR	Precision filter radiometer
PMOD/WRC	Physikalisch-Meteorologisches Observatorium Davos/World Radiation Center
PNSD	Particle number size distribution
ppb	Parts per billion
ppm	Parts per million
ppt	Parts per trillion
PSAP	Particle Soot Absorption Photometers

Abbreviation	Full name
RF	Radiative forcing
RI	Research Infrastructure
RIMA	Red Ibérica de Medida fotométrica de Aerosoles
SACC	Strategic Aerosol Observation and Modelling Capacities for Northern and Polar Climate and Pollution
SCIAMACHY	SCanning Imaging Absorption spectroMeter for Atmospheric CHartographY
SIS	Strategisk instituttsatsing
SMPS	Scanning Mobility Particle
TES	Tropospheric Emission Spectrometer
TOA	Top Of Atmosphere
TOMS OMI	Total Ozone Mapping Spectrometer Ozone Monitoring instrument
UN	United Nations
UNFCCC	United Nations Framework Convention on Climate Change
VOC	Volatile organic compounds
WDCA	World Data Centre for Aerosol
WDCS	World Data Centre of Aerosols
WMGHG	Well-mixed greenhouse gases
WMO	World Meteorological Organization

NILU

The climate and environmental research institute NILU is an independent, non-profit research institution established in 1969. Through its research NILU increases the understanding of atmospheric composition, climate change, air quality, environmental contaminants, health effects, sustainable systems, circular economy, and digitalisation. Based on its research, NILU markets integrated services and products within analysing, monitoring and consulting. NILU is concerned with increasing public awareness about climate change and environmental pollution.

NILU's values:	*Integrity - Competence - Benefit to society*
NILU's vision:	*Create sustainable development through internationally leading climate and environmental research*

NILU
P.O. Box 100, NO-2027 KJELLER, Norway

E-mail: nilu@nilu.no
http://www.nilu.no
Enterprise no.: 941 705 561

ISBN: 978-82-425-3137-7
ISSN: 2464-3327

NILU